
# From weakly to strongly correlated physics of bosons in the $p$ band

**Fernanda Pinheiro**

Licentiate Thesis

Akademisk avhandling
för avläggande av licentiatexamen i teoretisk fysik
vid Stockholms universitetet

Department of Physics
Stockholm University

August 2013

Material covered in this thesis:

Paper I - Confined *p*-band Bose-Einstein condensates
Fernanda Pinheiro, Jani-Petri Martikainen and Jonas Larson
*Phys. Rev. A* **85**, 033638 (2012)

Paper II - XYZ quantum Heisenberg models with p-orbital bosons
Fernanda Pinheiro, Georg M. Bruun, Jani-Petri Martikainen and Jonas Larson
*arXiv:1304.3178*

Other papers not in this thesis:

Quantum entanglement of bound particles under free center of mass dispersion
Fernanda Pinheiro and A. F. R. de Toledo Piza
*Phys. Scr.* **85** 065002, (2012)

Delocalization and superfluidity of ultracold bosonic atoms in a ring lattice
Fernanda Pinheiro and A. F. R. de Toledo Piza
*arXiv:1301.4672*

# Contents

# Acknowledgments

I thank my supervisors Jonas Larson and Jani-Petri Martikainen for all the learning and attention, for their support and for their comments on this thesis. I also would like to thank Georg Bruun and A. F. R. de Toledo Piza for participating on the different projects developed during the course of the work reported here, and Alessandro De Martino, Stephen Powell, Andreas Hemmerich and Tomasz Sowiński for valuable discussions. Finally, I would like to thank the Swedish Research Council Vetenskapsrådet for financial support.

# Abstract

In this thesis we explore the physics of bosonic atoms in the first excited band of an optical lattice - the p band. As is discussed here, due to the additional orbital degree of freedom, the physics in the p band is qualitatively different from the physics of the well characterized systems in the ground band. We first define the orbital states and discuss properties at the single particle level, from where we construct the framework for studying the many-body system. This serves as the basis for the mean-field analysis that is carried out in the sequence. The main body of this work covers the studies developed in Papers I and II. In Paper I we discuss properties of confined $p$-orbital bosons, that include condensation of the ideal gas of bosons in the $p$ band, the ideal gas at finite temperatures and zero temperature studies of the interacting system for both the symmetric and asymmetric lattices. We continue with the studies of Paper II, in which $p$-orbital bosons are considered in the strongly correlated regime. In particular, we show that the effective Hamiltonian describing $p$-orbital bosons in the Mott phase with a unit filling of the lattice sites can be mapped into the spin-1/2 quantum $XYZ$ Heisenberg model in external field. Here the system is considered in the context of quantum simulators and we complement the study by proposing detection and manipulation schemes for experimentally probing the physics discussed. Finally, we present some work in progress that suggests the possibility of using systems of bosons in the $p$ band for experimentally exploring the physics of spin chains beyond spin-1/2.

# 1. Introduction

After the experimental realization of the optical lattices in the lab and the subsequent observation in 2003 [1, 2] of the previously predicted Mott-insulator to superfluid transition, cold atom systems became a primary candidate for understanding many-body quantum phenomena [3, 4]. The degree of control and manipulation in these systems is so great, that nowadays it is possible to engineer lattices with all sorts of different configurations that allow for the study of many-body quantum physics in the strongly correlated regime [3, 4]. Put in other words, cold atoms in optical lattices provide highly controllable laboratories for testing models of solid state and condensed matter physics.

This is because similar to the behavior of electrons described by the celebrated *Hubbard model* [5], the many-body dynamics in the optical lattice is dominated by the two basic ingredients consisting of hopping and atom-atom repulsive interactions [6]. This is usually described in most simple terms by the *Bose-Hubbard Hamiltonian* in the tight-binding limit,

$$\hat{H}_{BH} = -t \sum_{\langle i,j \rangle} (\hat{a}_i^\dagger \hat{a}_j + \hat{a}_j^\dagger \hat{a}_i) + \frac{U}{2} \sum_i \hat{n}_i(\hat{n}_i - 1), \quad t,\, U > 0, \tag{1.1}$$

where $\sum_{\langle i,j \rangle}$ runs over the nearest neighbors and $\hat{a}_i$ and $\hat{a}_i^\dagger$ are the bosonic operators that annihilate and create an atom in a site-localized state in the $i$-th site. The first term describes nearest neighbors hopping, which happens with amplitude $t$, and the second term describes the onsite two-body interactions, characterized by a matrix element with magnitude proportional to $U$. The reason why nothing is said about the band structure – which results from the periodic structure superimposed on the system – is the truncation scheme adopted in the expansion of the many-body Hamiltonian. In fact, the majority of studies consider a single-band description of such systems, in terms of a basis constructed with the use of site-localized states of the first band only. This is not the case in this thesis. Instead, we would like to understand what happens, for example, if we also allow for the atoms to occupy states of higher bands of the optical lattice. How would this affect the properties of the Mott-insulator to superfluid transition? And what happens if the atoms are restricted to occupy only these higher-bands?

These issues are already interesting as they involve generalization of the Bose-Hubbard Hamiltonian [7, 8, 9]; and even though they might seem, at a first glance, nothing more than mere academic problems, recent studies and experimental work [10, 11] warrant answering these and other questions related to many-body quantum phenomena in excited bands of optical lattices. It has been argued, for example, that under the presence of (strong) repulsive interactions, the atomic population can migrate from the ground to the excited bands [12], thereby affecting the properties of the ground-state expected for the system. The interaction-induced broadening of the onsite wave-functions was also observed experimentally via microwave spectroscopy [13]. Furthermore, through

the mapping of collapse-revival structures in the atomic density of non-equilibrium configurations, it was possible to verify signatures of higher bands physics [14, 15]. As a result following this initial motivation, a large body of experimental research is nowadays focusing directly on the physics of cold atoms in the first excited (the $p$) and higher bands.

The physics of bosons in the $p$ band is qualitatively different from the physics of the usual Bose-Hubbard model (Eq. (1.1)) where the atoms are restricted to the lowest (the $s$) band. The reason for this can be most easily understood from analyzing the square and cubic lattices. In these cases, due to the lattice symmetry, the $p$ band becomes doubly (square lattice) and triply (cubic lattice) degenerate [7, 16]. This degeneracy introduces the concept of *orbitals* that are associated to the site-localized states in the lattice, and that are characterized by a node in each of the spatial directions. These are called the *$p$ orbitals* and are usually described in terms of the lattice *Wannier functions*. The Wannier functions, in turn, are broader in the direction of the node, and since their shapes determine the ease of tunneling between sites, this directly influences the dynamical properties of the system. Now, because the tunneling properties of $p$-orbital bosons considerably differ from the tunneling properties of bosons in the $s$ band, various types of novel quantum phases [17, 18, 19, 20, 21] can appear. In fact, due to the anomalous dispersions, mean-field analysis of the system reveals that the condensed state of bosons in the $p$ band is characterized by macroscopic occupation of nonzero momentum states [22].

The manner in which $p$-orbital atoms interact also differs significantly from interactions in the $s$-band. Again, this is a consequence of the orbital degeneracy. For the case of bosons, for example, in addition to the density-density interactions (as described by Eq. (1.1)), the system also contains multi-species (different orbital states) density-density interactions and interactions that move the atoms between the different orbital states. This gives rise to novel phenomena which include the formation of structures in the order parameter of the condensed phase [7, 16, 19].

The purpose of this thesis is to provide an introduction to the physics of cold atoms in the first excited bands of optical lattices, the $p$ band, and to report a number of studies that we have performed on this subject in the past years. We focus on the case of separable lattices[1] and mainly in the two-dimensional case. We start by defining and characterizing the orbital states in Chapter 2, where we also discuss the construction of the many-body Hamiltonian. In Chapter 3, properties of $p$-orbital bosons in isotropic square and cubic lattices are considered from the viewpoint of mean-field analysis. We then investigate how inclusion of the harmonic trap affects the physics of the two dimensional case in Chapter 4. This chapter is based on the study of Paper I and presents details of calculations that were omitted in the original work.

Moving away from the mean-field territory, we present properties of the $p$-orbital bosons in the strongly correlated regime in Chapter 5. The system is discussed here in the context of *quantum simulators* [23, 24] for studying critical properties of spin models relevant for the study of quantum magnetism. This chapter is based in the study of Paper II and also includes more details than what is presented in the original work. It also contains additional discussions on extensions of this work that are still work

[1] See definition in Sec. 2.1

in progress. Nevertheless it displays a different aspect of the physics of multi-orbital Hubbard systems that hints at an interesting direction for future research. We reserve final remarks to the Conclusion section.

# 2. $p$-orbital bosons: nice to meet you!

*"To P or not to P? (bands!)"*
William Shakespeare[1]

In this chapter we characterize the system of $p$-orbital bosons. We start with a quick note in Sec. 2.1 on the energy and length scales adopted here to define dimensionless variables, and follow with discussions on the general properties of single particle physics in periodic potentials in Sec. 2.2. In Sec. 2.3.1 we define the orbital states and discuss their properties. The many-body Hamiltonian for $p$-orbital bosons is derived in Sec. 2.4 and in Sec. 2.4.1 we briefly discuss symmetry properties of the many-body Hamiltonian.

## 2.1. Disclaimer notice

All the problems discussed in this thesis are concerned with the physics of cold atoms in optical lattices. Optical lattices are spatially periodic potentials, created from the superposition of counter-propagating laser beams, that can be used to trap atoms via Stark effect [2, 6]. Unless stated otherwise, we assume here that the lattices are sinusoidal and separable[2], as e.g.

$$V_{latt}(x,y) = V_x \sin^2(k_x x) + V_y \sin^2(k_y y) \tag{2.1}$$

in 2D, where $V_\alpha$ is the amplitude of the laser light with wavelength $\lambda_\alpha$ in the direction $\alpha = \{x,y\}$ and $k_\alpha$ is the corresponding wave vector. In this context, any of the inverse wave vectors, $l_\alpha^{-1} = 2\pi/\lambda_\alpha$ provides a natural choice for parametrizing the length scale, and any of the recoil energies $E_r^\alpha = \hbar^2 k_\alpha/2m$ (for an atom of mass $m$), provides a natural choice for fixing the energy scale.

Here whenever we use the word 'dimensionless' referring to any position, this means that the positions are scaled in terms of one of the $l_\alpha$, and whenever we use it referring to any energy, it means that the energies are scaled in terms of one of the $E_r^\alpha$. The direction $\alpha$ will be explicitly determined.

[1] Adapted from the tragedy of *Hamlet*.
[2] More explicitly, by separable lattice we mean that the eigenvalue problem for the given lattice potential admits solutions that can be factorized in the different directions.

## 2.2. General properties of one particle subjected to periodic potentials

Two main properties characterize the problem of a quantum particle interacting with a periodic potential [25]: (a) that the energy spectrum displays structure of bands where regions with allowed energies are separated from each other, and (b) that the solutions of the eigenvalue equation are given by *Bloch functions*. This is formulated in one dimension[3] as

$$\hat{H}\Psi(x) = E\Psi(x), \quad \text{where} \quad \hat{H} = \frac{-\hbar^2}{2m}\frac{d^2}{dx^2} + V(x) \tag{2.2}$$

with $m$ the mass of the particle and $V(x) = V(x+d)$ the periodic potential with periodicity $d$. The expression for the Bloch functions can be obtained from the Bloch theorem [26] and follows as

$$\Psi_{\nu q}(x) = e^{iqx}u_{\nu q}(x), \tag{2.3}$$

where $u_{\nu q}$ is a periodic function satisfying $u_{\nu q}(x) = u_{\nu q}(x+d)$ and $q$ and $\nu$ are the good quantum numbers labeling, respectively, quasi-momentum and band index. The fact that we are using the band index $\nu$ implicitly assumes the reduced scheme, where quasi-momentum varies along the first Brillouin zone [26]. To each of the values of $\nu$ and $q$ there is an associated energy, and in general the relation between the free particle momentum $p$ of $E = \hbar^2p^2/2m$ and the quasi-momentum $q$ appears in the form of a complicated (transcendental) equation. The eigenstates of Eq. (2.2) correspond thus to plane waves delocalized in the lattice and that experience a modulation due to the lattice periodicity.

An alternative basis for describing particles subjected to periodic potentials is given by the so called *Wannier functions* [25]. They are constructed in terms of the Bloch functions according to the prescription

$$w_{\nu j}(x) = \sum_q e^{-iqR_j}\Psi_{\nu q}(x), \tag{2.4}$$

where $R_j$ labels the coordinates of the $j$'th site and we sum over the quasi-momenta in the first Brillouin zone. The Wannier basis differs from the Bloch basis in two main aspects: First, at each site each of the energy bands is endowed only one Wannier function. Second, this is a site localized basis labeled by the position in the lattice. The Wannier functions at different sites satisfy the following orthonormality condition

$$\int dx\, w_{\nu j}(x)w_{\nu' i}(x) = \delta_{\nu\nu'}\delta_{ij}. \tag{2.5}$$

Let us now briefly illustrate this discussion by starting with Fig. 2.1, where the band structure for a system with periodic potential given by $V(x) = V_0\sin^2(k_x x)$ is shown for different values of the lattice amplitude $V_0$, and as a function of the quasi-momentum $q$. The general picture following is that for increasing values of the lattice amplitude, $V_0$, the widths of the bands experience a narrowing at the same time that the energy gaps between the bands become larger.

[3] Extensions for 2D and 3D systems are straightforward. We use the 1D case here just for illustrative purposes.

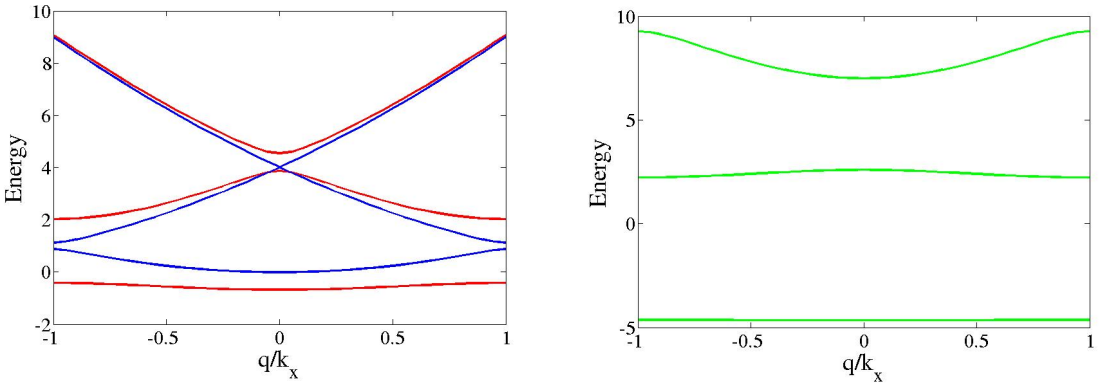


Figure 2.1.: Band structure of a system with $V_0 = 0.5E_r$ (blue), $V_0 = 5E_r$ (red) and $V_0 = 17E_r$ (green). As discussed in the text, the widths of the bands are larger for smaller values of the lattice amplitude. In addition, the energy gaps between the different bands increase for increasing values of $V_0$.

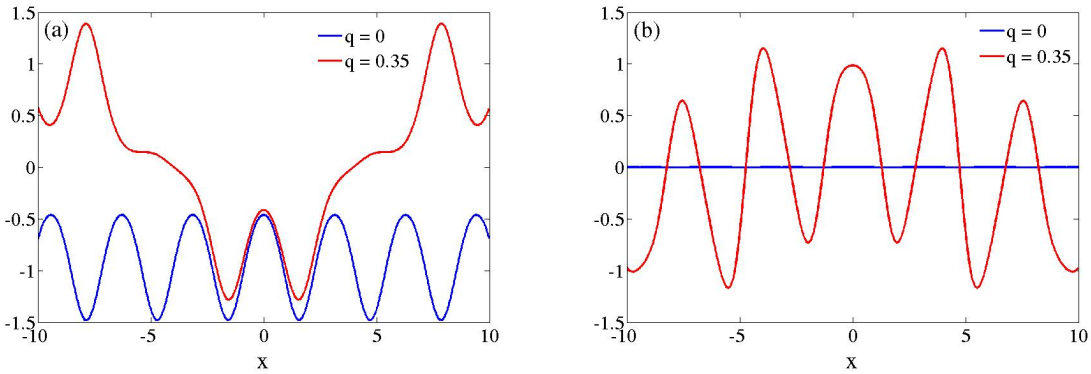


Figure 2.2.: Real part of the Bloch functions of the first (in (a)) and second (in (b)) bands for different values of quasi-momentum $q$ and for $V_0 = 5E_r$. Notice here that the Bloch function of the 2nd band is strictly imaginary if $q = 0$.

We continue by showing samples of the real and imaginary parts of the Bloch functions in Figs. 2.2 and 2.3, where we particularly raise attention to the delocalized character of the Bloch functions. This is clearly not the case for the Wannier functions, as illustrated in Fig. 2.4, which shows the Wannier functions of the first and second bands, and for different values of the lattice amplitude. In this picture, larger values of $V_0$ have corresponding Wannier functions that are more and more localized around the minimum of the potential well. For completeness, we show the probability density associated to each of these Wannier functions in Fig. 2.5 (a) and (b).

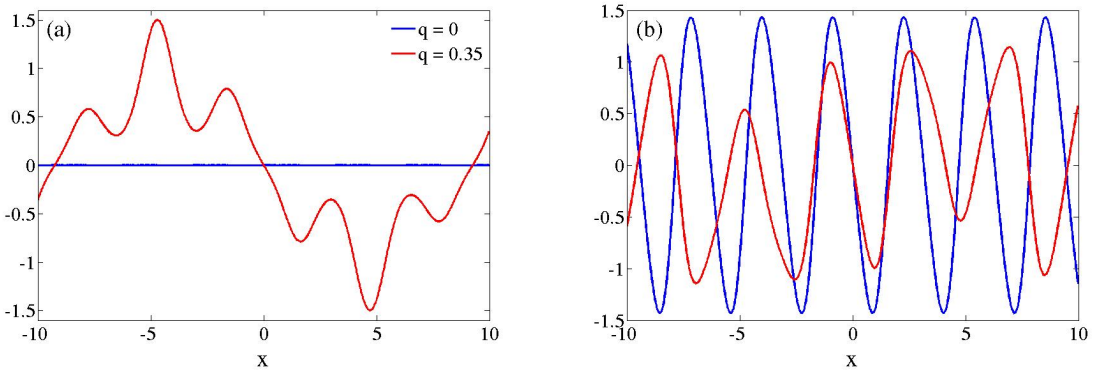


Figure 2.3.: Imaginary part of the Bloch functions of the first (in (a)) and second (in (b)) bands for different values of quasi-momentum $q$ and for $V_0 = 5E_r$. In contrast to the result of Fig. 2.2, here we notice that the 1st band Bloch function with $q = 0$ is strictly real. We point out that there is an arbitrary phase to be fixed in the definition of the Bloch functions. Once this phase is fixed, however, and say the Bloch function of the first band with $q = 0$ is purely real, then the Bloch function in the second band with $q = 0$ will be purely imaginary.

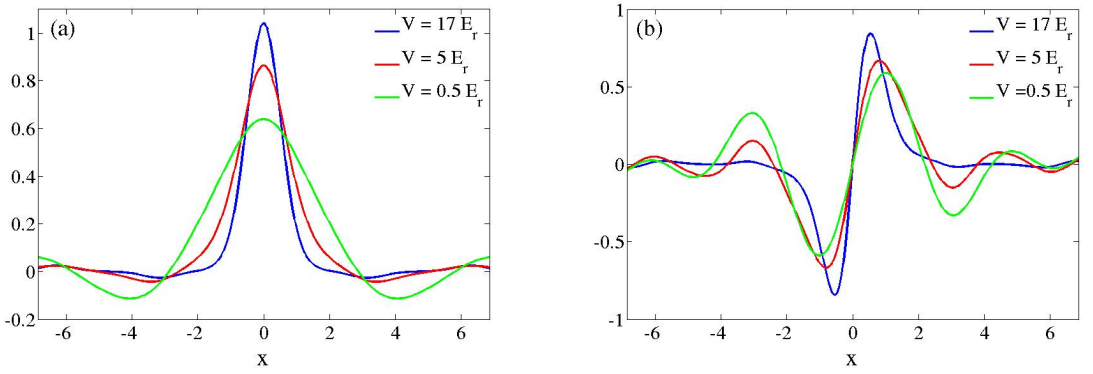


Figure 2.4.: Wannier functions of the first and second bands for systems with $V_0 = 0.5E_r$ (green), $V_0 = 5E_r$ (red) and $V_0 = 17E_r$ (blue).

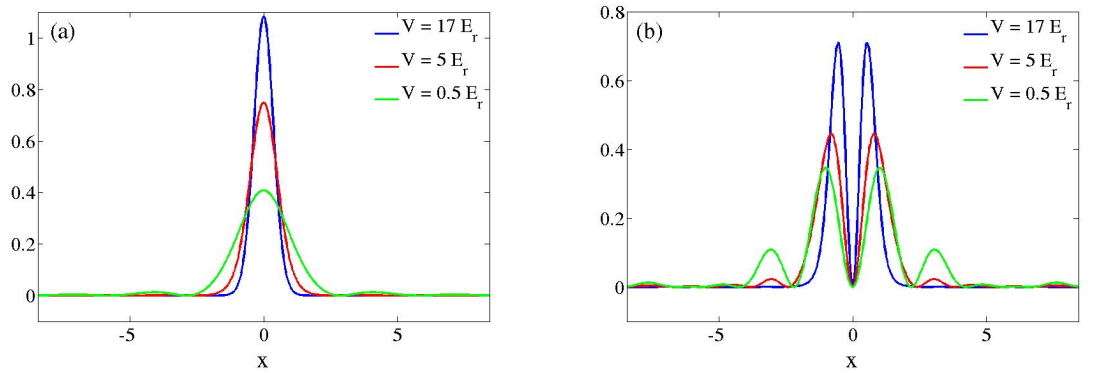


Figure 2.5.: Probability density of the first and second bands Wannier functions for systems with $V_0 = 0.5E_r$ (green), $V_0 = 5E_r$ (red) and $V_0 = 17E_r$ (blue).

## 2.3. What are the $p$-orbitals?

$p$-orbitals are the site-localized states of the first excited energy band, the $p$ band [7]. For isotropic square/cubic optical lattices in two or three dimensions, the first excited band is respectively two- and three-fold degenerate. This, in turn, renders a corresponding degeneracy for the site-localized states or $p$-orbitals. In particular, $p$ orbitals are anisotropic in magnitude and odd in parity [16], features of which are discussed in this section.

### 2.3.1. $p$-orbital bosons in the harmonic approximation

In order to get familiar with the physics in the $p$ band, we consider the system in the *harmonic approximation*, where analytical solutions are easily obtained and simple enough to expose properties of the physics in analytical terms. This consists in approximating each well of the sinusoidal potential with a harmonic potential, i.e., $V(x) = \sin^2(k_x x) \approx k_x^2 x^2$. Although the use of the harmonic approximation is limited [9, 27] and justified only in very particular cases[4], it is still a good starting point for building an intuitive picture about the objects used in the representation of the orbital states.

Let us then consider a two dimensional separable lattice with decoupled $x$- and $y$-directions, for which the expression of the lattice potential is given by $V(x,y) = V_x \sin^2(k_x x) + V_y \sin^2(k_y y)$, where $V_\alpha$ and $k_\alpha$, $\alpha = \{x, y\}$ correspond to the potential amplitude and wave number, respectively, in the direction $\alpha$. The Schrödinger equation for a particle under action of this potential assumes the form of the *Mathieu equation*:

$$\hat{H}\Psi = \left( -\frac{\hbar^2}{2m}\frac{d^2}{dx^2} + V_x \sin^2(k_x x) - \frac{\hbar^2}{2m}\frac{d^2}{dy^2} + V_y \sin^2(k_y y) \right) \Psi = E\Psi. \tag{2.6}$$

We now use dimensionless variables as $k_y y \to y'$ and $k_y x \to x'$ such that $k_y^{-1}$ sets the length scale at the lattice, and expand the potential around its minimum keeping only first order contributions, i.e.

$$\begin{aligned} \hat{H}\Psi &= \left( -\tfrac{\hbar^2 k_y^2}{2m}\tfrac{d^2}{dx'^2} + V_x \sin^2(\tfrac{k_x}{k_y}x') - \tfrac{\hbar^2 k_y}{2m}\tfrac{d^2}{dy'^2} + V_y \sin^2(y') \right) \Psi \\ \hat{H}\Psi &= \left( -\tfrac{\hbar^2 k_y^2}{2m}\tfrac{d^2}{dx'^2} + V_x \tfrac{k_x^2}{k_y^2}x'^2 - \tfrac{\hbar^2 k_y^2}{2m}\tfrac{d^2}{dy'^2} + V_y y'^2 \right) \Psi, \end{aligned} \tag{2.7}$$

which implies

$$\begin{aligned} \tfrac{\hat{H}}{E_r^y}\Psi &= \left( -\tfrac{d^2}{dx'^2} + (\tfrac{2m}{\hbar^2 k_y^2})V_x \tfrac{k_x^2}{k_y^2}x'^2 - \tfrac{d^2}{dy'^2} + (\tfrac{2m}{\hbar^2 k_y^2})V_y y'^2 \right) \Psi \\ \tfrac{\hat{H}}{E_r^y}\Psi &= \left( -\tfrac{d^2}{dx'^2} + \tilde{V}_x \tfrac{k_x^2}{k_y^2}x'^2 - \tfrac{d^2}{dy'^2} + \tilde{V}_y y'^2 \right) \Psi. \end{aligned} \tag{2.8}$$

In the last step we introduced $\tilde{V}_\alpha = V_\alpha / E_r^y$, where $E_r^y = \hbar^2 k_y^2 / 2m$ is the recoil energy in the $y$-direction. This step sets the energy scale.

[4] The limit of very deep potential wells is required.

When dealing with a separable lattice like in the example above, it is possible to find the solutions in the $x$- and $y$-directions by solving the corresponding equations independently. We solve first for $y'$ (dimensionless $y$-direction):

$$\left(-\frac{d^2}{dy'^2} + \tilde{V}_y y'^2\right)\Psi(y') = \epsilon_{y'}\Psi(y') \tag{2.9}$$

where $\epsilon_{y'}$ is the energy scaled in recoil energies of the lattice in the $y$-direction. We identify the characteristic length of the oscillator as $y_0^{-4} = \tilde{V}_y$ and therefore the ground and first excited states, with energies $\epsilon^0_{y'}$ and $\epsilon^1_{y'}$, are given by

$$\phi_0(y') = \frac{1}{\pi^{1/4}y_0^{1/2}}e^{-y'^2/2y_0^2} = \left(\frac{\tilde{V}_y^{1/8}}{\pi^{1/4}}\right)e^{-\sqrt{\tilde{V}_y}y'^2/2} \tag{2.10}$$

and

$$\phi_1(y') = \left(\frac{\sqrt{2}}{\pi^{1/4}y_0^{3/2}}\right)y'\ e^{-y'^2/2y_0^2} = \left(\frac{\sqrt{2}\tilde{V}_y^{3/8}}{\pi^{1/4}}\right)y'\ e^{-\sqrt{\tilde{V}_y}y'^2/2} \tag{2.11}$$

Equations for $x'$ (dimensionless $x$-direction) are solved in the same way

$$\left[-\frac{d^2}{dx'^2} + \tilde{V}_x\frac{k_x^2}{k_y^2}x'^2\right]\Psi(x') = \epsilon_{x'}\Psi(x') \tag{2.12}$$

and $\epsilon_{x'}$ is again the energy scaled in units of $E_r^y$. The characteristic length of the oscillator is identified here as $x_0^{-4} = \tilde{V}_x k_x^2/k_y^2$, and the ground and first excited states, with corresponding energies $\epsilon^0_{x'}$ and $\epsilon^1_{x'}$, are given by

$$\phi_0(x') = \frac{1}{\pi^{1/4}x_0^{1/2}}e^{-x'^2/2x_0^2} = \frac{1}{\pi^{1/4}}\left(\frac{\tilde{V}_x k_x^2}{k_y^2}\right)^{1/8}e^{-\frac{\sqrt{\tilde{V}_x}k_x}{k_y}x'^2/2} \tag{2.13}$$

and

$$\phi_1(x') = \left(\frac{\sqrt{2}}{\pi^{1/4}x_0^{3/2}}\right)x'\ e^{-x'^2/2x_0^2} = \frac{\sqrt{2}}{\pi^{1/4}}\left(\frac{\tilde{V}_x k_x^2}{k_y^2}\right)^{3/8}x'\ e^{-\frac{\sqrt{\tilde{V}_x}k_x}{k_y}x'^2/2} \tag{2.14}$$

With the expressions of the eigenfunctions in hand, we can now describe the energy levels and eigenstates of the 2 dimensional system in the harmonic approximation. For simplicity we consider here an isotropic lattice for which $\tilde{V}_x = \tilde{V}_y$ and $k_x = k_y$. The true ground state within this approximation has energy $E_0 = (\epsilon^0_{x'} + \epsilon^0_{y'})$ and its eigenfunction has a Gaussian profile in both $x$- and $y$-directions:

$$\Psi_0(x', y') = \frac{1}{\pi^{1/2}x_0^{1/2}y_0^{1/2}}e^{-x'^2/2x_0^2 - y'^2/2y_0^2}. \tag{2.15}$$

The first excited state is doubly degenerate. It has energy given by $E_1 = (\epsilon^1_{x'} + \epsilon^0_{y'}) = (\epsilon^0_{x'} + \epsilon^1_{y'})$ and the corresponding eigenfunctions are given, respectively, by

$$\Psi_x(x', y') = \left(\frac{\sqrt{2}}{\pi^{1/4}x_0^{3/2}}\right)x'\ e^{-x'^2/2x_0^2}\left(\frac{1}{\pi^{1/4}y_0^{1/2}}\right)e^{-y'^2/2y_0^2} \tag{2.16}$$

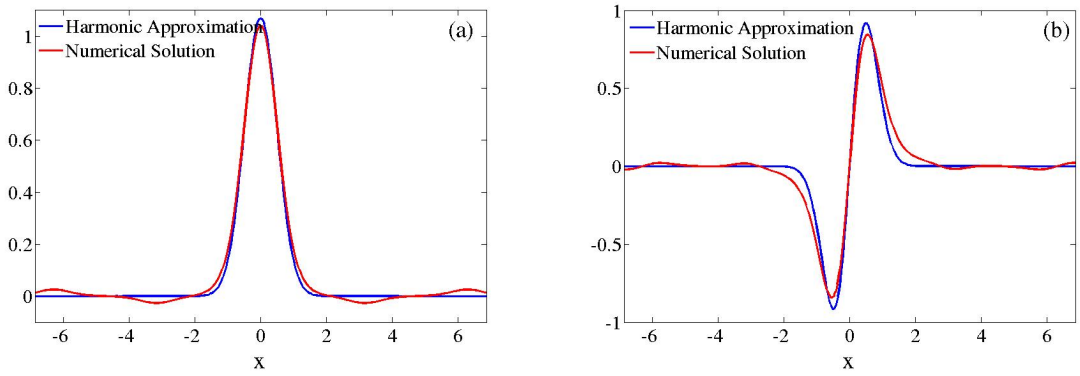


Figure 2.6.: Comparison between the numerically obtained Wannier functions and the Wannier functions in the harmonic approximation, Eqs. (2.10) and (2.11) for a $1D$ system with $V_0 = 17E_r$ (see discussion in the text).

and

$$\Psi_y(x', y') = \left(\frac{1}{\pi^{1/4}x_0^{1/2}}\right) e^{-x'^2/2x_0^2} \left(\frac{\sqrt{2}}{\pi^{1/4}y_0^{3/2}}\right) y' e^{-y'^2/2y_0^2}, \tag{2.17}$$

that are precisely the $p_x$- and $p_y$-orbital states in the harmonic approximation. As can be verified, the spatial profile of the two orbitals have different parities in the different directions, i.e., it is odd in the direction which introduces the node in the wave-function and even otherwise. In particular, the name of the orbital state is coined after the direction in which the wave-function is odd.

We compare in Fig. 2.6 the ground and first excited Wannier functions obtained from numerical diagonalization of the Mathieu equation with the ground and first excited states obtained in the harmonic approximation. It illustrates the situation where $V_0 = 17\,E_r$, of deep wells, where the harmonic approximation is expected to give a good qualitative picture of the system. While the harmonic oscillator ground-state eigenfunctions will never assume negative values, the negativity of the Wannier functions is an important property for the orthonormality condition (2.5). In addition, it is important to keep in mind that as opposed to the picture provided by the harmonic limit, the energy difference between different bands in the sinusoidal potential is not constant. In fact, due to the anharmonicity of the sinusoidal potential, the bands are usually not equally spaced in the optical lattices.

## 2.4. From the one-body to the many-body problem

The dynamics of a gas of $N$ atoms of mass $m$ under action of an external potential can be represented, in general terms, by a Hamiltonian of the type

$$H = \sum_{i=1}^{N} \left(\frac{p_i^2}{2m} + V_{ext}(\vec{r}_i)\right) + \sum_{i,j} V_{int}(\vec{r}_i, \vec{r}_j), \tag{2.18}$$

where the first two terms account for single-particle effects, while the last term describes interactions between the atoms, and therefore accounts for effects of collective nature.

In the ideal scenario $V_{int}$ should include all interactions in the system, i.e., the result of two-body collisions, three-body collisions and so on[5]. In real life, however, exact solutions for problems involving interacting many-body quantum particles are known only in very few or particular cases. The way out, of course, starts with the use of approximations that are capable of describing not all, but all the relevant interactions that warrant a good picture of the experimental reality.

We mentioned before that the interest here is in the physics of (many and also a few) interacting $p$-orbital bosons. We aim, therefore, at describing systems of very cold and dilute bosonic gases, where the atoms occupy the orbital states discussed in Sec. 2.2, of the $p$ band of an optical lattice. By 'very cold' we mean that the temperatures considered are close to the absolute zero[6]. In the same way, by 'very dilute' we mean that the distance between any two atoms fixed by $n = N/V$ - where $N$ is the total number of particles and $V$ the volume of the system - is very large. In the lab, for example, these systems are produced with densities of the order of $10^{-5}$ atoms per cm$^3$ ($\sim 10^{-27}$g/cm$^3$)[7], and under these circumstances, it is reasonable to truncate the interaction term in the two-body part [28, 29].

As a consequence from the characteristic low densities, the distances between the particles are always large enough to justify the use of the asymptotic expression of the wave function of the relative motion [28]. In addition, as a consequence from the low temperatures $T$, the relative momentum corresponding to kinetic energies $k_BT$, where $k_B$ is the Boltzmann constant, justifies that the collisions are effectively described by $s$-wave scattering processes, that are completely characterized by the corresponding phase shift [30]. At very low temperatures, however, the phase shift is not the best parameter for characterizing the cross section of the scattering processes.

> This can be illustrated[8], for example, by considering the cross section of two particles in a state with relative momentum $\vec{k}$ and energy $\hbar^2k^2/2\mu$, where $\mu$ is the reduced mass
>
> $$\frac{d\sigma}{d\Omega} = \frac{\sin^2(\delta_0(k))}{k^2} \xrightarrow{k\to 0} a^2 \tag{2.19}$$
>
> where $a$ has dimensions of length. At very low temperatures, i.e., in the $\lim k \to 0$, the presence of $k^2$ in the denominator of Eq. (2.19) would require that $\sin(\delta_0(k))$ vanishes linearly for any value of the cross section [30].

The trick here is to use instead the *scattering length* $a$ defined as

$$\lim_{k\to 0} \frac{k}{\sin(\delta_0(k))} \equiv -\frac{1}{a}, \tag{2.20}$$

that is, up to the choice of a sign, exactly the same length parameter of Eq. (2.19). Now this is a good quantity for parametrizing the low energy scattering cross section, for it can also be further interpreted as the first term of the expansion in powers of $k$ of the

[5] 'Ambition is the last refugee of failure.' - Oscar Wilde

[6] Or much less than the bandwidth. The temperature is typically of the order of $\sim 1\,n$K.

[7] For comparison, the density of the air at room temperature (notice however that the definition of room temperature might vary in countries like Sweden or Finland) is $\sim 1.25 \times 10^{-3}$g/cm$^3$, the density of the water is 1g/cm$^3$ and the density of a white dwarf can be estimated as $1.3 \times 10^6$g/cm$^3$.

[8] This discussion is based on the discussion presented in Ref. [30].

effective range expansion [30],

$$k\cot(\delta_0(k)) \equiv -\frac{1}{a} + \frac{r_0}{2}k^2 + ..., \tag{2.21}$$

where $r_0$ is the so called *effective range* of the potential. In these terms, low energy scattering processes can be characterized by only two parameters, $a$ and $r_0$, and regardless of their underlying forms or expressions, any two potentials that are characterized by the same $s$-wave scattering length $a$ and effective range $r_0$, will give rise to the same effective interaction [30].

The values of $a$ are determined with the use of the standard scattering theory. Now assuming that $a$ is a known quantity, our goal is to implement in the Hamiltonian (2.18) an effective interaction that captures the physics seen in the lab. The usual process consists in considering the real interaction potential $V_{int}(\vec{r}_i, \vec{r}_j)$ as a contact interaction $V_{int} = \lambda\delta(\vec{r}_i - \vec{r}_j)$ with coupling constant given by $\lambda = 2\pi\hbar^2 a/\mu$, where $\mu$ is the reduced mass of the two particles [31]. Accordingly, the effective potential for two identical particles of mass $m$ follows as

$$V_{int}(\vec{r}_i, \vec{r}_j) = \frac{4\pi\hbar^2 a}{m}\delta(\vec{r}_i - \vec{r}_j). \tag{2.22}$$

In the language of second quantization, this can be further re-written with the use of the bosonic field operators $\Psi(\vec{r}')$ and $\Psi^\dagger(\vec{r}')$, that annihilate and create a bosonic particle of mass $m$ at position $\vec{r}'$ as

$$\hat{V}_{int} = \frac{4\pi\hbar^2 a}{m}\int d\vec{r}' d\vec{r}\hat{\Psi}^\dagger(\vec{r})\hat{\Psi}^\dagger(\vec{r})\delta(\vec{r} - \vec{r}')\hat{\Psi}(\vec{r})\hat{\Psi}(\vec{r}') = \frac{4\pi\hbar^2 a}{m}\int d\vec{r}'\hat{\Psi}^\dagger(\vec{r}')\hat{\Psi}^\dagger(\vec{r}')\hat{\Psi}(\vec{r}')\hat{\Psi}(\vec{r}'). \tag{2.23}$$

These operators satisfy the bosonic commutation relations $[\Psi(\vec{r}''), \Psi(\vec{r}')] = \delta(\vec{r}'' - \vec{r}')$. The full expression of the Hamiltonian describing a weakly interacting Bose gas is given, therefore, by

$$\hat{H} = \int d\vec{r}'\left\{\hat{\Psi}^\dagger(\vec{r}')\left[-\frac{\hbar^2\nabla^2}{2m} + V(\vec{r}')\right]\hat{\Psi}(\vec{r}') + \frac{\tilde{U}_0}{2}\hat{\Psi}^\dagger(\vec{r}')\hat{\Psi}^\dagger(\vec{r}')\hat{\Psi}(\vec{r}')\hat{\Psi}(\vec{r}')\right\}, \tag{2.24}$$

where $V(\vec{r}')$ accounts for effects of external potentials superimposed to the system and $\tilde{U}_0 = 4\pi\hbar^2 a/m$ is the coupling constant in units of the recoil energies, as defined in Sec. 2.1.

In the usual procedure the field operators are then expanded with the use of a convenient basis, which in our case will be constructed in terms of the orbital states of the $p$ band of the optical lattice[9]. But before proceeding with the expansion, let us restrict the external potentials acting in this system $V(\vec{r})$ (in Eq. (2.18)) to account only for the optical potential. In the isotropic cubic lattice this follows as

$$V(\vec{r}) = V_{latt}(\vec{r}') = \tilde{V}_x\sin^2(kx') + \tilde{V}_y\sin^2(ky') + V_z\sin^2(kz'), \tag{2.25}$$

where again the lattice amplitudes and wave vectors are given, respectively by $\tilde{V}_\alpha$, $\alpha = \{x, y, z\}$ and $k = 2\pi/\lambda$, with $\lambda$ being the wavelength of the applied lasers. As before

[9] Since in this step we restrict the atoms to live in the $p$ band of the optical lattice, this also means that we are considering what is called the *single band approximation*.

we define dimensionless parameters by taking the recoil energy $E_r = \hbar^2 k^2/2m$ as the energy scale and the inverse wave vector as the typical length scale $l = \lambda/2\pi$[10]. In these terms, the expression for the field operators then follows as

$$\begin{aligned} \Psi^\dagger(\vec{r}) &= \sum_{\alpha\mathbf{j}} w^*_{\alpha\mathbf{j}}(\vec{r})\hat{a}^\dagger_{\alpha\mathbf{j}}(\vec{r}) \\ \Psi(\vec{r}) &= \sum_{\alpha\mathbf{j}} w_{\alpha\mathbf{j}}(\vec{r})\hat{a}_{\alpha\mathbf{j}}(\vec{r}) \end{aligned} \tag{2.26}$$

where $\hat{a}^\dagger_{\alpha\mathbf{j}}$ and $\hat{a}_{\alpha\mathbf{j}}$ create and annihilate an atom in the $\alpha = \{x, y, z\}$ orbital state and in the $j$-th site of the lattice ($\mathbf{j} = (j_x, j_y, j_z)$, $j_x, j_y, j_z \in \mathcal{N}$).

> Notice here that the orbital states in the $p$ band are not eigenstates of the single-particle Hamiltonian. They are constructed in terms of the site-localized Wannier functions[11] $w_{\nu\mathbf{j}}(\vec{r})$, $\nu = 1, 2$[12] with the prescription[13]
>
> $$\begin{aligned} w_{x\mathbf{j}}(\vec{r}) &= w_{2j_x}(x)w_{1j_y}(y)w_{1j_z}(z) \\ w_{y\mathbf{j}}(\vec{r}) &= w_{1j_x}(x)w_{2j_y}(y)w_{1j_z}(z) \\ w_{z\mathbf{j}}(\vec{r}) &= w_{1j_x}(x)w_{1j_y}(y)w_{2j_z}(z), \end{aligned} \tag{2.27}$$
>
> which according to Eq. (2.4), relate with the Bloch functions (the eigenstates of the single-particle Hamiltonian) as
>
> $$w_{\nu\mathbf{R_j}(\vec{r})} = \sum_{\mathbf{q}} e^{-i\mathbf{q}\cdot\mathbf{R_j}}\phi_{\nu\mathbf{q}}(\vec{r}),$$
>
> where we use $\mathbf{R_j} = (x_\mathbf{j}, y_\mathbf{j}, z_\mathbf{j}) = (\pi j_x, \pi j_y, \pi j_z)$ and $\mathbf{q} = (q_x, q_y, q_z)$ is the index which labels the quasi-momentum.

Now before arriving to the final expression of the second quantized version of the Hamiltonian describing bosonic atoms in the $p$ band, we assume, in addition, the *tight-binding* regime. In this approximation, the range of the tunneling is restricted to the first nearest neighbors, and the interactions to happen only onsite. The final result then follows as

$$\hat{H} = \hat{H}_0 + \hat{H}_{nn} + \hat{H}_{FD}. \tag{2.28}$$

The first term here corresponds to the kinetic part of the Hamiltonian and is given by

$$\hat{H}_0 = -\sum_{\alpha,\beta}\sum_{\langle\mathbf{ij}\rangle_\beta} t_{\alpha\beta}\hat{a}^\dagger_{\alpha\mathbf{i}}\hat{a}_{\alpha\mathbf{j}} \tag{2.29}$$

with $\sum_{\langle\mathbf{ij}\rangle_\beta}$ the nearest neighbor sum in the direction $\beta$. The second and third terms account for different types of interactions:

$$\hat{H}_{nn} = \sum_{\alpha}\sum_{\mathbf{j}} \hat{n}_{\alpha\mathbf{j}}(\hat{n}_{\alpha\mathbf{j}} - 1) + \sum_{\alpha\beta,\alpha\neq\beta}\sum_{\mathbf{j}} U_{\alpha\beta}\hat{n}_{\alpha\mathbf{j}}\hat{n}_{\beta\mathbf{j}}, \tag{2.30}$$

[10] These units are used in all derivations from here on, which also makes the resulting equations dimensionless.

[11] Which themselves are also not eigenstates of the single particle-Hamiltonian.

[12] Remember here that $\nu$ is the index which labels the energy band of the corresponding Wannier function.

[13] Remember that we are considering the case where the equations describing the lattice are separable in the different directions.

describes various types of density-density interactions, where $\hat{n}_{\alpha\mathbf{j}}$ is the atom number operator for particles in the $p_\alpha$-orbital, and

$$\hat{H}_{FD} = \sum_{\alpha\beta,\alpha\neq\beta} \sum_{\mathbf{j}} \frac{U_{\alpha\beta}}{4} \left( \hat{a}^\dagger_{\alpha\mathbf{j}} \hat{a}^\dagger_{\alpha\mathbf{j}} \hat{a}_{\beta\mathbf{j}} \hat{a}_{\beta\mathbf{j}} + \hat{a}^\dagger_{\beta\mathbf{j}} \hat{a}^\dagger_{\beta\mathbf{j}} \hat{a}_{\alpha\mathbf{j}} \hat{a}_{\alpha\mathbf{j}} \right), \tag{2.31}$$

describes interactions which move atomic population between the different orbital states.

To complement we write the expressions for the various coupling parameters. They are given in terms of the orbital states as

$$U_{\alpha\beta} = U_0 \int d\vec{r} |w_{\alpha\mathbf{j}}(\vec{r})|^2 |w_{\beta\mathbf{j}}(\vec{r})|^2, \tag{2.32}$$

where $U_0 = \tilde{U}_0 l^3/E_r$ is the dimensionless interparticle strength, and

$$t_{\alpha\beta} = -\int d\vec{r} w^*_{\alpha\mathbf{j}}(\vec{r}) [-\nabla^2 + V(\vec{r})] w_{\alpha\mathbf{j}+\mathbf{1}_\beta(\vec{r})}, \tag{2.33}$$

with $V(\vec{r})$ is the external potential of Eq. (2.25).

Substitution of Eq. (2.27) in the above Eq. (2.33) shows that the tunneling coefficients in the directions perpendicular to the node depend uniquely on the properties of the Wannier functions in the ground band (i.e., $\nu = 1$), while in the direction parallel to the node, it depends solely on the Wannier functions of the second band of the lattice ($\nu = 2$)[14]. This is the basis of the tunneling anisotropy in the $p$ band, and explicitly shows why an atom in the the $p_\alpha$-orbital state has larger probability of tunneling in the $\alpha$ direction than in the transverse ones[15].

### 2.4.1. Brief discussion on the symmetries of the model

Because each term in Eq. (2.28) has the same number of operators and Hermitian conjugates, the Hamiltonian describing bosonic particles in the $p$ band is clearly invariant under global $U(1)$ transformations. This reflects the overall conservation of particle number in the system, and therefore

$$[\hat{H}, \sum_{\mathbf{j}} (\hat{n}^x_{\mathbf{j}} + \hat{n}^y_{\mathbf{j}} + \hat{n}^z_{\mathbf{j}})] = 0. \tag{2.34}$$

In addition to the overall number conservation, the number of particles modulo 2 in each of the orbital states is also conserved. This follows from the properties of the terms describing transfer of population between the different orbitals, Eq. (2.31), which introduce a set of $Z_2$ symmetries under which the full Hamiltonian is invariant. In fact, in isotropic lattices[16], any permutations of the type

$$\hat{a}_{x\mathbf{j}} \to \pm\hat{a}_{y\mathbf{j}}, \quad \hat{a}_{y\mathbf{j}} \to \pm\hat{a}_{z\mathbf{j}}, \quad \hat{a}_{z\mathbf{j}} \to \pm\hat{a}_{x\mathbf{j}} \tag{2.35}$$

[14] Notice here that these bands refer to the band in the $1D$ lattice from where one considers the quasi-momentum of the Bloch functions used in the construction of the localized states.

[15] Remember that the $p_\alpha$ orbital state has a broader spatial profile in the $\alpha$ direction.

[16] Where all the $t_{\alpha\alpha}$ for different orbitals are equal, as well as all the $t_{\alpha\beta}$, and $U_{xx} = U_{yy} = U_{zz}$ with again all the $U_{\alpha\beta}$ equal for different $\alpha$ and $\beta$.

leave the Hamiltonian invariant.

Let us take a closer look on the symmetries of the two-dimensional case. We start with the isotropic square lattice, where $U_{xx} = U_{yy}$, $U_{xy} = U_{yx}$, $t_{xx} = t_{yy}$ and $t_{xy} = t_{yx}$. In this case, transformations of the type

$$\begin{pmatrix} \hat{a}'_{x\mathbf{j}} \\ \\ \hat{a}'_{y\mathbf{j}} \end{pmatrix} \rightarrow \begin{pmatrix} \cos\theta & -\sin\theta \\ \\ \sin\theta & \cos\theta \end{pmatrix} \begin{pmatrix} \hat{a}_{x\mathbf{j}} \\ \\ \hat{a}_{y\mathbf{j}} \end{pmatrix} \tag{2.36}$$

leave the Hamiltonian invariant for different values of $\theta = (0, \pi/2, \pi) \pm k\pi$, where $k \in Z$. This is not the case for an asymmetric lattice. Here, even though the lattice can be tuned in such a way to preserve the degeneracy between the orbitals, the coupling constants $U_{xx} \neq U_{yy}$ and $t_{\alpha\alpha} \neq t_{\beta\beta}$, $t_{\alpha\beta} \neq t_{\beta\alpha}$, which means that transformations of the type $\hat{a}_{x\mathbf{j}} \rightarrow \hat{a}_{y\mathbf{j}}, \hat{a}_{y\mathbf{j}} \rightarrow \hat{a}_{x\mathbf{j}}$ will not leave the Hamiltonian invariant. There is a particular case, however, for which even in asymmetric lattices the system is characterized by an additional $SO(2)$ symmetry [32]. This corresponds to the harmonic approximation in the limit of vanishing tunneling[17], where $U_{\alpha\alpha} = 3U_{\alpha\beta} = U$. As pointed out in Ref. [32], this special case is better studied with the use of the angular-momentum like annihilation operators $\hat{a}_{\pm\mathbf{j}} = (\hat{a}_{x\mathbf{j}} \pm i\hat{a}_{y\mathbf{j}})/\sqrt{2}$, in terms of which the local part of the Hamiltonian can be written as [32]

$$\begin{aligned} \hat{H} &= \tfrac{U}{2}\left[\hat{n}_{\mathbf{j}}\left(\hat{n}_{\mathbf{j}} - \tfrac{2}{3}\right) - \tfrac{1}{3}\right] + \delta\left[(\hat{n}_{\mathbf{j}} - 1)(\hat{L}_{+\mathbf{j}} + \hat{L}_{-\mathbf{j}})\right] \\ &\quad + \lambda\left[\tfrac{1}{4}\hat{L}^2_{z\mathbf{j}} - 3(\hat{L}_{+\mathbf{j}} - \hat{L}^2_{-\mathbf{j}})^2 - \hat{n}_{\mathbf{j}}\right] \end{aligned} \tag{2.37}$$

where $U = (U_{xx} + U_{yy})/2$, $\delta = (U_{xx} - U_{yy})/2$ and $\lambda = U_{xy} - U/3$. The density operator can be expressed as $\hat{n}_{\mathbf{j}} = \hat{a}^\dagger_{+\mathbf{j}}\hat{a}_{+\mathbf{j}} + \hat{a}^\dagger_{-\mathbf{j}}\hat{a}_{-\mathbf{j}}$, and the angular momentum operators are $\hat{L}_{z\mathbf{j}} = \hat{a}^\dagger_{+\mathbf{j}}\hat{a}_{+\mathbf{j}} - \hat{a}^\dagger_{-\mathbf{j}}\hat{a}_{-\mathbf{j}}$ and $\hat{L}_{\pm\mathbf{j}} = \hat{a}^\dagger_{\pm\mathbf{j}}\hat{a}_{\mp\mathbf{j}}/2$. Now it follows from the properties of the harmonic oscillator eigenstates that in the harmonic approximation $\lambda = \delta = 0$ for any lattice configuration, and therefore $[\hat{H}_{\mathbf{j}}, \hat{L}_{z\mathbf{j}}] = 0$ [32]. This is not the case for real optical lattices, for there $\lambda,\ \delta \neq 0$, which destroys the axial symmetry, and consequently $[\hat{H}_{\mathbf{j}}, \hat{L}_{z\mathbf{j}}] \neq 0$ [32]. It is important to point out here that this additional $SO(2)$ symmetry is not of geometric character. Instead, this is a dynamical symmetry [33], which appears as a consequence of the specific form that the eigenvalue problem assumes when the harmonic approximation is used.

[17] This is only valid in the case of separable lattices.

# A. Hamiltonian parameters in the harmonic approximation

We briefly compute here the various coupling constants in the harmonic approximation. As discussed before, under this assumption the Wannier functions are approximated by harmonic oscillator eigenfunctions, and therefore (2.32) and (2.33) can be obtained from computation of simple Gaussian integrals. Here

$$\begin{aligned} U_{xx} &= U_0 \int dx \left(\frac{\sqrt{2}}{\pi^{1/4}x_0^{3/2}}\right)^4 x^4\, e^{-2x^2/x_0^2} \int dy \left(\frac{1}{\pi^{1/4}y_0^{1/2}}\right)^4 e^{-2y^2/y_0^2} \\ &= U_0 \left(\frac{\sqrt{2}}{\pi^{1/4}x_0^{3/2}}\right)^4 \frac{3}{4}\frac{\sqrt{\pi}}{2^{5/2}} x_0^5 \left(\frac{1}{\pi^{1/4}y_0^{1/2}}\right)^4 \sqrt{\frac{\pi}{2}} y_0 = U_0 \left(\frac{3}{8\pi}\frac{1}{x_0 y_0}\right) \end{aligned} \tag{A.1}$$

Analogous calculation yields $U_{yy} = U_0 \left(\frac{3}{8\pi}\frac{1}{x_0 y_0}\right)$.

We now compute $U_{xy}$:

$$\begin{aligned} U_{xy} &= U_0 \int dx \left(\frac{\sqrt{2}}{\pi^{1/4}x_0^{3/2}}\right)^2 x^2\, e^{-x^2/x_0^2} \left(\frac{1}{\pi^{1/4}x_0^{1/2}}\right)^2 e^{-x^2/x_0^2} \times \\ &\qquad \int dy \left(\frac{\sqrt{2}}{\pi^{1/4}y_0^{3/2}}\right)^2 y^2\, e^{-y^2/y_0^2} \left(\frac{1}{\pi^{1/4}y_0^{1/2}}\right)^2 e^{-y^2/y_0^2} \\ &= U_0 \int dx \left(\frac{\sqrt{2}}{\pi^{1/2}x_0^2}\right)^2 x^2 e^{-2x^2/x_0^2} \int dy \left(\frac{\sqrt{2}}{\pi^{1/2}y_0^2}\right)^2 y^2 e^{-2y^2/y_0^2} \\ &= U_0 \left(\frac{1}{8\pi}\frac{1}{x_0 y_0}\right), \end{aligned} \tag{A.2}$$

and thus we verify that in the harmonic approximation $U_{xx} = U_{yy} = 3U_{xy}$. In particular, notice that $U_{\alpha\alpha}/U_{\alpha\beta} = 3$ is always valid in the harmonic approximation regardless of the wave vectors of the lattice, $k_x$ and $k_y$. In addition, it is very surprising that in this limit the coupling constants don't even depend on the values of the lattice vector, but only on the lattice amplitudes $V_x$ and $V_y$[1] [32]. This is again another feature of the harmonic approximation, which in general is not valid when the lattice Wannier functions are used for computation of the Hamiltonian parameters.

Now according to Eq. (2.33), the tunneling coefficients are computed in the harmonic approximation (see Eqs. (2.16) and (2.17)) as

$$\begin{aligned} -t_{xx} &= \left(\frac{\sqrt{2}}{\pi^{1/4}x_0^{3/2}}\right)^2 V_x \int dx\, x(x+d) \sin^2 x\, e^{-x^2/2x_0^2} e^{-(x+d)^2/2x_0^2} \\ &\quad + \left(\frac{\sqrt{2}}{\pi^{1/4}x_0^{3/2}}\right)^2 \int dx \frac{d}{dx}(x e^{-x^2/2x_0^2}) \frac{d}{dx}\left((x+d)e^{(x+d)^2/2x_0^2}\right) \end{aligned} \tag{A.3}$$

[1] In the harmonic approximation this happens because the use of the degeneracy condition fixes the ratio $k_x/k_y$.

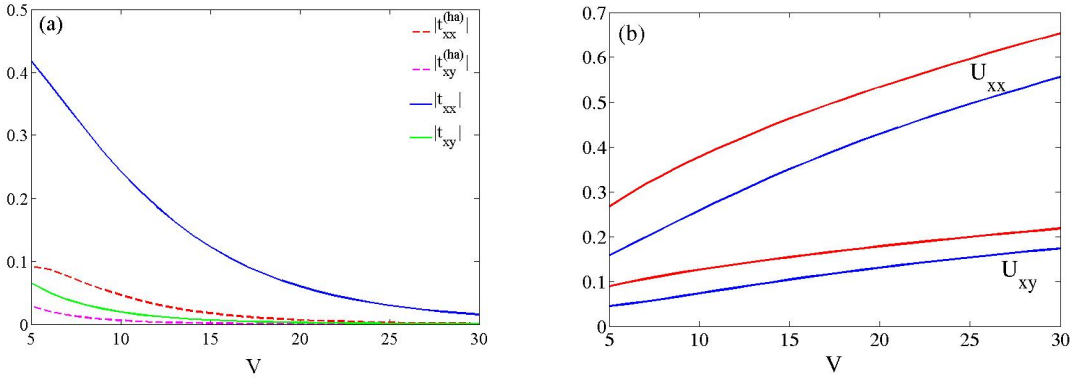


Figure A.1.: Comparison between the values of the couplings obtained from analytical and numerical computations as a function of $V$. It is shown in (a) that the harmonic approximation fails to reproduce the results obtained numerically for the tunneling coefficients when tunneling occurs in the direction of the node. In (b) we show the results for the interaction coefficients. In particular the estimates obtained from the harmonic approximation are always larger than the values of the couplings computed numerically.

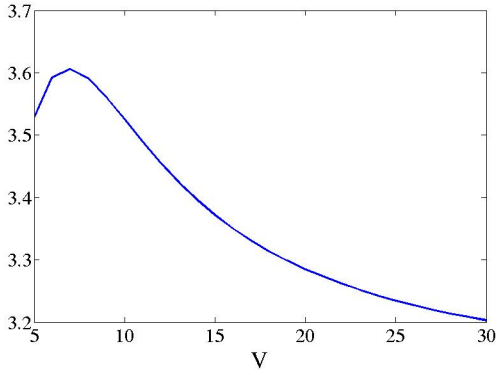


Figure A.2.: Ratio $U_{xx}/U_{xy}$ for different values of the amplitude of the optical potential. Notice here that $U_{xx}/U_{xy}$ is always larger than 3 for numerical computations with the lattice Wannier functions.

where $d$ is used here as the lattice constant and where we already used that the integral in the $y$-direction yields 1. In the same way,

$$\begin{aligned} -t_{xy} &= \left(\frac{1}{\pi^{1/4}y_0^{1/2}}\right)^2 V_y \int dy\, \sin^2 y\, e^{-y^2/2x_0^2} e^{-(y+d)^2/2y_0^2} \\ &+ \left(\frac{1}{\pi^{1/4}y_0^{1/2}}\right)^2 \int dy \frac{d}{dy} e^{-y^2/2y_0^2} \frac{d}{dy} e^{-(y+d)^2/2y_0^2}, \end{aligned} \tag{A.4}$$

but now it is the integral in the $x$-direction that yields 1, and therefore we only write the part that contributes to the tunneling coefficient. The expressions for $t_{yx}$ and $t_{yy}$ are obtained by making $x \to y$ and $y \to x$ with $x_0 \to y_0$ and $y_0 \to x_0$.

# 3. $p$-orbital bosons in the mean-field approximation

In this chapter[1] we focus on the mean-field description of $p$-orbital bosons in isotropic square and cubic lattices. After presenting details of the formalism in Sec. 3.1, we characterize general properties of the order parameters of the two and three dimensional cases in Secs. 3.1.1 and 3.1.2.

## 3.1. The mean-field Hamiltonian

At the mean-field level, the system is characterized in terms of order parameters which acquire a finite value in the phases with broken symmetry [34]. This is usually related to the appearance of a long-wavelength collective mode, and description in such terms neglects details of microscopic nature of the corresponding model [35]. This is therefore not a good approach for studying properties of more correlated regimes. For cold atoms in optical lattices, for example, mean field analysis is not suitable for describing properties of the Mott phase. On the other hand, if the system is deep in the superfluid phase, a mean-field treatment is still capable of revealing qualitative aspects of the underlying physics [29].

In order to give a mean-field description and to study the superfluid phase[2] of the system described by Eq. (2.28) we start by replacing the operators $\hat{a}_{\alpha,\mathbf{j}}$ with the complex numbers $\psi_{\alpha\mathbf{j}}$. If the Hamiltonian is normally ordered[3], then this corresponds to attributing a coherent state at each site, $|\Psi\rangle = \otimes_{\mathbf{j}}|\psi\rangle_{\mathbf{j}} = \otimes_{\mathbf{j}}|\psi_{x\mathbf{j}}, \psi_{y\mathbf{j}}, \psi_{z\mathbf{j}}\rangle_{\mathbf{j}}$ such that $\hat{a}_{\alpha\mathbf{j}}|\Psi\rangle = \psi_{\alpha\mathbf{j}}|\Psi\rangle_{\mathbf{j}}$. Now since this has the form of a product state, it does not contain information about quantum correlations between sites. Nevertheless, as we anticipate here, this ansatz is used with self-consistent equations and therefore provides a self-consistent solution for our problem.

In terms of the Fock basis, the single site many-body wave function is given thus by

$$|\Psi\rangle_{\mathbf{j}} = \exp\left(-\frac{|\psi_{x\mathbf{j}}|^2 + |\psi_{y\mathbf{j}}|^2 + |\psi_{z\mathbf{j}}|^2}{2}\right) \sum_{n_x,n_y} \frac{\psi_{x\mathbf{j}}^{n_x}\psi_{y\mathbf{j}}^{n_y}\psi_{z\mathbf{j}}^{n_z}}{\sqrt{n_x!n_y!n_z!}}|\mathbf{n}\rangle_{\mathbf{j}}, \tag{3.1}$$

from where $|\mathbf{n}\rangle_{\mathbf{j}} = |n_x, n_y, n_z\rangle_{\mathbf{j}}$ represents the state with $n_x$ $p_x$-orbital atoms, $n_y$ $p_y$-orbital atoms, and $n_z$ $p_z$-orbital atoms at the site $\mathbf{j}$. In this language the order parameter

[1] This chapter describes part of the study developed in Paper I.

[2] This is a phase where the $U(1)$ symmetry related to conservation of particle number is broken.

[3] Notice here that since the Hamiltonian in Eq. (2.28) is not in the normal form, it is necessary to normally order it before taking the expectation values for proceeding with the mean-field analysis.

of site $\mathbf{j}$ and orbital $\alpha$ is given by $\psi_{\alpha\mathbf{j}} = \langle\Psi|\hat{a}_{\alpha\mathbf{j}}|\Psi\rangle$, and for being a coherent state it has number fluctuations which obey Poissonian statistics [36]. In addition, this is also part of what we call the *full onsite order parameter*, defined as the expectation value of the annihilation operator in Eq. (2.26)

$$\psi_{\mathbf{j}}(\vec{r}) \equiv \langle\hat{\Psi}_{\mathbf{j}}(\vec{r})\rangle = \sum_{\alpha} w_{\alpha\mathbf{j}}(\vec{r})\langle\hat{a}_{\alpha\mathbf{j}}\rangle. \tag{3.2}$$

We can now derive the equations of motion for the order parameter $\psi_\alpha$ from the Euler-Lagrange equations:

$$\frac{\partial L}{\partial\psi^*_{\alpha\mathbf{j}}} - \frac{d}{dt}\left(\frac{\partial L}{\partial\dot{\psi}^*_{\alpha\mathbf{j}}}\right) = 0, \tag{3.3}$$

where the Lagrangian is given by

$$L = \sum_{\alpha}\sum_{\mathbf{j}}\frac{i}{2}\left[\psi^*_{\alpha\mathbf{j}}\frac{d}{dt}\psi_{\alpha\mathbf{j}} - \psi_{\alpha\mathbf{j}}\frac{d}{dt}\psi^*_{\alpha\mathbf{j}}\right] - H_{MF}, \tag{3.4}$$

with the mean-field Hamiltonian

$$\begin{aligned} H_{MF} \;=\; & -\textstyle\sum_{\alpha\beta}\sum_{\langle\mathbf{i},\mathbf{j}\rangle_\beta} t_{\alpha\beta}\psi^*_{\alpha\mathbf{i}}\psi_{\alpha\mathbf{j}} + \sum_\alpha\sum_{\mathbf{j}}\tfrac{U_{\alpha\alpha}}{2}n_{\alpha\mathbf{j}}n_{\alpha\mathbf{j}} + \sum_{\alpha\beta,\alpha\neq\beta}\sum_{\mathbf{j}}U_{\alpha\beta}n_{\alpha\mathbf{j}}n_{\beta\mathbf{j}} \\ & + \textstyle\sum_{\alpha\beta,\alpha\neq\beta}\sum_{\mathbf{j}}\frac{U_{\alpha\beta}}{4}\left(\psi^*_{\alpha\mathbf{j}}\psi^*_{\alpha\mathbf{j}}\psi_{\beta\mathbf{j}}\psi_{\beta\mathbf{j}} + \psi^*_{\beta\mathbf{j}}\psi^*_{\beta\mathbf{j}}\psi_{\alpha\mathbf{j}}\psi_{\alpha\mathbf{j}}\right), \end{aligned} \tag{3.5}$$

and where computation of the coherent-state expectation value is carried out with the normally order version of the Hamiltonian (2.28). The density of the $p_\alpha$-orbital state is given by $n_{\alpha\mathbf{j}} = |\psi_{\alpha\mathbf{j}}|^2$ and normalization was imposed in the whole lattice as

$$N = N_x + N_y + N_z = \sum_{\mathbf{j}}|\psi_{x\mathbf{j}}|^2 + \sum_{\mathbf{j}}|\psi_{y\mathbf{j}}|^2 + \sum_{\mathbf{j}}|\psi_{z\mathbf{j}}|^2, \tag{3.6}$$

with $N$ the total number of atoms.

The Euler-Lagrange equations lead to a set of coupled (discrete) Gross-Pitaevskii equations, one for each of the orbital states at each site $\mathbf{j}$:

$$\begin{aligned} -i\tfrac{\partial\psi_{x\mathbf{j}}}{\partial t} \;=\; & -\textstyle\sum_{\beta\in\{x,y,z\}} t_{x\beta}(\psi_{x\mathbf{j}+\mathbf{i}_\beta} - 2\psi_{x\mathbf{j}} + \psi_{x\mathbf{j}-\mathbf{1}_\beta}) \\ & +(U_{xx}|\psi_{x\mathbf{j}}|^2 + (U_{xy}+U_{yx})|\psi_{y\mathbf{j}}|^2 + (U_{xz}+U_{zx})|\psi_{z\mathbf{j}}|^2)\psi_{x\mathbf{j}} \\ & + \left(\tfrac{U_{xy}+U_{yx}}{2}\right)\psi^2_{y\mathbf{j}}\psi^*_{x\mathbf{j}} + \left(\tfrac{U_{xz}+U_{zx}}{2}\right)\psi^2_{z\mathbf{j}}\psi^*_{x\mathbf{j}} \\ -i\tfrac{\partial\psi_{y\mathbf{j}}}{\partial t} \;=\; & -\textstyle\sum_{\beta\in\{x,y,z\}} t_{y\beta}(\psi_{y\mathbf{j}+\mathbf{i}_\beta} - 2\psi_{y\mathbf{j}} + \psi_{y\mathbf{j}-\mathbf{1}_\beta}) \\ & +(U_{yy}|\psi_{y\mathbf{j}}|^2 + (U_{xy}+U_{yx})|\psi_{x\mathbf{j}}|^2 + (U_{yz}+U_{zy})|\psi_{z\mathbf{j}}|^2)\psi_{y\mathbf{j}} \\ & + \left(\tfrac{U_{xy}+U_{yx}}{2}\right)\psi^2_{x\mathbf{j}}\psi^*_{y\mathbf{j}} + \left(\tfrac{U_{zy}+U_{yz}}{2}\right)\psi^2_{z\mathbf{j}}\psi^*_{y\mathbf{j}} \end{aligned} \tag{3.7}$$

$$\begin{aligned} -i\frac{\partial\psi_{z\mathbf{j}}}{\partial t} &= -\sum_{\beta\in\{x,y,z\}} t_{z\beta}(\psi_{z\mathbf{j}+\mathbf{i}_\beta} - 2\psi_{z\mathbf{j}} + \psi_{z\mathbf{j}-\mathbf{1}_\beta}) \\ &\quad +(U_{zz}|\psi_{x\mathbf{j}}|^2 + (U_{xz}+U_{zx})|\psi_{x\mathbf{j}}|^2 + (U_{yz}+U_{zy})|\psi_{y\mathbf{j}}|^2)\psi_{z\mathbf{j}} \\ &\quad + \left(\tfrac{U_{xz}+U_{zx}}{2}\right)\psi_{x\mathbf{j}}^2\psi_{z\mathbf{j}}^* + \left(\tfrac{U_{yz}+U_{zy}}{2}\right)\psi_{y\mathbf{j}}^2\psi_{z\mathbf{j}}^*, \end{aligned}$$

Moreover, using the fact that the order parameters in the Hamiltonian (3.5) are complex numbers, say

$$\psi_{\alpha\mathbf{j}} = e^{i\theta_{\alpha\mathbf{j}}}|\psi_{\alpha\mathbf{j}}|, \tag{3.8}$$

further properties at the level of the mean-field analysis can be additionally inferred from the conditions that lead to minimum energy[4].

We start this analysis by first considering the non-interacting part of the mean-field Hamiltonian

$$H^0_{MF} = -\sum_{\alpha,\beta}\sum_{\langle i,j\rangle_\beta} t_{\alpha\beta}\psi^*_{\alpha\mathbf{i}}\psi_{\alpha\mathbf{j}} = -2\sum_{\alpha\beta}\sum_{\langle\mathbf{i},\mathbf{j}\rangle} t_{\alpha\beta}|\psi_{\alpha\mathbf{i}}||\psi_{\alpha\mathbf{j}}|\cos(\theta_{\alpha\mathbf{j}} - \theta_{\alpha\mathbf{i}}). \tag{3.9}$$

Here the role of the tunneling becomes clear: it connects the phases of the order parameters between neighboring sites, establishing phase coherence within the corresponding orbital state. In particular, since the tunneling coefficients are $t_\parallel < 0$ in the direction parallel to the node and $t_\perp > 0$ in the perpendicular direction, intersite phase coherence is implemented in the form of a stripped pattern. In fact, taking as an example the $p_x$-orbital state, the phase of the corresponding order parameter can be expressed as $\theta_{x\mathbf{j}} = \theta_x(j_x, j_y, j_z) - \pi \mod (j_x, 2)$. Analogous relations hold for the $p_y$- and $p_z$-orbitals. It follows, therefore, from the properties of tunneling in the $p$ band, that neighboring sites will always maintain the same phase relation in the directions perpendicular to the node, while in the parallel direction the phase alternates with $\pi$ difference.

We consider now the interacting part of the mean-field Hamiltonian. Substituting Eq. (3.8) in the term that describes density-density interactions

$$\begin{aligned} H^{(\mathbf{j})}_{nn} &= \tfrac{U_{xx}}{2}|\psi_{x\mathbf{j}}|^4 + \tfrac{U_{yy}}{2}|\psi_{y\mathbf{j}}|^4 + \tfrac{U_{zz}}{2}|\psi_{z\mathbf{j}}|^4 \\ &\quad +2U_{xy}|\psi_{x\mathbf{j}}|^2|\psi_{y\mathbf{j}}|^2 + 2U_{xz}|\psi_{x\mathbf{j}}|^2|\psi_{z\mathbf{j}}|^2 + 2U_{yz}|\psi_{y\mathbf{j}}|^2|\psi_{z\mathbf{j}}|^2. \end{aligned} \tag{3.10}$$

no information regarding phase relation can be extracted. But this was already expected, for this term in Eq. (2.30) depends only on number operators. This is not the case, however, in the term describing transfer of population between different orbitals,

$$\begin{aligned} H^{(\mathbf{j})}_{FD} &= U_{xy}|\psi_{x\mathbf{j}}|^2|\psi_{y\mathbf{j}}|^2\cos(2(\theta_{x\mathbf{j}} - \theta_{y\mathbf{j}})) + U_{xz}|\psi_{x\mathbf{j}}|^2|\psi_{z\mathbf{j}}|^2\cos(2(\theta_{x\mathbf{j}} - \theta_{z\mathbf{j}})) \\ &\quad + U_{yz}|\psi_{y\mathbf{j}}|^2|\psi_{z\mathbf{j}}|^2\cos(2(\theta_{y\mathbf{j}} - \theta_{z\mathbf{j}})), \end{aligned} \tag{3.11}$$

and therefore the configuration which minimizes energy will impose a corresponding specific onsite phase locking for the different orbital states order parameters. In what follows we discuss the cases of two and three dimensional lattices separately.

[4] This discussion follows Refs. [9] and Paper I.

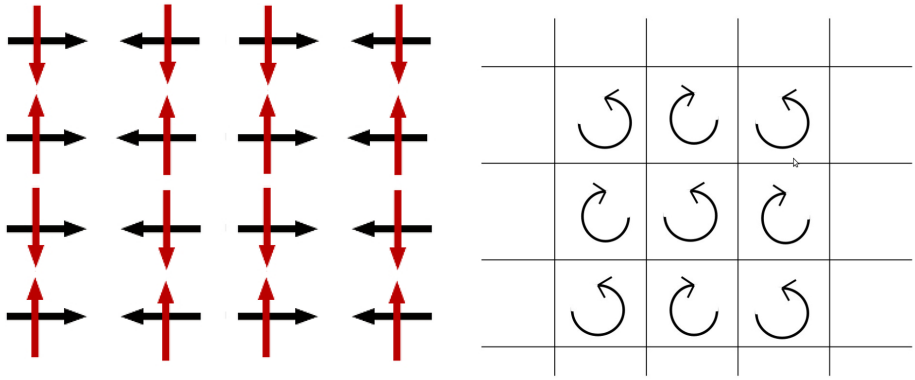

Figure 3.1.: Here we illustrate the phase ordering established in the different orbital states order parameters. Black arrows in the left pannel describe $\theta_{x\mathbf{j}}$ while the red arrows are used to describe $\theta_{y\mathbf{j}}$. Notice that $\theta_{x\mathbf{j}}$ and $\theta_{y\mathbf{j}}$ always keep a $\pi/2$ phase difference as required by Eq. (3.12) for minimizing the ground-state energy. In the right pannel we illustrate the vortex/anti-vortex structure in the different lattice sites.

### 3.1.1. The two-dimensional lattice

In the two-dimensional case, the phases between the $p_x$- and $p_y$-orbitals are locked with a $\pi/2$ phase difference. This can be easily noticed from the fact that

$$H^{(\mathbf{j})}_{FD_{2D}} = U_{xy}|\psi_{x\mathbf{j}}|^2|\psi_{y\mathbf{j}}|^2\cos(2(\theta_{x\mathbf{j}} - \theta_{y\mathbf{j}})) \tag{3.12}$$

is at a minimum value for $\theta_{x\mathbf{j}} - \theta_{y\mathbf{j}} = \pm\pi/2$ ($U_{xy} > 0$). When this is combined with the stripped pattern required for minimizing contributions of the tunneling terms, the phases of the order parameters become constrained. This is illustrated in the left pannel of Fig. 3.1 where the directions of the arrows define an angle.

Now in terms of the orbital states, the expression of the full onsite order parameter defined in Eq. (3.2) is given in the position representation as [27]

$$\psi_{\mathbf{j}}(\vec{r}) = \psi_{x\mathbf{j}}w_{x\mathbf{j}}(\vec{r}) + \psi_{y\mathbf{j}}w_{y\mathbf{j}}(\vec{r}), \tag{3.13}$$

which can be further re-written as

$$\psi_{\mathbf{j}}(\vec{r}) = |\psi_{x\mathbf{j}}|w_{x\mathbf{j}}(\vec{r}) \pm i|\psi_{y\mathbf{j}}|w_{y\mathbf{j}}(\vec{r}), \tag{3.14}$$

after use is made of the specific phase relations that minimize the energy. In particular, the $\pm$ sign alternates between neighboring sites (see Eq. (3.12)). Making use of Eq. (2.5), which states the orthonormality condition satisfied by the Wannier functions, the onsite order parameter can be interpreted as a spinor

$$\psi_{\mathbf{j}} = \begin{bmatrix} |\psi_{x\mathbf{j}}| \\ \pm i|\psi_{y\mathbf{j}}| \end{bmatrix}, \tag{3.15}$$

where the basis states $w_{x\mathbf{j}}(\vec{r})$ and $w_{y\mathbf{j}}(\vec{r})$ contain any spatial dependence, and where the length of the spinor gives the onsite atom number, i.e., $N_{\mathbf{j}} = \sqrt{|\psi_{x\mathbf{j}}|^2 + |\psi_{y\mathbf{j}}|^2}$. Since here

the onsite order parameter has essentially the same properties of a two-level system, it can be completely characterized by a *Bloch vector* $\mathbf{J_j} = (J_{x\mathbf{j}}, J_{y\mathbf{j}}, J_{z\mathbf{j}})$ with components

$$\begin{aligned} J_{x\mathbf{j}} &= \psi^*_{x\mathbf{j}}\psi_{y\mathbf{j}} + \psi^*_{y\mathbf{j}}\psi_{x\mathbf{j}}, \\ J_{y\mathbf{j}} &= i(\psi^*_{x\mathbf{j}}\psi_{y\mathbf{j}} - \psi^*_{y\mathbf{j}}\psi_{x\mathbf{j}}), \\ J_{z\mathbf{j}} &= |\psi_{x\mathbf{j}}|^2 - |\psi_{y\mathbf{j}}|^2. \end{aligned} \tag{3.16}$$

The length of the Bloch vector is related with the total number of atoms[5] at the site $\mathbf{j}$, $|\mathbf{J_j}| = N_\mathbf{j}$, and $J_{z\mathbf{j}}$ computes the onsite population imbalance between the $p_x$- and the $p_y$-orbital states. In addition, due to the required onsite phase-locking relation, $J_{x\mathbf{j}}$ is always zero.

Now we still need to analyze the spatial dependence of the order parameter, which is absent in the Bloch vector description. This is most conveniently done by considering first what happens in the limit where the harmonic approximation is reasonable: the Wannier functions can be replaced by harmonic oscillator ground states (see Sec. 2.3.1) and the expression of the onsite order parameter becomes

$$\psi^{(ha)}_\mathbf{j} = \left[|\psi_{x\mathbf{j}}|x \pm i|\psi_{y\mathbf{j}}|y\right] e^{-\frac{x^2+y^2}{\sigma^2}}, \tag{3.17}$$

where $\sigma^2$ is the effective width of the oscillator, determined from the lattice parameters. Now if $|\psi_{x\mathbf{j}}| = |\psi_{y\mathbf{j}}|$, this is an angular momentum eigenstate, $L_{z\mathbf{j}} = -i\partial_{\theta_\mathbf{j}}$, $L_{z\mathbf{j}}\psi^{(ha)}_\mathbf{j} = \pm\psi^{(ha)}_\mathbf{j}(\vec{r})$, which allows for interpretation of the onsite order parameter as a vortex/anti-vortex state which covers the entire lattice. In terms of the Bloch sphere, this means that $J_{x\mathbf{j}} = 0$ for every $\mathbf{j}$ and that the Bloch vector points parallel to the direction defined by $J_{y\mathbf{j}}$. This vortex/anti-vortex structure is illustrated in the right pannel of Fig. 3.1. We remark that this solution is only true in the harmonic approximation. Outside this regime there is no requirement which ensures the existence of a true vortex/anti-vortex state[6] even when $J_{z\mathbf{j}} = 0$. It still stands though, that due to the properties of the Wannier functions and the onsite interorbital phase relation, the density vanishes at the center of the site $\mathbf{j}$, and therefore the onsite order parameter do show a vortex-like singularity. In addition, it also holds that the neighboring sites are then characterized by anti-vortex-like states. This is the extent to which the order parameter of the general case shares properties of the staggered vortex solution.

### 3.1.2. The three-dimensional lattice

Similar analysis[7] also reveals many features of the physics in the three-dimensional system. But in the isotropic cubic lattice, due to the triple degeneracy of the orbital states on the $p$ band, the angular momentum becomes a vector with components $L_\alpha$, $\alpha = \{x, y, z\}$. Let us assume first that $|\psi_{x\mathbf{j}}| = |\psi_{y\mathbf{j}}| = |\psi_{z\mathbf{j}}|$ and check the requirements

[5] This is a mean-field version of the Schwinger bosons.
[6] In the sense of eigenvalues of $L_{z\mathbf{j}}$.
[7] We follow analysis done in Ref. [9].

for minimizing Eq. (3.11). Under these conditions the phase relation to be satisfied is $\theta_{x\mathbf{j}} - \theta_{y\mathbf{j}} = \theta_{y\mathbf{j}} - \theta_{z\mathbf{j}} = \theta_{z\mathbf{j}} - \theta_{x\mathbf{j}} = \pm 2\pi/3 \pm \pi$, which can be written, for example, as

$$\Psi_{\mathbf{j}} = \begin{bmatrix} \psi_{x\mathbf{j}} \\ \psi_{y\mathbf{j}} \\ \psi_{z\mathbf{j}} \end{bmatrix} = \sqrt{\frac{N_{\mathbf{j}}}{3}} e^{i\theta} \begin{bmatrix} 1 \\ e^{2\pi i/3} \\ e^{4\pi i/3} \end{bmatrix}, \tag{3.18}$$

where $N_{\mathbf{j}}$ is the total onsite atom number and $\theta$ is an arbitrary phase. The onsite wave function with equal number of atoms on each of the orbital states has a unit angular momentum per atom which points along the axis $\mathbf{L} \propto (\pm 1, \pm 1, \pm 1)$. And because $U_{xy} > 0$, the relative phases of the three orbital order parameters are frustrated[8]. In particular, it was pointed out in Ref. [7] that "the onsite frustrated phase configurations come in two different "chiralities" that cannot be converted into each other by shifting any one of the phases by the $\pi$ shift allowed by the $Z_2$ symmetry."[9]

With information about the onsite orbitals phase locking and in particular the frustrated character of the phase relation in the three orbital case, one can then pose the inverse question. Let us assume that this property is inherent of the model, and that the phases of the different orbital states are arranged as in Eq. (3.18). Is this phase relation still valid regardless of the values of $U_{\alpha\alpha}$ and $U_{\alpha\beta}$, or is there any condition imposed over the values of these coupling constants?

We follow again the approach of Ref. [9], and re-write the interacting part of the mean-field Hamiltonian as[10]

$$\begin{aligned} H_{nn} &= \tfrac{U_{xx}}{2}(n_x^2 + n_y^2 + n_z^2) + 2U_{xy}(n_x n_y + n_x n_z + n_y n_z), \\ H_{FD} &= U_{xy}\left(\cos(\Delta_{xy}) n_x n_y + \cos(\Delta_{xz}) n_x n_z + \cos(\Delta_{xz} - \Delta_{xy}) n_y n_z\right), \end{aligned} \tag{3.19}$$

where $n_\alpha = |\psi_\alpha|^2$, and $\Delta_{\alpha\beta} = 2(\theta_\alpha - \theta_\beta)$. In these terms, defining $\mathbf{n} = (n_x, n_y, n_z)$, the energy functional can be written in the quadratic form of the $n_\alpha$ variables,

$$E[\psi_x, \psi_y, \psi_z] = \mathbf{n}^T \mathbf{M} \mathbf{n}, \tag{3.20}$$

with

$$\mathbf{M} = \begin{bmatrix} U_{xx}/2 & U_{xy}(2 + \cos(\Delta_{xy})) & U_{xy}(2 + \cos(\Delta_{xz})) \\ U_{xy}(2 + \cos(\Delta_{xy})) & U_{xx}/2 & U_{xy}(2 + \cos(\Delta_{xz} - \Delta_{xy})) \\ U_{xy}(2 + \cos(\Delta_{xz})) & U_{xy}(2 + \cos(\Delta_{xz} - \Delta_{xy})) & U_{xx}/2 \end{bmatrix}. \tag{3.21}$$

Solving for the eigenvalues we find that

$$\begin{aligned} \lambda_1 &= U_{xx} - 3U_{xy} \\ \lambda_2 &= U_{xx} - 3U_{xy} \\ \lambda_3 &= U_{xx} + 6U_{xy}, \end{aligned} \tag{3.22}$$

[8] Notice that the phase relation to be satisfied is a (dependent) linear combination of the phases of the different orbital states.

[9] We refer to the original reference [7] for more discussions on the symmetry properties of the broken symmetry phase of three orbital system.

[10] Due to typos in Ref. [9], there are different factors in the calculations presented here. We point out, however, that this does not change the conclusions drawn by the authors.

which requires $U_{xx} > 3U_{xy}$ for otherwise $\mathbf{M}$ is not positive definite. This is usually satisfied in sinusoidal lattices (see Fig. A.2). However when this condition is violated, the onsite phase of the order parameters cannot establish the phase relation described in Eq. (3.20) because for this range of the parameter values $\mathbf{M}$ is not positive definite. In particular, this also means that minimization of the overall energy has to be studied now in the case where $|\psi_{x\mathbf{j}}| \neq |\psi_{y\mathbf{j}}| \neq |\psi_{z\mathbf{j}}|$ and therefore qualitative features of the ground-state are expected to be different (see Ref. [9] for discussions of this case). Furthermore this also reveals limitations in the description provided by the harmonic approximation, in which case $U_{xx} = 3U_{xy}$ as discussed previously.

# 4. Confined $p$-orbital bosons

In this chapter we study the superfluid phase of $p$-orbital bosons confined by a harmonic trap[1]. Mean-field analysis carried out in Chapter 3 revealed the existence of specific on and inter site phase relations to be satisfied by the phase of the orbital order parameters in order to minimize the system's energy. More explicitly, it was shown that in a situation of equal number of atoms in the different orbital states, the ground state in the isotropic square lattice is characterized by a staggered vortex-like solution. But how is this scenario altered by the presence of an external confining trap?

By rendering the atomic density an inhomogeneous spatial profile, the presence of a confining potential immediately adds an extra feature for the physics in the $p$ band. In the case of a harmonic trap, for example, the atomic density has an approximate Gaussian distribution in the lattice. Now how will the combination of inhomogeneous atomic density + the anisotropic tunneling in the $p$ band affect the properties of the ground state?

In order to answer this question we proceed with a mean field analysis for a system of harmonically confined $p$-orbital bosons. We first discuss how confinement changes the equations of the order parameters in Sec. 4.1, where we also discuss the approximations considered. We continue with the study of Bose-condensation for the ideal gas in the $p$ band in Sec. 4.2, and also analyze finite temperature properties. We consider the interacting case in Sec. 4.2.2, and conclude the study by analyzing the properties of the system with an anisotropic optical lattice in Sec. 4.2.3.

## 4.1. Mean-field equations of the two-dimensional confined system

In Sec. 2.4 the general expression of the many-body Hamiltonian, Eq. (2.24), was expanded with the use of orbital states of the $p$ band. In this section we extend this procedure in order to include effects stemming from an external confining harmonic trap. We do this by modifying the term in Eq. (2.24) that describes contributions of external potentials as

$$V(\vec{r}') \rightarrow V_{latt}(\vec{r}') + V_{trap}(\vec{r}'), \tag{4.1}$$

where

$$V_{latt}(\vec{r}') = V_x \sin^2(kx') + V_y \sin^2(ky') \tag{4.2}$$

and

$$V_{trap}(\vec{r}') = \frac{m\tilde{\omega}^2}{2}(x'^2 + y'^2) = \frac{\omega^2}{2}(x^2 + y^2). \tag{4.3}$$

[1]This chapter is based on Paper I, which is attached in the end of this thesis.

Here, as usual, $k$ is the wave vector of the lattice, $V_\alpha$ the lattice amplitude in the direction $\alpha = \{x, y\}$, $\tilde{\omega}$ is the trap frequency. $\omega = \sqrt{2}m\tilde{\omega}/\hbar k^2$ is the dimensionless trap frequency, and $x = kx'$ and $y = ky'$ are dimensionless positions. We now assume that the parameters of the system satisfy the requirements necessary for validity of the *local density approximation*[2]. We consider thus a very smooth confining potential, with characteristic length $l_{trap} = \sqrt{h/m\tilde{\omega}} \gg \lambda/2$. Under this condition, the system can still be considered periodic on the length scale characteristic of the trap, and corresponding trap effects can be implemented at each site, as a shift of the onsite energies[3]. In addition, the site-localized Wannier functions are assumed the same as in the non-trapped case, which also implies that the orbital states remain unaltered from the ones discussed previously.

The expression of the second quantized Hamiltonian describing $p$-orbital bosons in the square lattice and with harmonic confinement then follows as

$$\begin{aligned}\hat{H}_{2D} &= -\sum_{\alpha\beta}\sum_{\langle \mathbf{i},\mathbf{j}\rangle_\beta} t_{\alpha\beta}\hat{a}^\dagger_{\alpha\mathbf{i}}\hat{a}_{\alpha\mathbf{j}} + \sum_\alpha\sum_{\mathbf{j}}\tfrac{\omega}{2}(x_{\mathbf{j}}^2 + y_{\mathbf{j}}^2)\hat{n}_{\alpha\mathbf{j}} \\ &\quad + \sum_\alpha\sum_{\mathbf{j}}\tfrac{U_{\alpha\alpha}}{2}\hat{n}_\alpha(\hat{n}_{\alpha\mathbf{j}} - 1) + \sum_{\alpha\beta,\alpha\neq\beta}\sum_{\mathbf{j}} U_{\alpha\beta}\hat{n}_{\alpha\mathbf{j}}\hat{n}_{\beta\mathbf{j}} \\ &\quad + \sum_{\alpha\beta,\alpha\neq\beta}\sum_{\mathbf{j}}\tfrac{U_{\alpha\beta}}{4}(\hat{a}^\dagger_{\alpha\mathbf{j}}\hat{a}^\dagger_{\alpha\mathbf{j}}\hat{a}_{\beta\mathbf{j}}\hat{a}_{\beta\mathbf{j}} + \hat{a}^\dagger_{\beta\mathbf{j}}\hat{a}^\dagger_{\beta\mathbf{j}}\hat{a}_{\alpha\mathbf{j}}\hat{a}_{\alpha\mathbf{j}}),\end{aligned} \tag{4.4}$$

where again $\hat{n}_{\alpha\mathbf{j}} = \hat{a}^\dagger_{\alpha\mathbf{j}}\hat{a}_{\alpha\mathbf{j}}$, with $\alpha = \{x, y\}$ the number operator for the orbital state $\alpha$. In particular, notice here that the first, second and third lines correspond, respectively, to the former $\hat{H}_0$, $\hat{H}_{nn}$ and $\hat{H}_{FD}$ of Eq. (2.28).

As a quick remark, we explicitly write the expression of $\hat{H}_U = \hat{H}_{nn} + \hat{H}_{FD}$ for the case of an isotropic square lattice, where $U_{\alpha\beta} = U_{\beta\alpha}$[4]:

$$\begin{aligned}\hat{H}_U &= \tfrac{U_{xx}}{2}\hat{n}_{x\mathbf{j}}(\hat{n}_{x\mathbf{j}} - 1) + \tfrac{U_{yy}}{2}\hat{n}_{y\mathbf{j}}(\hat{n}_{y\mathbf{j}} - 1) + 2U_{xy}\hat{n}_{x\mathbf{j}}\hat{n}_{y\mathbf{j}} \\ &\quad + \tfrac{U_{xy}}{2}\hat{a}^\dagger_{x\mathbf{j}}\hat{a}^\dagger_{x\mathbf{j}}\hat{a}_{y\mathbf{j}}\hat{a}_{y\mathbf{j}} + \tfrac{U_{xy}}{2}\hat{a}^\dagger_{y\mathbf{j}}\hat{a}^\dagger_{y\mathbf{j}}\hat{a}_{x\mathbf{j}}\hat{a}_{x\mathbf{j}}.\end{aligned} \tag{4.5}$$

Our goal now is to obtain equations similar to Eqs. (3.7), i.e, the equations of motion for the order parameter, but for the system described by the Hamiltonian (4.4). We thus start with the coherent state ansatz, Eq. (3.1), and obtain the mean-field Hamiltonian that will be used to compute the Euler-Lagrange equations. In the same way as for the three-dimensional case in Sec. 3.1, normalization is imposed in the whole lattice as

$$N = N_x + N_y = \sum_{\mathbf{j}}|\psi_{x\mathbf{j}}|^2 + \sum_{\mathbf{j}}|\psi_{y\mathbf{j}}|^2, \tag{4.6}$$

where $N$ is the total number of atoms.

The equations for the order parameters then follow. They correspond to a set of coupled

[2] We remark that the term local density approximation means different things in different contexts. What we mean by local density approximation is explicitly defined in the sequence of the text and no other significance is implied.

[3] This is equivalent to having a position dependent chemical potential.

[4] We do this here just because the literature has considerable amount of typos in this part.

(discrete) Gross-Pitaevskii equations, one for each of the orbital states at each site $\mathbf{j}$

$$\begin{aligned} -i\frac{\partial\psi_{x\mathbf{j}}}{\partial t} &= -\sum_{\beta\in\{x,y\}} t_{x\beta}(\psi_{x\mathbf{j}+\mathbf{i}_\beta} - 2\psi_{x\mathbf{j}} + \psi_{x\mathbf{j}-\mathbf{1}_\beta}) + \tfrac{\omega^2}{2}(x_{\mathbf{j}}^2 + y_{\mathbf{j}}^2)\psi_{x\mathbf{j}} \\ &\quad +(U_{xx}|\psi_{x\mathbf{j}}|^2 + (U_{xy} + U_{yx})|\psi_{y\mathbf{j}}|^2)\psi_{x\mathbf{j}} + \left(\tfrac{U_{xy}+U_{yx}}{2}\right)\psi_{y\mathbf{j}}^2\psi_{x\mathbf{j}}^* \\ -i\frac{\partial\psi_{y\mathbf{j}}}{\partial t} &= -\sum_{\beta\in\{x,y\}} t_{y\beta}(\psi_{y\mathbf{j}+\mathbf{i}_\beta} - 2\psi_{y\mathbf{j}} + \psi_{y\mathbf{j}-\mathbf{1}_\beta}) + \tfrac{\omega^2}{2}(x_{\mathbf{j}}^2 + y_{\mathbf{j}}^2)\psi_{y\mathbf{j}} \\ &\quad +(U_{yy}|\psi_{y\mathbf{j}}|^2 + (U_{xy} + U_{yx})|\psi_{x\mathbf{j}}|^2)\psi_{y\mathbf{j}} + \left(\tfrac{U_{xy}+U_{yx}}{2}\right)\psi_{x\mathbf{j}}^2\psi_{y\mathbf{j}}^*, \end{aligned} \tag{4.7}$$

where the expressions of the couplings are given by Eqs. (2.32) and (2.33), which are computed here with the lattice Wannier functions obtained from numerical solution as the Mathieu equation for the potential (4.2).

## 4.2. The ideal gas

We start by considering first the simplest case of the non interacting gas, where expression of the mean-field Hamiltonian follows as

$$H_{MF}^0 = -\sum_{\alpha,\beta}\sum_{\langle i,j\rangle_\beta} t_{\alpha\beta}\psi_{\alpha\mathbf{i}}^*\psi_{\alpha\mathbf{j}} + \sum_\alpha\sum_{\mathbf{j}}\frac{\omega^2}{2}(x_{\mathbf{j}}^2 + y_{\mathbf{j}}^2)n_{\alpha\mathbf{j}}, \tag{4.8}$$

where $n_{\alpha\mathbf{j}} = |\psi_{\alpha\mathbf{j}}|^2$ is the onsite density of the orbital state $\alpha$.

The analysis again makes use of the same ideas discussed in Chapter 3: the order parameters are complex numbers,

$$\psi_{\alpha\mathbf{j}} = |\psi_{\alpha\mathbf{j}}|e^{i\theta_{\alpha\mathbf{j}}}, \tag{4.9}$$

and therefore we are required to characterize properties of both amplitudes and phases in the lattice. Here Eq. (4.8) accounts only for contributions of the free part of the full Hamiltonian (4.4), and the additional term describing contributions of the trap depends only on number operators. This means that the confining potential does not require any particular phase relation to be satisfied, and that the phases of the order parameters behave in exactly the same way as in the non-confined system discussed in Sec. 3.1.1: neighboring sites will always keep the same phase relation in the directions perpendicular to the node, while in the parallel direction the phase alternates with a $\pi$ phase difference.

We proceed with the Schrödinger equation for (4.8),

$$i\frac{\partial}{\partial t}\Psi = H_{MF}^{(0)}\Psi.$$

We first notice that the the Hamiltonian of this discrete model, Eq. (4.8), has structure similar to the Mathieu equation expanded in momentum eigenstates [37], and therefore

the eigenvalue problem for each of the $p_\alpha$ orbitals can be written in the form

$$i\frac{\partial}{\partial t}\begin{pmatrix}\vdots\\ \psi_{\alpha\mathbf{j}-\mathbf{1}_\beta}\\ \psi_{\alpha\mathbf{j}_\beta}\\ \psi_{\alpha\mathbf{j}+\mathbf{1}_\beta}\\ \vdots\end{pmatrix} = \begin{pmatrix} \ddots & & \vdots & & & \\ & \frac{\omega^2}{2}R^2_{\mathbf{j}-2\beta} & -t_{\alpha\beta} & 0 & 0 & \\ \cdots & -t_{\alpha\beta} & \frac{\omega^2}{2}R^2_{\mathbf{j}-\mathbf{1}_\beta} & -t_{\alpha\beta} & 0 & \cdots \\ \cdots & 0 & -t_{\alpha\beta} & \frac{\omega^2}{2}R^2_{\mathbf{j}} & -t_{\alpha\beta} & \cdots \\ & 0 & 0 & -t_{\alpha\beta} & \frac{\omega^2}{2}R^2_{\mathbf{j}+\mathbf{1}_\beta} & \\ & & \vdots & & & \ddots \end{pmatrix}\begin{pmatrix}\vdots\\ \psi_{\alpha\mathbf{j}-\mathbf{1}_\beta}\\ \psi_{\alpha\mathbf{j}_\beta}\\ \psi_{\alpha\mathbf{j}+\mathbf{1}_\beta}\\ \vdots\end{pmatrix}, \tag{4.10}$$

where as usual $\alpha,\beta = \{x,y\}$ and $R^2_{\mathbf{j}} = x^2_{\mathbf{j}} + y^2_{\mathbf{j}}$. Special cases of this equation can be solved analytically. However, since the solution is given in terms of Fourier expansions of the Mathieu functions, there is not much to learn from analytical expressions in this case [37]. In any way, it is still possible to understand the influence of the trap in rather simple terms by considering the continuum limit, where analytical solutions have a closed form. This consists in making $\psi_{\alpha\mathbf{j}} \to \psi_\alpha(x,y)$, such that the kinetic energy transforms as

$$\psi_{\alpha\mathbf{j}+\mathbf{1}_\beta} - 2\psi_{\alpha\mathbf{j}} + \psi_{\alpha\mathbf{j}-\mathbf{1}_\beta} \to \frac{\partial^2}{\partial\beta^2}\psi_\alpha(x,y).$$

But another step before arriving at the final form of the equations, is to impose in the wave function ansatz the correct phase imprint which renders the stripped order in the lattice. The phase factors are then further absorbed into the redefinition of the tunneling coefficients by making $t_{\alpha\alpha} \to -t_{\alpha\alpha}$, and the equations of the orbital states are given by

$$\begin{aligned} i\tfrac{\partial}{\partial t}\psi_x(x,y) &= \left[-|t_{xx}|\tfrac{\partial^2}{\partial x^2} - |t_{xy}|\tfrac{\partial^2}{\partial y^2} + \tfrac{\omega^2}{2}(x^2+y^2)\right]\psi_x(x,y) \\ i\tfrac{\partial}{\partial t}\psi_y(x,y) &= \left[-|t_{yx}|\tfrac{\partial^2}{\partial x^2} - |t_{yy}|\tfrac{\partial^2}{\partial y^2} + \tfrac{\omega^2}{2}(x^2+y^2)\right]\psi_y(x,y) \end{aligned} \tag{4.11}$$

By introducing the *effective mass* $m_{\alpha\beta} = |t_{\alpha\beta}|^{-1}/2$, and parallel and transverse frequencies

$$\begin{aligned} \omega_\parallel &= \omega\sqrt{2|t_{\alpha\beta}|}, \quad \alpha = \beta \\ \omega_\perp &= \omega\sqrt{2|t_{\alpha\beta}|}, \quad \alpha \neq \beta, \end{aligned} \tag{4.12}$$

Eq. (4.11) can be re-written as

$$i\frac{\partial}{\partial t}\psi_x(x,y) = \left[\frac{p_x^2}{2m_{xx}} + \frac{p_y^2}{2m_{xy}} + \frac{m_{xx}\omega_\parallel^2}{2}x^2 + \frac{m_{xy}\omega_\perp^2}{2}y^2\right]\psi_x(x,y), \tag{4.13}$$

with a corresponding equation for the $p_y$ orbital state. We find therefore that the continuum approximation considerably simplifies the problem, for now the system we have to deal with resumes to the 2D anisotropic harmonic oscillator. This also shows that implementation of the striped pattern in the wave-function ansatz prior to taking the the continuum limit helps avoiding a final Hamiltonian that is not bounded from below. It

has an overall effect in the system, in the sense that it inverts the $p$ band and shifts its minimum to the center of the Brillouin zone, but the physics remain unchanged.

Now the anisotropy arising from the different tunneling elements $t_{xx}$ and $t_{xy}$ will affect $m_{\alpha\beta}$ and therefore also $\omega_{\alpha\beta}$. As a consequence, the density of the resulting ground state of Eq. (4.13) will be characterized by a Gaussian distribution, but with different widths in $x$- and $y$-directions. We use this fact to define the anisotropy parameter

$$S_x = \sqrt{\frac{(\Delta_x x)^2}{(\Delta_x y)^2}}, \tag{4.14}$$

where $(\Delta_\alpha \beta)^2 = \langle \beta^2 \rangle_\alpha - \langle \beta \rangle_\alpha^2$, and $\langle .. \rangle_\alpha$ represents the expectation value taken with respect to $\psi_\alpha(x, y)$. The anisotropy in the density for atoms occupying the $p_y$-orbital state is characterized by an equivalent expression, that satisfies $S_x S_y = 1$ for symmetry reasons, and thus from now on we use $S = S_x$ whenever discussing such anisotropies. In particular, in the continuum case discussed here

$$S_{con} = \left( \frac{|t_{xx}|}{|t_{xy}|} \right)^{1/4} = \left( \frac{\omega_\parallel}{\omega_\perp} \right). \tag{4.15}$$

The limit where $\omega_\parallel = \omega_\perp$ corresponds to the case of isotropic tunneling, and yields $S = 1$. But as soon as this isotropy is broken, $S \neq 1$. Accordingly this reveals a narrowing in the density of atoms in the orbital states along one of the directions.

### 4.2.1. The ideal gas at finite temperatures

The possibility of rewriting the Schrödinger equation of the non-interacting system in a rather simple form allows for the study of thermodynamic properties of condensation in the $p$ band.

We start by analyzing the properties of the continuum limit, described by Eqs. (4.11). Here known properties of condensation in harmonically trapped systems can be directly used [29]. The *critical temperature* for the Bose-Einstein condensation, for example is given by

$$T_c^{(2D)} = \omega_{eff}^{(2D)} \sqrt{6N/\pi^2} \tag{4.16}$$

and

$$T_c^{(3D)} = \omega_{eff}^{(3D)} (N/\zeta(3))^{1/3} \tag{4.17}$$

in the two and three dimensional cases. It also follows that $\zeta(3) \approx 1.20206$ and the effective trapping frequencies are defined [29] as

$$\omega_{eff}^{(2D)} = 3\omega \sqrt{|t_{xx}||t_{xy}|} \tag{4.18}$$

and

$$\omega_{eff}^{(3D)} = 4\omega (|t_{xx}||t_{xy}||t_{xz}|)^{1/3} = 4\omega (|t_{xx}||t_{xy}|^2)^{1/3}. \tag{4.19}$$

For the discrete model described by Eq. (4.8), the critical temperature can be computed by noticing that the number of thermal atoms is determined by

$$N_T = \sum_{n \neq 0} \frac{1}{e^{\beta(E_n - \mu)} - 1}, \tag{4.20}$$

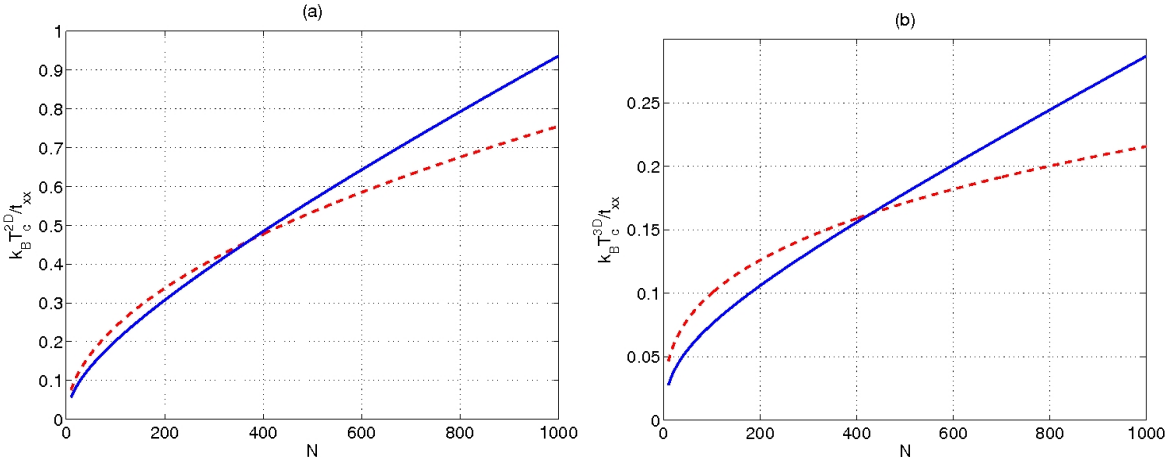


Figure 4.1.: Critical temperature for the establishment of Bose-Einstein condensation in the $p$ band as a function of the atom number denoted by $N$. (a) shows the results of the $2D$ system while (b) shows the results for the $3D$ system. We also compare the results obtained for the continuum approximation (dashed line) with the results of the discrete model obtained numerically (solid line). The parameters here are $\omega^2/2 = 0.001$ for the dimensionless trap strength and $|t_{xx}/t_{xy}| = 20.1$, which corresponds to the ratio between the tunneling coefficients for $V_x = V_y = 17$.

where $\beta = E_r/k_BT$ is the inverse (dimensionless) temperature and $\mu$ is the chemical potential. In these terms, the chemical potential is found by fixing the total atom number $N$, and the energy levels $E_n$ are obtained via diagonalization of (4.10).

In Fig. 4.1 we compare the results for the critical temperature in both the continuum and discrete cases. In the limit of very small atom number, the continuum limit predicts larger values for the critical temperature of the discrete model, while in the other limit, of large atom number, it predicts considerable smaller critical temperatures. We attribute this difference as being a consequence of the different density of states between the lattice and continuum models.

Now in the $2D$ version of the system, is there any change in the profile of the atomic density distribution as the temperature is lowered below the critical temperature $T_c$ associated to the transition to the condensed phase? In the limit of high temperature, we expect the system to display isotropic atomic density. This is because in this region the system is described by the Boltzmann distribution, which is isotropic. But after the system reaches the critical temperature, is there any direct signature of this intrinsic tunneling anisotropy? The answer is yes. In fact, in the low temperature limit, the condensed state of $p$-orbital bosons is characterized by a bimodal structure. In particular, below $T_c$ the condensate density has properties similar to the properties of the ground state, which feature anisotropies because of the different tunneling strengths in the different directions. This is illustrated in Figs. 4.2 (a) and (b), where we show the density

$$n_{total}(\mathbf{j}) = N_0|\psi_0(\mathbf{j})|^2 + \sum_{n\neq 0} \frac{|\psi_n(\mathbf{j})|^2}{e^{\beta(E_n-\mu)}-1} \tag{4.21}$$

for two different temperatures, above $T_c$ and for the ground state (where $T = 0$).

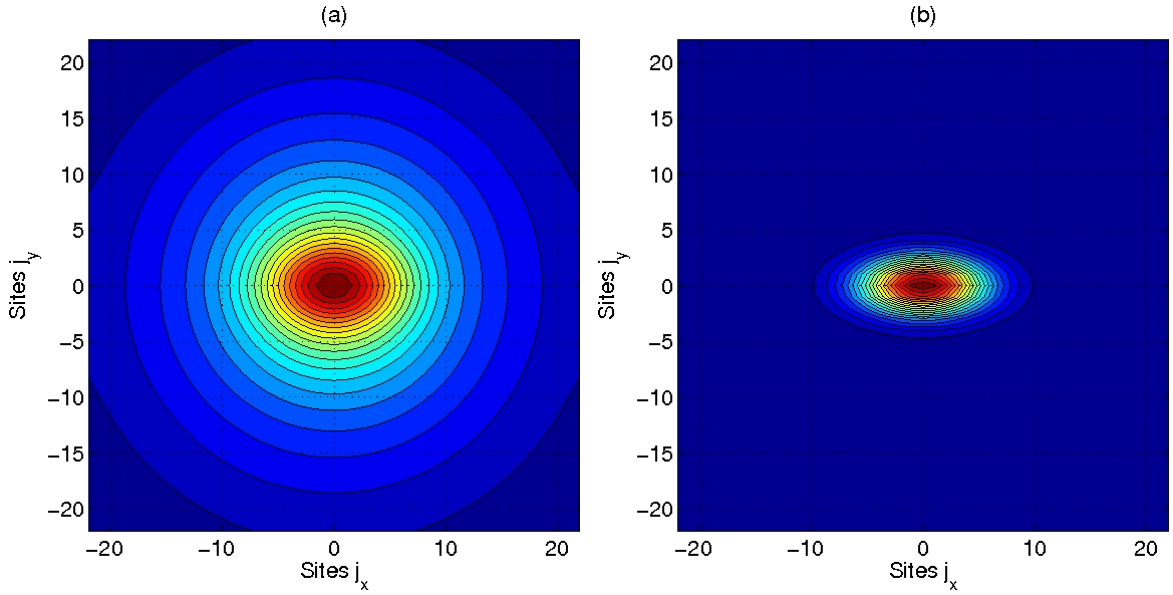


Figure 4.2.: Populations per site of the 2D Bose gas in the $p$ band and for a single orbital state. (a) shows a situation where $T > T_c$, while in (b) $T = 0$. In both cases the total number of atoms in the system $N_{tot} = 1000$, the dimensionless trap strength $\omega^2/2 = 0.001$ and potential depths are $V_x = V_y = 17$.

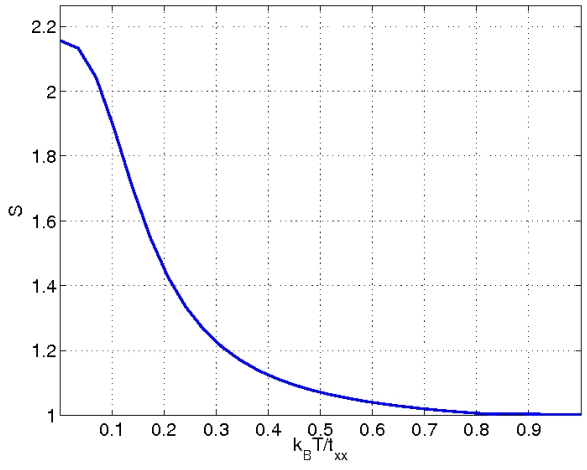


Figure 4.3.: The anisotropy parameter $S$ (see text) that is used to characterize the anisotropy in the density in the $2D$ system, and as a function of the temperatures scaled with $t_{xx}$. The number of atoms considered is $N = 1000$, the dimensionless trap strength is $\omega^2/2 = 0.001$ and $V_x = V_y = 17$.

To conclude this section, we use the anisotropy parameter defined in Eq. (4.14) and characterize how the anisotropy in the $p$-orbital ideal gas changes with temperature for a system with 1000 atoms in Fig. 4.3. As Fig. 4.1 (a) indicates, after the (scaled) critical temperature $T_c \approx 0.9$, the atomic density becomes isotropic in the $xy$-plane.

### 4.2.2. Interacting system

In order to characterize the ground state of the interacting system we propagate the mean-field equations (4.7) in imaginary time with an initial trial wave-function.

To illustrate how this procedure works [38], let us consider the Schrödinger equation $\hat{H}\psi = E\psi$ such that the wave function $\psi$ evolves in time according to $\psi(t) = e^{-i\hat{H}t}\psi(0)$, where we used $\hbar = 1$. Writing $\psi$ in the basis of its energy eigenstates, $\psi = \sum_n c_n\phi_n$, with $c_n = \langle\psi|\phi_n\rangle$,

$$\psi(t) = \sum_n c_n e^{-iE_n t}\phi(0),$$

where $E_n$ corresponds to the $n$-th energy level of the system. Now using $t \to i\tau$, with

$$\psi(\tau) = \sum_n c_n e^{-E_n\tau}\phi(0),$$

the overlap between the ground state with the $\psi(\tau)$ propagated in imaginary time, and after a long propagation time, is given by

$$\langle\psi(\tau)|c_0\phi(\tau)\rangle \to \lim_{\tau\to\infty} \frac{c_0^2 e^{-2E_0\tau}}{c_0^2 e^{-2E_0\tau} + \sum_{n=1} c_n^2 e^{-2E_n\tau}} = 1$$

Therefore in the limit of $\tau \to \infty$, $\psi(\tau)$ will converge to the true ground state of the system, as long as the overlap between these states is non-vanishing:

$$\psi(\tau) = c_0 e^{-\tau H}\phi(0) + \mathcal{O}(e^{-\tau(E_1-E_0)}),$$

with a correction of the order of $\mathcal{O}(e^{-\tau(E_1-E_0)})$.

This method can also be applied to non-linear systems as e.g the system described by Eqs. (4.7), but in this case propagation has to be carried out self-consistently.

We re-write Eqs. (4.7) as

$$i\frac{\partial\Psi_{\mathbf{j}}}{\partial t} = \begin{bmatrix} H_{11} & H_{12} \\ H_{21} & H_{22} \end{bmatrix}\Psi_{\mathbf{j}}, \tag{4.22}$$

where $\Psi_{\mathbf{j}} = \begin{bmatrix} \psi_{x\mathbf{j}} \\ \psi_{y\mathbf{j}} \end{bmatrix}$ and

$$\begin{aligned} H_{11} &= -t_{xx}\frac{\partial^2}{\partial x^2} - t_{xy}\frac{\partial^2}{\partial y^2} + U_{xx}|\psi_{x\mathbf{j}}|^2 + (U_{xy}+U_{yx})|\psi_{y\mathbf{j}}|^2, \\ H_{22} &= -t_{yx}\frac{\partial^2}{\partial x^2} - t_{yy}\frac{\partial^2}{\partial y^2} + U_{yy}|\psi_{y\mathbf{j}}|^2 + (U_{xy}+U_{yx})|\psi_{x\mathbf{j}}|^2, \\ H_{12} &= \left(\tfrac{U_{xy}+U_{yx}}{2}\right)\psi_{y\mathbf{j}}\psi^*_{x\mathbf{j}}, \\ H_{21} &= \left(\tfrac{U_{xy}+U_{yx}}{2}\right)\psi_{x\mathbf{j}}\psi^*_{y\mathbf{j}}. \end{aligned} \tag{4.23}$$

Since the Hamiltonian governing time-evolution contains both spatial and momentum dependent terms, we study the system numerically, with the use of the *split-operator* method [39]. This method is based on factorization of the evolution operator, and therefore becomes exact only in the limit of vanishingly small time steps. Propagation is thus carried out in very tiny time steps, and numerical accuracy of the procedure is checked by varying the size of the time steps.

In what follows, we illustrate the details of the calculation. The time evolution operator is written as

$$U(\delta t) = e^{-iH\delta t} = \exp\left\{-i\begin{bmatrix} H_{11} & H_{12} \\ H_{21} & H_{22} \end{bmatrix}\delta t\right\} = \exp\left\{-i\left(\begin{bmatrix} H_{11} & 0 \\ 0 & H_{22} \end{bmatrix} + \begin{bmatrix} 0 & H_{12} \\ H_{21} & 0 \end{bmatrix}\right)\delta t\right\}$$

and since we assume the $\lim \delta t \to 0$, this equation is further approximated as

$$U(\delta t) \approx \underbrace{e^{-i\delta t\begin{bmatrix} H_{11} & 0 \\ 0 & H_{22} \end{bmatrix}}}_{U_1(\delta t)}\underbrace{e^{-i\delta t\begin{bmatrix} 0 & H_{12} \\ H_{21} & 0 \end{bmatrix}}}_{U_2(\delta t)}. \tag{4.24}$$

We now expand $U_2(\delta t)$. In particular,

$$\begin{bmatrix} 0 & H_{12} \\ H_{21} & 0 \end{bmatrix}^2 = \begin{bmatrix} \left(\frac{U_{xy}+U_{yx}}{2}\right)^2 |\psi_{x\mathbf{j}}|^2|\psi_{y\mathbf{j}}|^2 & 0 \\ 0 & \left(\frac{U_{xy}+U_{yx}}{2}\right)^2 |\psi_{x\mathbf{j}}|^2|\psi_{y\mathbf{j}}|^2 \end{bmatrix} \tag{4.25}$$

and

$$\begin{bmatrix} 0 & H_{12} \\ H_{21} & 0 \end{bmatrix}^3 = \left(\frac{U_{xy}+U_{yx}}{2}\right)^3 |\psi_{x\mathbf{j}}|^2|\psi_{y\mathbf{j}}|^2 \begin{bmatrix} 0 & \psi_{y\mathbf{j}}\psi^*_{x\mathbf{j}} \\ \psi_{x\mathbf{j}}\psi^*_{y\mathbf{j}} & 0 \end{bmatrix}, \tag{4.26}$$

from where it follows that expansion of $U_2(\delta t)$ has the form

$$\frac{(-i\delta t)^n}{n!}A^n = \frac{(-i\delta t)^n}{n!}|\psi_{x\mathbf{j}}|^{n-1}|\psi_{y\mathbf{j}}|^{n-1}\begin{bmatrix} 0 & \psi_{y\mathbf{j}}\psi^*_{x\mathbf{j}} \\ \psi_{x\mathbf{j}}\psi^*_{y\mathbf{j}} & 0 \end{bmatrix} \tag{4.27}$$

for odd $n$, and

$$\frac{(-i\delta t)^n}{n!}A^n = \frac{(-i\delta t)^n}{n!}|\psi_{x\mathbf{j}}|^n|\psi_{y\mathbf{j}}|^n\begin{bmatrix} 1 & 0 \\ 0 & 1 \end{bmatrix} \tag{4.28}$$

for even $n$. Gathering all the terms of the expansion, we have

$$U_2(\delta t) = \begin{bmatrix} U_2^{(11)} & U_2^{(12)} \\ U_2^{(21)} & U_2^{(22)} \end{bmatrix}, \tag{4.29}$$

where

$$U_2^{(11)} = U_2^{(22)} = \cos\left(\left(\frac{U_{xy}+U_{yx}}{2}\right)\delta t|\psi_{x\mathbf{j}}||\psi_{y\mathbf{j}}|\right),$$

$$U_2^{(12)} = -i\delta t\left(\frac{U_{xy}+U_{yx}}{2}\right)\operatorname{sinc}\left(\left(\frac{U_{xy}+U_{yx}}{2}\right)\delta t|\psi_{x\mathbf{j}}||\psi_{y\mathbf{j}}|\right)\psi_{y\mathbf{j}}\psi^*_{x\mathbf{j}}$$

and

$$U_2^{(21)} = -i\delta t\left(\frac{U_{xy}+U_{yx}}{2}\right)\operatorname{sinc}\left(\left(\frac{U_{xy}+U_{yx}}{2}\right)\delta t|\psi_{x\mathbf{j}}||\psi_{y\mathbf{j}}|\right)\psi_{x\mathbf{j}}\psi^*_{y\mathbf{j}}$$

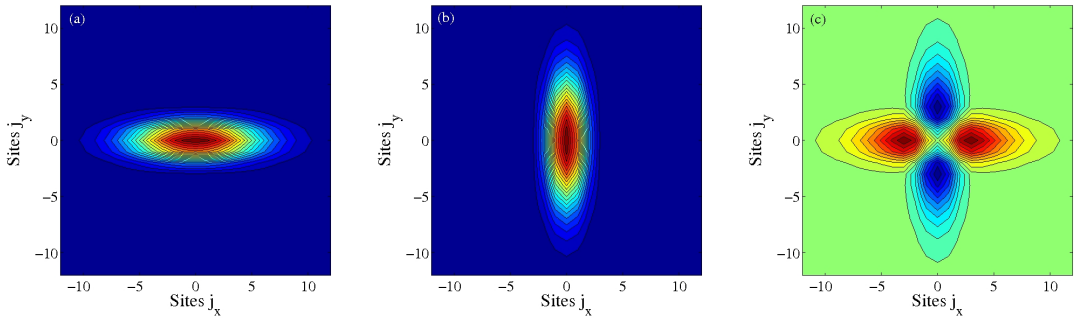


Figure 4.4.: (a) and (b) show populations in the $p_x$- and in the $p_y$-orbital states respectively. (c) illustrates the corresponding population imbalance $J_{z\mathbf{j}}$. The dimensionless system parameters are $V_x = V_y = 17$, $\omega = 0.005$, and $U_0 N = 1$. Excess of atoms in the $p_x$-orbital state appears in the horizontal axis and is indicated by red color, while in the vertical axis the system displays excess of atoms in the $p_y$-orbital state.

Now the idea is to make $\Psi(\delta t) = U_1(\delta t)U_2(\delta t)\Psi = U_1(\delta t)\Psi_1$, where $\Psi_1 = U_2(\delta t)\Psi$ with $U_1(\delta t)$ defined in (4.24). This involves evolution with a diagonal matrix that contains two different types of contributions (see the expressions of $H_{11}$ and $H_{22}$ in Eqs. (4.23)), one that depends on derivatives with respect to $x$ and $y$, and the other that contains a quadratic dependency of the orbitals order parameters. We will first evolve $\Psi_1$ with the part of $U_1$ that does not depend on the derivatives and thus $\Psi_1 \rightarrow \tilde{\Psi}_1$. After this step is taken into account, the remaining part is considered in momentum space. By means of a Fourier transform we obtain the expression of $\tilde{\Psi}_1$ in the momentum representation, $\mathcal{F}[\tilde{\Psi}_1] = \tilde{\Psi}$, which can then be easily evolved with the corresponding dispersion relations[5]

$$\begin{bmatrix} \tilde{\psi}_{x\mathbf{j}}(\delta t) \\ \tilde{\psi}_{y\mathbf{j}}(\delta t) \end{bmatrix} = \begin{bmatrix} e^{-i\delta t[2t_{xx}(1-\cos k_{xx})+2t_{xy}(1-\cos k_{xy})]} & 0 \\ 0 & e^{-i\delta t[2t_{yx}(1-\cos k_{yx})+2t_{yy}(1-\cos k_{yy})]} \end{bmatrix} \begin{bmatrix} \tilde{\psi}_{x\mathbf{j}} \\ \tilde{\psi}_{y\mathbf{j}} \end{bmatrix}. \tag{4.30}$$

By Fourier transforming it back to the position representation, the final result is $\Psi(\delta t)$ (cf. Eq. (4.22)), that is used now as the trial wave function and propagated in imaginary time again. This procedure is repeated until convergence has been reached.

Fig. 4.4 displays the density profiles of the $p_x$- and $p_y$-orbitals in the confined system, in (a) and (b), respectively. As can be seen from comparison with Fig. 4.2 (b), here the density of the $p_x$-orbital state is also elongated in the $x$-direction, with analogous result holding for the density of the $p_y$-orbital. Fig. 4.4 (c) shows the population imbalance in the lattice, i.e., the difference between the number of atoms occupying the $p_x$ and $p_y$ orbital states at the site $\mathbf{j}$ ($J_{z\mathbf{j}}$). Now the next question that arises is what happens in the regime where tunneling stops playing an important role in the dynamics of the system?

There are two ways of weakening the role of tunneling in the lattice: either by making the lattice sites very deep, either by making the coupling parameter $\tilde{U}_0$ (see Eq. (2.24)) very large. In these situations, i.e., in the limit where interactions are so strong that

[5] In momentum space the term $-t_{\alpha\beta}\frac{\partial^2}{\partial\beta^2}$ corresponds to $t_{\alpha\beta}k_{\alpha\beta}^2$. Here however we use $k_{\alpha\beta}^2 \rightarrow 2t_{\alpha\beta}(1-\cos k_{\alpha\beta})$ to account for the (inverted) shape of the $p$ band and the discrete character of the system.

other effects can be neglected in the dynamics, the system is said to be in the *Thomas-Fermi limit* [29]. Now since we already know that the tunneling is the main factor rendering this anisotropic profile for the atomic cloud, it is natural to expect that by suppressing its effects, the density should display more and more symmetric profile. But how does this transition from anisotropic to symmetric profile happens as the relative strength of tunneling gets weaker as compared to other terms in the mean-field version of Hamiltonian (4.4)?

In order to characterize anisotropies in the density, we use again the anisotropy parameter defined in Sec. 4.2:

$$S = \sqrt{\frac{(\Delta_x x)^2}{(\Delta_x y)^2}}$$

and calculate if for different values of the system's parameters. As showed in Fig. 4.5, the anisotropy parameter approaches $S = 1$ smoothly in both cases. However, as opposed to the behavior of $S$ obtained for suppressing the tunneling by increasing the interaction strength (axis $U_0N$ in Fig. 4.5), when the lattice sites are made deeper and deeper ($V$ axis), the anisotropy of the density increases until it reaches a maximum value, and from there it decreases monotonically until it reaches 1. Although we had no reason to expect such behavior, which in fact is not predicted by $S_{cont}$ in the continuum limit[6], this can be a consequence of the poor description provided by the tight-binding approximation in situations which assume shallow lattice sites and therefore the results should not be taken too literally in this region. To complement the analysis, Figs. 4.6 (a) and (b) display the density profile of the $p_x$- and $p_y$-orbitals for a situation with moderate interaction, where $U_0N = 15$, $\omega = 0.005$ and $V = V_x = V_y = 17$, which confirms the results discussed here.

When the system is not confined, mean-field analysis reveals that the ground state is characterized by the staggered vortex-like solution. This corresponds to the most favorable configuration satisfying both requirements of tunneling and interaction parts which lead to the lowest energy. What happens now with the staggered vortex solution, when the system is harmonically confined?

As opposed to the non-confined system, the atomic cloud in the present case is not evenly distributed in the lattice, and as discussed previously, it has the approximate form of a Gaussian distribution. Here we investigate ground state properties and characterize the fate of the staggered vortex-like solution in terms of the mean-field version of Schwinger bosons, as discussed previously in Sec. 3.1.1. It was argued there, that the phase of the full onsite order parameter, Eq. (3.2), was characterized by a true vortex/anti-vortex profile only in the harmonic approximation. Outside this limit, even $J_{\mathbf{zj}} = 0$ didn't provide sufficient condition for rendering a perfect staggered vortex solution. And as discussed above, the confined system has already a natural imbalance in the number of atoms occupying the $p_x$ and $p_y$ orbital states, as seen in Fig. 4.4. Here it holds thus

[6]It should be noticed, however, that the expression provided by $S_{cont}$ is obtained in the limit of $U_0 = 0$ and it does not approach 1 as $V \to \infty$. On the other hand, under these circumstances any small $U_0 > 0$ is sufficient to make $S_{cont} \to 1$ since the kinetic term is going to be negligible relatively to interactions. For moderate values of the lattice depth $V$, $S_{cont}$ increases monotonically with increasing of $V$. This behavior is not confirmed by the predictions of the discrete model (Eq. (4.8)) and thus it should be kept in mind that the behavior predicted for the density anisotropy in the limit of deep lattices is qualitatively different in the continuum and discrete models.

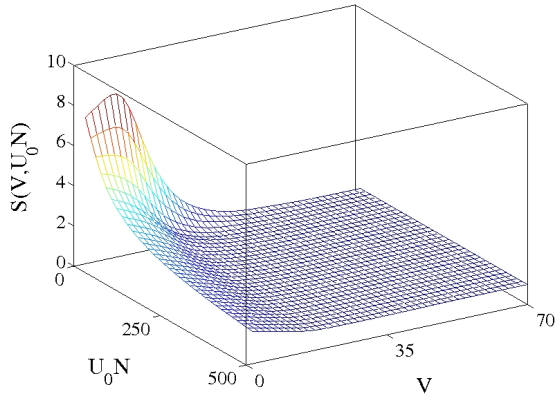


Figure 4.5.: The condensate anisotropy parameter $S$ (see Eq. (4.14)) as a function of the interaction strength $U_0N$ and of the lattice amplitude $V = V_x = V_y$ for the system with dimensionless trap frequency $\omega = 0.005$. It illustrates that the system enters the Thomas-Fermi regime whenever the relative strength of the tunneling compared to interactions becomes small, i.e., $S \to 1$.

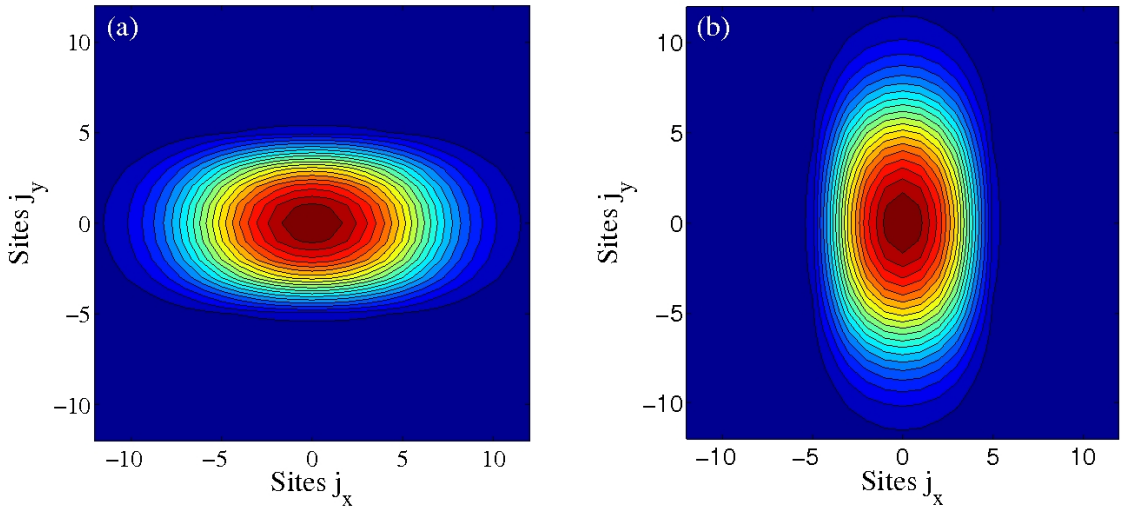


Figure 4.6.: These plots display populations in the $p_x$- (a) and $p_y$- (b) orbital states, for $V_x = V_y = 17$, $\omega = 0.005$ and $U_0N = 15$. Due to the strength of the interactions, the anisotropy in the density is not so pronounced as compared to the results in Figs. 4.4 (a) and (b).

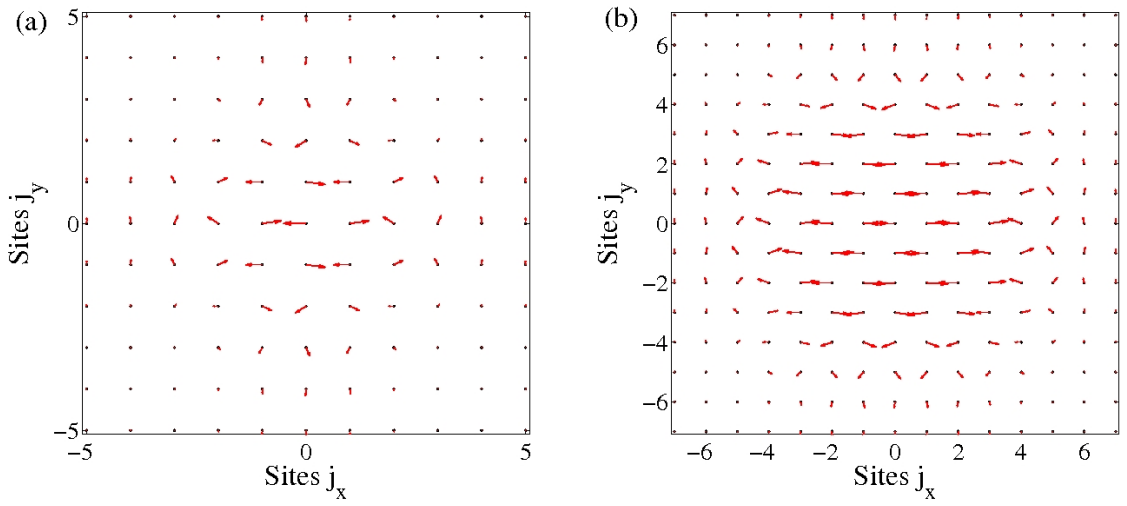


Figure 4.7.: Bloch vector at different sites of the optical lattice. We use the horizontal axis to represent the $y$-component of the spin and the vertical axis to represent the spin $z$-component. The $x$-component of the spin is strictly zero due to the specific onsite phase locking between the $p_x$-and the $p_y$-orbital states. Information about the density is encoded in the length of the Bloch vector (see Eq. (3.16)) and the offset from the horizontal axis encodes information about the breakdown of the antiferromagnetic order. The black dots are used to denote the lattice sites. In (a) $U_0N = 1$ and in (b) $U_0N = 15$. The other parameters are the same as in Fig. 4.6. This illustrates, in particular, that the staggered-vortex solution remains valid in a larger number of sites in the center of the trap in the limit of large interactions.

that in general $J_{z\mathbf{j}} \neq 0$, and the staggered vortex solution is certainly lost at the edges of the condensed cloud. In the center of the cloud, however, where $J_{z\mathbf{j}} \approx 0$, it is still possible to find characteristics of non-trapped like physics. This is illustrated in Figs. 4.7 (a) and (b), which display the Bloch vector in the $yz$-plane[7], $\mathbf{J_j} = (0, J_{y\mathbf{j}}, J_{z\mathbf{j}})$. By calling the horizontal axis the $y$-spin direction and the vertical axis the $z$-spin direction, we see that the $J_{y\mathbf{j}}$ component dominates at the center of the trap, while at the edges the Bloch vector no longer points along the horizontal direction. This reveals the breakdown of the staggered vortex solution in these regions. It also shows, however, that in the limit of larger interactions where the density becomes more symmetric, the staggered vortex-like solution holds true for a larger number of sites in the center of the trap.

### 4.2.3. Properties of the system in the anisotropic lattice

All the properties discussed so far addressed the case of a symmetric lattice, where the requirements ensuring the degeneracy of the orbital states were automatically fulfilled. This picture is modified in anisotropic or asymmetric lattices, where any small anisotropy/imperfection is in principle capable of lifting the degeneracy between the orbital states.

In particular, there are two ways of introducing anisotropies in the lattice discussed

[7]Recall here that $J_{x\mathbf{j}}$ is always zero.

here, either as a result of choosing different wave vectors, $k_x \neq k_y$, either as a result of having a lattice with different amplitudes $V_x \neq V_y$ in the different directions. What are the properties of the physics then, and how robust are the properties of the symmetric lattice with respect to small imperfections?

We investigate these issues by considering the second scenario, of a lattice with different amplitudes, and in terms of the anisotropy parameter

$$R = \frac{V_y}{V_x} \tag{4.31}$$

which controls the ratio between the lattice depths. The case of $R = 1$ recovers the symmetric lattice that was already discussed.

We have checked (numerically) that the main effect of the asymmetry is to shift the energy levels between the degenerate orbital states. The amount can be estimated in the harmonic approximation, for example, by considering the onsite energies of the $p_x$ and $p_y$ orbitals at the $\mathbf{j}$-th lattice site:

$$\Delta = E_y - E_x = 2\sqrt{V_x}(\sqrt{R} - 1), \tag{4.32}$$

where $E_\alpha = \int d\vec{r}\; w^*_{\alpha\mathbf{j}}(\vec{j})[-\nabla^2 + V_{lat}(\vec{r})]w_{\alpha\mathbf{j}}(\vec{j})$ is the energy of the $p_\alpha$ orbital state. This splitting is actually site independent, and as long as the value of $\Delta$ is much smaller than the energy scale set by the interaction terms, $E_U \sim U_0 N|\psi_x|^2$, it doesn't really affect the physics.

This picture becomes more complicated when more sites are taken into account. It can be the case, for example, that interaction is capable of coupling the order parameters of the orbital states in a small region $\delta$ around $R = 1$, such that small changes of the lattice parameters can lead to drastic changes in the properties of the ground state[8]. This is an important point to be considered here, because in case it is possible to accurately control these parameters, the physics in a neighborhood around the degeneracy point might reveal novel phenomena similar to adiabatic ramping through an avoided crossing[9] (as discussed in Ref. [40]). In this sense the parameter which computes population imbalance between the different orbital states

$$J_z = \frac{1}{N}\sum_{\mathbf{j}} J_{z\mathbf{j}}, \tag{4.33}$$

arises as a natural candidate for characterizing sensitivity of the system with respect to $R$. When $J_z = -1$, all the particles occupy only $p_y$ orbital states, and in the same way, when $J_z = 1$ all the particles occupy only $p_x$ orbital states. In addition, the case of $J_z = 0$ recovers the symmetric lattice, which is characterized by the equal sharing of population among the different orbitals. Now it is important to remember that the trap defines an effective size for the system that is fixed by $\omega$. Since this will set the extent to which finite size effects affect the system[10], we expect that sensitivity under variations of $R$ is greatly influenced by the values of the trap frequency.

[8] In the sense of changing its symmetry properties.

[9] It is important to point out, however, that since here the densities of different orbital states are spatially different, adiabatic driving could lead to macroscopic flow of particles within the trap.

[10] By transforming energy level crossings into avoided crossings, for example.

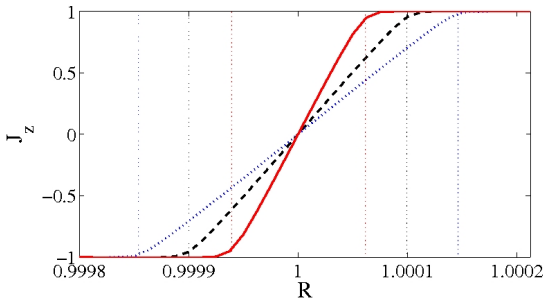


Figure 4.8.: The parameter for measuring population imbalance $J_z$ as a function of the lattice asymmetry parameter, $R$, and for different values of the trapping frequency. Here $U_0N = 1$ and $V_x = 17$. The vertical dashed lines are used to denote the typical sizes $\delta$ of the transition region where atoms coexist in the two orbital states. In particular, smaller values of $\omega$ are associated with smaller values of $\delta$. This means that the transition becomes sharper as the system's size increases.

Figure 4.8 depicts the behavior of $J_z$ around $R = 1$ for systems of different sizes, i.e., with different trapping frequencies $\omega$. It illustrates that the range of $\delta$ is smaller for larger systems, which implies that qualitative properties of the ground state will change more abruptly for increasing system sizes. We also verified numerically that $\delta$ increases with increasing values of the interaction strength $U_0N$, which is in agreement with the picture that the orbital order parameters are coupled by interactions.

This suggests thus that if the system interacts very weakly, a very fine tuning of the lattice parameters is required in order to investigate the properties of the ground state of the symmetric lattice. In addition, these properties become more robust in the limit of stronger interactions. In fact, even a small temperature could actually contibute to the establishment of phase coherence between the order parameters of the $p_x$ and $p_y$ orbital states in experimental realizations. This follows from the reduction of the energy gap between the ground and first excited states around the $R = 1$ point, that makes it easier for the atoms to occupy the first excited state. In particular, this is needed for balancing the population of the two orbitals. We furthermore notice that the transition from one to the other extreme of $J_z$ is smooth for nonzero $\omega$, and that by controlling the lattice amplitudes this system could realize a many-body Landau-Zener transition [41], which when $R$ is tuned externally could form a play-ground of the Kibble-Zurek [42] mechanism.

# 5. Beyond the mean-field approximation: Effective spin Hamiltonians via exchange mechanism

In the previous chapters we studied the physics of $p$-orbital bosons from a mean-field perspective. In this chapter we move away from the mean-field regime and study the physics of the strongly correlated Mott insulator phase of $p$-orbital bosons. We are particularly interested in the Mott-insulator state with a unit filling of the lattice sites[1] and mainly in the case of a $2D$ lattice.

As will be shown in Sec. 5.1, there is a regime for which the dynamics of the two orbital case can be effectively described by the Hamiltonian of the $XYZ$ quantum Heisenberg model in external field[2]. This spin model, in turn, is one of the classical models employed for describing quantum magnetism [44, 45], and particularly special for falling in the class of non-integrable models [46]. This means that there is no known heuristics leading to analytical solutions in closed form. On the other hand, as we show here, this physics is accessible with the use of bosons in the $p$ band of an optical lattice. In this context, therefore, $p$-orbital bosons constitute a nice controllable system that can be used as a *quantum simulator*[3] [3, 24].

This will be discussed in Sec. 5.1.1, where we characterize the phase diagram for the particular case of an effective $1D$ spin chain for both the infinite and finite cases. We continue then by presenting detection schemes which are capable of experimentally addressing the physics discussed, in Sec. 5.2. We conclude this study by extending the calculations for the three orbital case[4] in Sec. 5.5.

[1] We remark that this is the easiest case for experimental realizations of Mott phases for bosons in excited bands [43].

[2] This chapter is based in the study done in Paper II.

[3] The idea of quantum simulation dates back to 1982, in the work of Feynman entitled *Simulating Physics with Computers* [23]. In this work Feynman suggests that an alternative way to understanding computationally intractable systems (due to the exponential growth of the Hilbert space, for example) would be to find another system of experimental feasibility that has the same equations of motion. In this sense one physical system would be 'simulated' by another.

[4] That is, where an effective one-dimensional chain is constructed from a three-dimensional lattice.

## 5.1. $p$-orbital Bose system and effective spin Hamiltonian

Let us consider once more the second quantized Hamiltonian describing a system of $p$-orbital bosons in two dimensions[5]:

$$\begin{aligned}\hat{H} &= -\sum_{\alpha}\sum_{\langle i,j\rangle} t_{ij}^{\alpha}\hat{a}_{i,\alpha}^{\dagger}\hat{a}_{j,\alpha} + \sum_{i,\alpha}\left[\frac{U_{\alpha\alpha}}{2}\hat{n}_{i,\alpha}(\hat{n}_{i,\alpha}-1) + E_{\alpha}^{os}\hat{n}_{i,\alpha}\right] \\ &\quad + \sum_{i\alpha\neq\beta}\left(U_{\alpha\beta}\hat{n}_{i,\alpha}\hat{n}_{i,\beta} + \frac{U_{\alpha\beta}}{2}\hat{a}_{i,\alpha}^{\dagger}\hat{a}_{i,\alpha}^{\dagger}\hat{a}_{i,\beta}\hat{a}_{i,\beta}\right),\end{aligned} \tag{5.1}$$

where $\hat{a}_{i,\alpha}^{\dagger}$ creates a particle in the $p_{\alpha}$-orbital with $\alpha = \{x, y\}$ at site $i$, $\hat{n}_{i,\alpha} = \hat{a}_{i,\alpha}^{\dagger}\hat{a}_{i,\alpha}$, and where $\sum_{\langle i,j\rangle}$ is the sum over nearest neighbors. We remind again that the tunneling elements[6] $t_{ij}^{\alpha}$ and coupling constants $U_{\alpha\beta}$ depend on the orbital states and are given by Eqs. (2.33) and (2.32), and $E_{\alpha}^{os}$ denotes the onsite energy of the $p_{\alpha}$-orbital state.

Our interest here is in the physics of the Mott insulator phase with a unit filling of the lattice sites. In this regime the system admits description in terms of an effective Hamiltonian, obtained from the perturbative expansion of the tunneling processes up to second order in $t/U$. We give here a detailed description of the procedure [45, 47].

First let $\hat{H}$ act on the Hilbert space $\mathcal{H}$. Define $\mathcal{H}_P$ as the projection on the subspace $\hat{P}\mathcal{H}$ of states which describe sites occupied by one atom, and $\mathcal{H}_Q$, where $\hat{Q} = \hat{1} - \hat{P}$ the subspace of states with at least one doubly occupied site. Since both $\hat{P}$ and $\hat{Q}$ are projection operators, the following relations hold: $\hat{P}^2 = \hat{P}$ and $\hat{Q}^2 = \hat{Q}$. The eigenvalue problem associated to $\hat{H}$ can be decomposed as

$$\hat{H}\Psi = E\Psi \rightarrow \hat{H}\left(\hat{P}+\hat{Q}\right)\Psi \rightarrow \left(\hat{H}_K + \hat{H}_U\right)\left(\hat{P}+\hat{Q}\right)\Psi = E\Psi, \tag{5.2}$$

where $H_K$ and $H_U$ describe, respectively, the kinetic and the interaction terms of Eq. (5.1).

We then act with $\hat{Q}$ and $\hat{P}$ from the left

$$\begin{aligned}\left(\hat{Q}\hat{H}_K\hat{P} + \hat{Q}\hat{H}_K\hat{Q} + \hat{Q}\hat{H}_U\hat{P} + \hat{Q}\hat{H}_U\hat{Q}\right)\Psi &= E\Psi, \\ \left(\hat{P}\hat{H}_K\hat{P} + \hat{P}\hat{H}_K\hat{Q} + \hat{P}\hat{H}_U\hat{Q} + \hat{P}\hat{H}_U\hat{P}\right)\Psi &= E\Psi,\end{aligned} \tag{5.3}$$

and use that $\hat{Q}\hat{H}_K\hat{Q}$, $\hat{Q}\hat{H}_U\hat{P}$, $\hat{P}\hat{H}_K\hat{P}$ and $\hat{P}\hat{H}_U\hat{P}$ are all equal to zero[7] to obtain the following expression

$$\hat{Q}\Psi = -\frac{1}{\hat{Q}\hat{H}_U\hat{Q} - E}\hat{Q}\hat{H}_K\hat{P}\Psi, \tag{5.4}$$

which leads to

$$\hat{H}_{Mott_1} = -\hat{P}\hat{H}_K\hat{Q}\frac{1}{\hat{Q}\hat{H}_U\hat{Q} - E}\hat{Q}\hat{H}_K\hat{P}. \tag{5.5}$$

[5] In order to match the notation used in the previous chapters of this thesis, the notation here differs from what we used in Paper II.

[6] Notice here that $t_{ij}^{\alpha}$ is used to denote the tunneling of a $p_{\alpha}$-orbital atom from site $i$ to site $j$ in a generic way, and that the direction of the tunneling should be implicit in the $ij$ indices.

[7] The first three terms are equal to zero for connecting orthogonal projections of the Hilbert space, while the last term is equal to zero for computing interactions in states that have a unit occupation of the lattice sites.

So far this result is exact. It explicitly shows the effects of the tunneling, which acts as an intermediate and couples the different projections of the Hilbert space $\hat{P}\mathcal{H}$ and $\hat{Q}\mathcal{H}$. We summarize it here by considering the physics in two neighboring sites, and denote the states of the 2-site problem as $|\text{site}_{\mathbf{j}}, \text{site}_{\mathbf{j+1}}\rangle$. Let us start from a situation where each of these lattice sites are occupied by only one atom. Suppose then that the particle at the site $\mathbf{j}$ tunnels to the site $\mathbf{j+1}$. This yields a state where the $(\mathbf{j+1})$-th site is doubly occupied, and that has a corresponding matrix element which accounts for the interaction processes allowed by $\hat{H}_U$. After interaction has taken place, one of the particles is brought back to the site $\mathbf{j}$[8], and again, in the final state, the lattice sites are characterized by unit filling. This is the starting point for derivation of the effective Hamiltonian describing the $n = 1$ Mott ($\text{Mott}_1$) phase of $p$-orbital bosons. But up till now we have not yet specified the equations that describe the optical lattice. We use here the same sinusoidal potential as in Chapter 4,

$$V_{latt}(\mathbf{r}) = V_x \sin^2(k_x x) + V_y \sin^2(k_y y), \tag{5.6}$$

and remind once more that $V_\alpha$ and $k_\alpha$ are the amplitude and wave vector of the potential in the direction $\alpha = \{x, y\}$.

Under the assumptions of the Mott phase, the operator $1/(\hat{Q}\hat{H}_U\hat{Q} - E)$ in Eq. (5.5) can then be expanded to lowest order in $t/U_{\alpha\beta}$ in analogy to the customary procedure used for the large $U$ expansion of the Hubbard model at half filling [45, 47]. Let us consider the 2-site problem again[9] and define a basis for the $\mathcal{H}_P$ and $\mathcal{H}_Q$ subspaces:

$$\mathcal{H}_P \rightarrow \{|X, X\rangle, |X, Y\rangle, |Y, X\rangle, |Y, Y\rangle\} \tag{5.7}$$

and

$$\mathcal{H}_Q \rightarrow \{|0, 2X\rangle, |0, XY\rangle, |0, 2Y\rangle\}. \tag{5.8}$$

Notice, in particular, that the states listed above for a basis in $\mathcal{H}_Q$ are only the ones that are relevant for the perturbative calculation[10]. It also follows that the full energy in Eq. (5.5) is of the order of $E \sim t^2/U$, which makes it possible to consider $(\hat{H}_Q - E)^{-1} \approx \hat{H}_Q^{-1}$, where $\hat{H}_Q = \hat{Q}\hat{H}_U\hat{Q}$. However, due to the possibility of transferring population between the different orbital states via action of $\hat{H}_{FD}$, the projection of the Hamiltonian on the $\mathcal{H}_Q$ subspace is not diagonal in the basis of the intermediate states with doubly occupied sites. We therefore adapt the usual procedure for this situation and estimate the matrix elements for characterizing the virtual interaction resulting from the exchange processes by using the inverse matrix $\hat{H}_Q^{-1}$. Explicitly,

$$\hat{H}_Q = \begin{pmatrix} U_{xx} & 0 & U_{xy} \\ 0 & 2U_{xy} & 0 \\ U_{xy} & 0 & U_{yy} \end{pmatrix} \tag{5.9}$$

[8] Again via action of the tunneling Hamiltonian.
[9] Under the assumption of the tight-binding regime it is enough to consider what happens in two sites.
[10] In fact, these are precisely the intermediate states of the perturbative analysis.

and its inverse

$$\hat{H}_Q^{-1} = \begin{pmatrix} U_{yy}/U^2 & 0 & -U_{xy}/U^2 \\ 0 & 1/2U_{xy} & 0 \\ -U_{xy}/U^2 & 0 & U_{xx}/U^2 \end{pmatrix}, \tag{5.10}$$

where $U^2 \equiv U_{xx}U_{yy} - U_{xy}^2$. On this basis we arrive at the final form of the effective Hamiltonian by computing the relevant matrix elements of (5.5).

From states of the type $|\alpha_i, \alpha_j\rangle$

$$\hat{a}^\dagger_{\alpha,i}\hat{a}_{\alpha,j}\hat{H}_Q^{-1}\hat{a}^\dagger_{\alpha,j}\hat{a}_{\alpha,i}|\alpha_i,\alpha_j\rangle = \hat{a}^\dagger_{\alpha,i}\hat{a}_{\alpha,j}\hat{H}_Q^{-1}\sqrt{2}|0,2\alpha_j\rangle$$

$$= \sqrt{2}\hat{a}^\dagger_{\alpha,i}\hat{a}_{\alpha,j}\left(\frac{U_{\beta\beta}}{U^2}|0,2\alpha_j\rangle - \frac{U_{\alpha\beta}}{U^2}|0,2\alpha_j\rangle\right) = \frac{2U_{\beta\beta}}{U^2}|\alpha_i,\alpha_j\rangle$$

the effective Hamiltonian acquires a term of the form

$$-\sum_{\langle i,j\rangle}\sum_{\alpha}\frac{2|t_{ij}^{\alpha}|^2U_{\beta\beta}}{U^2}\hat{n}_{\alpha,i}\hat{n}_{\alpha,j}.$$

In the same way, from the states of the type $|\alpha_i, \beta_j\rangle$, with $\alpha \neq \beta$,

$$\hat{a}^\dagger_{\alpha,i}\hat{a}_{\alpha,j}\hat{H}_Q^{-1}\hat{a}^\dagger_{\alpha,j}\hat{a}_{\alpha,i}|\alpha_i,\beta_j\rangle = \hat{a}^\dagger_{\alpha,i}\hat{a}_{\alpha,j}\hat{H}_Q^{-1}|0,\alpha_j\beta_j\rangle$$

$$= \frac{1}{2U_{xy}}\hat{a}^\dagger_{\alpha,i}\hat{a}_{\alpha,j}|0,\alpha_j\beta_j\rangle = \frac{1}{2U_{xy}}|\alpha_i,\beta_j\rangle,$$

corresponding to the operator

$$-\sum_{\langle i,j\rangle}\sum_{\alpha}\frac{|t_{ij}^{\alpha}|^2}{2U_{xy}}\hat{n}_{\alpha,i}\hat{n}_{\beta,j}.$$

From the states of the type $|\beta_i, \alpha_j\rangle$ and the following process

$$\hat{a}^\dagger_{\alpha,i}\hat{a}_{\alpha,j}\hat{H}_Q^{-1}\hat{a}^\dagger_{\beta,j}\hat{a}_{\beta,i}|\beta_i,\alpha_j\rangle = \hat{a}^\dagger_{\alpha,i}\hat{a}_{\alpha,j}\hat{H}_Q^{-1}|0,\alpha_j\beta_j\rangle$$

$$= \frac{1}{2U_{xy}}\hat{a}^\dagger_{\alpha,i}\hat{a}_{\alpha,j}|0,\alpha_j\beta_j\rangle = \frac{1}{2U_{xy}}|\alpha_i,\beta_j\rangle,$$

the Hamiltonian gains a contribution as

$$-\sum_{\langle i,j\rangle}\sum_{\alpha}\frac{t_{ji}^{\alpha}t_{ij}^{\beta}}{2U_{xy}}\hat{a}^\dagger_{\alpha,i}\hat{a}_{\beta,i}\hat{a}^\dagger_{\alpha,j}\hat{a}_{\beta,j}.$$

Finally, we consider the states of the type $|\beta_i, \beta_j\rangle$,

$$\hat{a}^\dagger_{\alpha,i}\hat{a}_{\alpha,j}\hat{H}_Q^{-1}\hat{a}^\dagger_{\beta,j}\hat{a}_{\beta,i}|\beta_i,\beta_j\rangle = \hat{a}^\dagger_{\alpha,i}\hat{a}_{\alpha,j}\hat{H}_Q^{-1}\sqrt{2}|0,2\beta_j\rangle$$

$$= \sqrt{2}\hat{a}^{\dagger}_{\alpha,i}\hat{a}_{\alpha,j}\left(\frac{U_{\alpha\alpha}}{U^2}|0,2\beta_j\rangle - \frac{U_{xy}}{U^2}|0,2\alpha_j\rangle\right) = -\frac{2U_{xy}}{U^2}|\alpha_i,\alpha_j\rangle,$$

that contribute to the effective Hamiltonian with a term that changes the orbital states of the atoms in both sites

$$\sum_{<i,j>}\sum_{\alpha,\alpha\neq\beta}\frac{2t^{\alpha}_{ji}t^{\beta}_{ij}U_{xy}}{U^2}\hat{a}^{\dagger}_{\alpha,i}\hat{a}_{\beta,i}\hat{a}^{\dagger}_{\beta,j}\hat{a}_{\alpha,j}.$$

The resulting expression for the effective Hamiltonian corresponds thus to

$$\begin{aligned}\hat{H}_{Mott} = -\sum_{\langle i,j\rangle}\sum_{\alpha}\Bigg(&\frac{2|t_\alpha|^2U_{\beta\beta}}{U^2}\hat{n}_{\alpha,i}\hat{n}_{\alpha,j} + \frac{|t_\alpha|^2}{2U_{xy}}\hat{n}_{\alpha,i}\hat{n}_{\beta,j}\\ &-\frac{2t^{\alpha}_{ji}t^{\beta}_{ij}U_{xy}}{U^2}\hat{a}^{\dagger}_{\alpha,i}\hat{a}_{\beta,i}\hat{a}^{\dagger}_{\alpha,j}\hat{a}_{\beta,j} + \frac{t^{\alpha}_{ji}t^{\beta}_{ij}}{2U_{xy}}\hat{a}^{\dagger}_{\alpha,i}\hat{a}_{\beta,i}\hat{a}^{\dagger}_{\beta,j}\hat{a}_{\alpha,j}\Bigg).\end{aligned} \tag{5.11}$$

We now use the orbital states to define the Schwinger spin operators [48]

$$\begin{aligned}\hat{S}^z &= \frac{1}{2}(\hat{a}^{\dagger}_x\hat{a}_x - \hat{a}^{\dagger}_y\hat{a}_y)\\ \hat{S}^+ &= \hat{S}^x + i\hat{S}^y = \hat{a}^{\dagger}_x\hat{a}_y\\ \hat{S}^- &= \hat{S}^x - i\hat{S}^y = \hat{a}^{\dagger}_y\hat{a}_x,\end{aligned} \tag{5.12}$$

and together with the constraint of unit occupation of the lattice sites in the Mott$_1$ phase, i.e. $\hat{n}_{x,i} + \hat{n}_{y,i} = 1$, we rewrite Eq. (5.11) as

$$\hat{H}_{Mott} = -\sum_{\langle i,j\rangle}\left(J^{zz}\hat{S}^z_i\hat{S}^z_j + J^{xx}\hat{S}^x_i\hat{S}^x_j + J^{yy}\hat{S}^y_i\hat{S}^y_j\right) - \sum_i J^z\hat{S}^z_i.$$

This shows that within the perturbative regime, the physics of bosonic atoms in the orbital states of a $2D$ optical lattice is well described by the $XYZ$ quantum Heisenberg model in an external field, where all the parameters of the spin model depend on the lattice configuration. We notice, in addition, that no assumption regarding the geometry of the lattice was used, and thus this derivation applies to square lattices, hexagonal lattices, etc.

From now on we restrict the study to the case of asymmetric lattices with very deep potential wells in one of the axis, say the $y$-direction, in such a way to yield an effective $1D$ dynamics[11] (here along the $x$ axis). At the same time the wave vectors are adjusted so that the quasi-degeneracy of the orbital states is maintained[12]. In other words, we are considering the case where $|t_{xy}|, |t_{yy}| \to 0$ and also that $U_{\alpha\beta} \gg |t_{xx}|, |t_{yx}|$ due to the

[11] Here we focus on the effective $1D$ system, but generalizations of the procedure for computing the couplings of the effective Hamiltonian for the $2D$ system is straightforward.

[12] In the harmonic approximation this is achieved by imposing that $V_x k_x^2 = V_y k_y^2$. For sinusoidal lattices there is no simple relation which states the degeneracy condition, but this can be numerically checked for various lattice configurations.

strong coupling regime condition. Therefore, in terms of the lattice parameters, the expression for the various couplings follow

$$J^{xx} = \frac{2t_x t_y}{U_{xy}}\left(1 - 4\frac{U_{xy}^2}{U^2}\right), \tag{5.13}$$

$$J^{yy} = \frac{2t_x t_y}{U_{xy}}\left(1 + 4\frac{U_{xy}^2}{U^2}\right), \tag{5.14}$$

$$J^{zz} = 4\frac{|t_x|^2 U_{yy}}{U^2} + 4\frac{|t_y|^2 U_{xx}}{U^2} - \frac{|t_x|^2}{U_{xy}} - \frac{|t_y|^2}{U_{xy}}, \tag{5.15}$$

$$J^{z} = \frac{2|t_x|^2 U_{yy}}{U^2} - \frac{2|t_y|^2 U_{xx}}{U^2} + (E_x^{os} - E_y^{os}). \tag{5.16}$$

We adopt here the standard notation used for the $XYZ$ Heisenberg model and define $J = -2t_x t_y/U_{xy}$, $\Delta = -J^{zz}$, $h = -J^z$, and $\gamma = -4U_{xy}^2/U^2$, in terms of which the Hamiltonian is then rewritten as

$$\hat{H}_{XYZ} = \sum_{\langle i,j\rangle} J\left[(1+\gamma)\hat{S}_i^x\hat{S}_j^x + (1-\gamma)\hat{S}_i^y\hat{S}_j^y + \frac{\Delta}{J}\hat{S}_i^z\hat{S}_j^z\right] + h\sum_i \hat{S}_i^z. \tag{5.17}$$

Notice that the tunneling in the $p$ band satisfies $t_x t_y < 0$ and therefore $J > 0$. In addition, since $|\gamma| < 1$ the interactions between the $x$-component and the $y$-component of neighboring spins always favor for anti-ferromagnetic order. This is an interesting property, for bosonic particles always preserve the sign of the wave function under exchange processes, and thus it is more natural for a bosonic system to display ferromagnetic order. This is not the case here, however, and its only possible because of the specific properties of the tunneling in the $p$ band.

Another important feature of this spin model which follows solely due to the properties of the $p$-orbital bosonic system, is the appearance of the anisotropy parameter $\gamma$ which breaks the rotational symmetry characteristic of the $XXZ$ Heisenberg model[13]. In fact, this is a consequence of the terms describing transit of population between the different orbital states, in $\hat{H}_{FD}$, which break the continuous $U(1)$ symmetry of the Hamiltonian to a set of $Z_2$ symmetries. Accordingly, the resulting $XYZ$ spin model is also invariant only to discrete $Z_2$ symmetries. This property is related to the 'parity' of the states of the many-body Hamiltonian, which divides the eigenstates into states with even or odd number of atoms in the $p_x$ and $p_y$ orbitals.

The importance of the orbital changing term in the dynamics of the effective spin model can be further investigated in terms of the Jordan-Wigner transformation [51]

$$\begin{aligned}\hat{S}_i^- &= e^{i\pi\sum_{j=1}^{i-1}\hat{c}_j^\dagger\hat{c}_j}\hat{c}_i \\ \hat{S}_i^+ &= \hat{c}_j^\dagger e^{i\pi\sum_{j=1}^{i-1}\hat{c}_j^\dagger\hat{c}_j},\end{aligned} \tag{5.18}$$

[13]The same procedure applied to the usual (ground band) Bose-Hubbard Hamiltonian with one atom per site yields spin chains with continuous symmetries (as is the case of the $XXZ$ model), and which typically favor for ferromagnetic order [49, 50].

where the $\hat{c}_j$ are fermionic operators satisfying $\{\hat{c}_i, \hat{c}_j\}=\{\hat{c}_i^\dagger, \hat{c}_j^\dagger\}= 0$ and $\{c_i, c_j^\dagger\}= \delta_{ij}$. This yields the fermionic Hamiltonian

$$\begin{aligned}\hat{H}_K/J = \sum_n \Big[&(\hat{c}_n^\dagger \hat{c}_{n+1} + \hat{c}_{n+1}^\dagger \hat{c}_n) + \gamma(\hat{c}_n^\dagger \hat{c}_{n+1}^\dagger + \hat{c}_{n+1}\hat{c}_n) \\ &+ \tfrac{\Delta}{J}(\hat{c}_n^\dagger \hat{c}_n - \tfrac{1}{2})(\hat{c}_{n+1}^\dagger c_{n+1}^\dagger - \tfrac{1}{2}) + \tfrac{h}{J}(\hat{c}_n^\dagger \hat{c}_n - \tfrac{1}{2})\Big]\end{aligned} \tag{5.19}$$

that contains a pairing term proportional to $\gamma$. The presence of a pairing term typically opens a gap in the energy spectrum, and therefore we expect the spectrum to be gapped whenever $\gamma \neq 0$. In addition, we notice furthermore that the limit of $\Delta \to 0$ is a realization of the Kitaev chain [52].

### 5.1.1. Properties of the ground state: the phase diagram of the $XYZ$ model

We illustrate the rich physics of the $XYZ$ model in external field by discussing the phase diagram for the $1D$[14] open chain[15]. One dimensional quantum systems are particularly interesting, for quantum effects are specially pronounced in low dimensions.

> One dimensional quantum systems require a description which accounts for the collective rather than individual behavior of their constituent parts [53]. To see this more explicitly, let us consider, for example, a system of spinless bosons with repulsive interactions in one dimension. Such a system is described in general terms by a symmetric wave-function. But in the limit of infinitely repulsive interactions - the *Tonks-Girardeau limit*, it is reasonable to assume that the amplitude of this wave-function should decrease in the neighborhood of any of the bosonic particles, and vanish completely at the exact values for which the probability of finding any of these particles is maximum, as shown in Fig. 5.1.
>
> Now the symmetric wave-function shown in Fig. 5.1 can be used to construct an alternative anti-symmetric wave-function via reflection to the negative axis, with nodes that reproduce the nodes of the symmetric case. At the level of the wave-functions, the description provided by the symmetric and anti-symmetric wave-functions will be very different. In fact, collective anti-symmetric wave-functions describe systems of non-interacting fermions, not of bosons. But the construction of this anti-symmetric wave-function can be considered in such a way that its absolute value reproduce the absolute value of the symmetric wave-function. This means, therefore, that the properties of the bosonic system at the level of densities, as e.g. density-density correlation functions, can be completely inferred from the properties of a system of non-interacting fermions. This process is usually referred to as the *fermionization of bosons* [54], and is used here to illustrate how interesting and maybe counter intuitive nature can become when collective behavior is allowed to play a role in low dimensional quantum systems.

[14] We remark that little is known about the $XYZ$ Heisenberg model in external field in higher dimensions. In addition to not having analytical solutions, numerical treatment of this problem is very limited due to the exponential growth of the Hilbert space and becomes intractable already for a small number of spins in $2D$ (less than 8x8 sites).

[15] That is, with open boundary conditions.

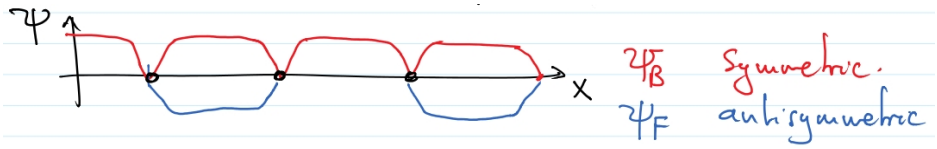


Figure 5.1.: One dimensional system of infinitely repulsive bosonic particles. The position of the bosons are the black dots in the $x$-axis and the red and blue wave functions are the corresponding symmetric and anti-symmetric descriptions. This figure is taken from Ref. [54].

Now in $1D$ the ground state of the system described by Eq. (5.17) experiences four different phases as the parameters of this Hamiltonian are varied. A schematic phase diagram is illustrated in Fig. 5.2. At zero field, the $XYZ$ Heisenberg model is integrable[16] with known analytical expressions for the eigenvalues and the eigenvectors [55]. At large positive values of $\Delta/J$ the system has anti-ferromagnetic order in the $z$-direction. For small values of $\Delta/J$, the system displays Nèel ordering in the $y$-direction and is in the so called spin-flop phase [56]. The $h = 0$ line for large negative values of $\Delta/J$ is characterized by a ferromagnetic phase in the $z$-direction, and for all the cases, the limit of large external field displays a magnetized phase, where the spins align along the orientation of the field in the $z$-direction. These three phases also characterize the phase diagram of the $XXZ$ model in a longitudinal field [44]. For non-zero anisotropy $\gamma$, however, the system has an additional phase in between the anti-ferromagnetic and spin-flop phases that is called as the floating phase [56]. This is a gapless phase characterized by algebraic decay of the correlations[17]. Notice, in particular, that this property is unexpected from the point of view of the fermionic chain, where as stated before for values of $\gamma \neq 0$ the Hamiltonian contains a pairing term, which typically opens a gap in the energy spectrum.

All these phases are separated by different types of phase transitions. The transition from the anti-ferromagnetic to the floating phase is of the commensurate to incommensurate (C-IC) type, whereas the transition from the floating phase to the spin flop phase is a Berezinski-Kosterlitz-Thouless (BKT) transition. For $\Delta < -(1 + |\gamma|)$ there is a first order phase transition at $h = 0$ between the two polarized phases (all spins up or all spins down) and finally, between the spin flop and the polarized phases there is an Ising transition.

In what follows we give a brief description of the properties of the different phases and the different types of phase transitions. Here we illustrate these concepts in the context of interacting spins, where we consider an Ising-like Hamiltonian given by $H_{Ising} = -J\sum_{\langle i,j\rangle} \hat{\mathbf{S}}_i\hat{\mathbf{S}}_j + h\sum_i \hat{\mathbf{S}}_i$.

- Nèel order: Nèel order is the term generally used to describe a state with

[16] It was shown by Sutherland, in 1970 [46, 55], that the transfer matrix of any zero-field *eight-vertex model* commutes with the Hamiltonian of the $XYZ$ Heisenberg model. In addition, it was shown by Baxter in 1971 and 1972 that for any values of the couplings in the Hamiltonian of the $XYZ$ model, Eq. (5.17), this operator is effectively a logarithmic derivative of an eight-vertex transfer matrix and therefore the minimum eigenvalue of Eq. (5.17) can be obtained [46, 55]. Baxter study properties of the ground state of the $XYZ$ model by generalizing the Bethe ansatz [55], and in 1973 Baxter's results were generalized by other authors and used for computing the energy of the excitations of the $XYZ$ model.

[17] In terms of bosonization [53, 57] and renormalization group arguments, the floating phase is characterized by irrelevant *Umklapp* terms and accordingly described by the Luttinger Liquid theory. Upon entering the $XY$ phase these terms are no longer irrelevant and the phase becomes gapped [56].

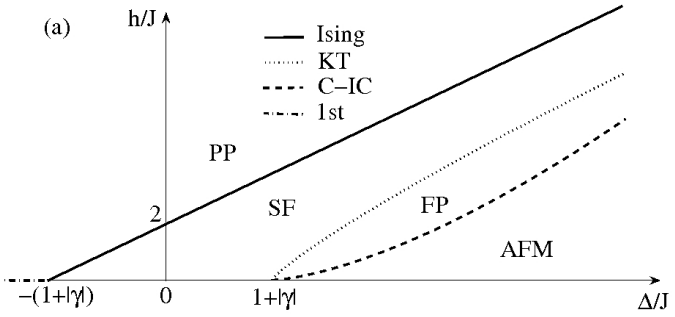


Figure 5.2.: Schematic phase diagram of the *XYZ* chain. AFM denotes the anti-ferromagnetic phase, FP the floating phase, SF the spin flop phase and PP the polarized phase. The properties of these phases and of the different types of phase transitions are discussed in the text.

broken symmetry and for which

$$\langle \hat{\mathbf{S}}_i \rangle \neq 0$$

for all the spins [58]. And although this is most commonly used to refer to the bipartite lattice, i.e., the Nèel anti-ferromagnet, where the direction neighboring spins alternate in opposite directions [58], there are more complex patterns that also correspond to a Nèel state [58].

- Anti-ferromagnetic phase ($J < 0$): as stated above, the anti-ferromagnetic phase is characterized by Nèel order with alternating neighboring spins. States of this type are characterized by staggered magnetization [58], and therefore the net magnetization is vanishing:

$$M = \sum_i \langle \hat{\mathbf{S}}_i \rangle = 0.$$

- Floating phase ($J < 0$): this is a gapless phase without long range order, and for which the correlations decay algebraically [59].
- Spin-flop phase ($J < 0$): this corresponds to a gapped phase with Nèel order in the $x$ and $y$ components of the spin. It is again a gapped phase, with exponential decay of the correlations.
- Highly magnetized state or polarized phase ($J < 0$): for sufficiently large $h$, the phase diagram of spin models subjected to external fields will always display a highly magnetized state, where the spins align in the direction of the field. This corresponds to a 'forced' order, in the sense that there is no symmetry breaking involved in the ordering processes and the spins are uncorrelated.
- Ferromagnetic phase ($J > 0$): for the case of positive $J$ both the spins and their neighbors align in the same direction, which therefore builds a highly magnetized state. Here, however, as opposed to the polarized phase, the ordering is accompanied of symmetry breaking, with an order parameter similar to the order parameter of the anti-ferromagnetic phase [58].

We now briefly discuss the properties of the different types of phase transitions that appear in the phase diagram of the infinite system, Fig. 5.2:

- Ising transition: the transition between the polarized and the spin flop phases belongs to the universality class of the $2D$ Ising model. It is classified as a continuous or second order phase transition, and therefore the discontinuities

appear at the level of the order parameter (or second derivatives of the energy). In the Ising transition the critical exponent related to the divergence of the *correlation length* goes as $\xi \propto$ (distance from the transition)$^{-1}$ as one approaches the critical point, and in addition, the dynamical critical exponent[18] ($z$) is also equal to one [61, 62].

- Berezinski-Kosterlitz-Thouless (BKT) transition: BKT transitions also belong to the class of continuous phase transitions. They are rather special, however, for the derivatives of the energy don't present discontinuities (they are sometimes referred to as infinite order phase transitions), and there is no local order parameter [63]. In fact, BKT transitions do not involve symmetry breaking and are not described by the Landau theory.
- Commensurate to incommensurate (C-IC) transition: the C-IC transition happens due to the interplay of competing length scales in the system. In a periodic system, the collective excitations can develop a periodic structure that has different period from the 'natural period of the system'. These structures could comprise kinks, walls or solitons[19] [64].
- First order phase transition: in thermodynamic systems, first order phase transitions are defined as transitions that involve coexistence of phases, latent heat, and the discontinuities appear in the first derivative of the free energy [61]. In the same way, in quantum phase transitions[20], the discontinuities appear in the first derivative of the ground state energy as one of the parameters of the Hamiltonian is varied.

Since any implementation of the Heisenberg model will contain effects of finite size due to the harmonic confinement inevitably required for experimental realizations with cold atoms, it is important to reproduce these studies in systems with finite sizes. In the presence of confinement, in addition, it might also be the case that the inhomogeneities in the density affect the properties of the system. Here, however, as long as the trap is smooth enough such that the system satisfies the requisites of the local density approximation (as discussed in Sec. 4.1), effects stemming from the confinement renormalize the couplings such that they become spatially dependent. In the same way, as long as the sizes of the orbitals are very small compared to the length scale imposed by the trap, this spatial dependency is not relevant for the physics, and can therefore be neglected [27]. For this reason we restrict our study of finite size effects to the case of the open chain with constant coupling coefficients. We perform exact diagonalization for the system with 18 spins and focus on the behavior of the total magnetization of the ground state

$$M = \sum_i \langle \hat{S}_i^z \rangle \tag{5.20}$$

for different values of $h/J$ and $\Delta$. $\gamma$ is assumed to be fixed and the result is presented in Fig. 5.3: While both the anti-ferromagnetic (AFM) and the polarized (PP) phases are clearly visible, numerical treatment of this system exposes that in between these phases, the total magnetization develops a step-like structure. We attribute these steps in $M$ to a *devil's staircase structure* of spin density waves (SDW) [59]. In fact, the

[18] The dynamical critical exponent is the exponent defined to characterize the behavior of the correlation time near the critical point. In the same way as it works for the correlation length, the correlation time also diverges in the vicinity of the phase transition. The divergence of the correlation time implies that the fluctuations on any observable become incredibly slow, a phenomenon that is known as the *critical slowing down* [60, 61].

[19] A very good review on the subject is given in Ref. [59].

[20] Here there is no concept of temperature, i.e., quantum phase transitions happen at $T = 0$ and due to competition between non-commuting terms in the Hamiltonian of the system [65].

change in the total magnetization appears as a consequence of the modulation of the anti-ferromagnetic pattern (of the anti-ferromagnetic phase), which happens as one runs through larger and larger values of $h$. his also mean, for the finite system, that it is only possible to give a precise quantitative estimate for the Ising transition between the polarized and the spin flop phase[21]. While it is not clear whether the C-IC transition can be captured by this procedure, the BKT transition is certainly overshadowed by the sharp transitions between the different spin density waves. In the thermodynamic limit this staircase becomes complete and one then recovers the phase diagram displayed in Fig. 5.2[22]. These transitions between the different SDW are more pronounced for moderate system sizes and we estimate approximately 15 different SDW between the anti-ferromagnetic and polarized phases of a system with 50 spins[23].

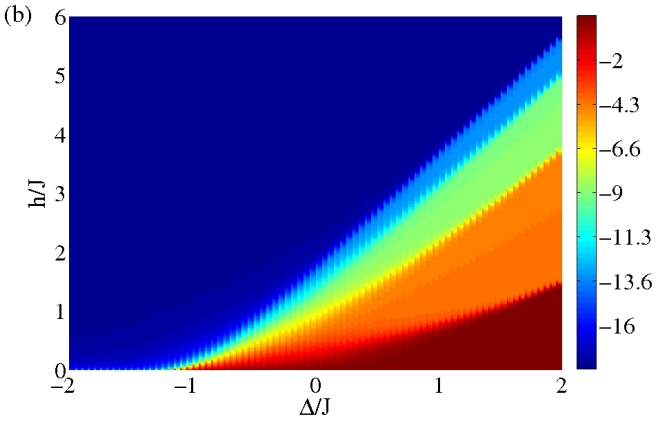


Figure 5.3.: Finite size 'phase diagram' obtained from exact diagonalization of a system with 18 spins and with the anisotropy parameter $\gamma = 0.2$. It displays the total magnetization $M$ (as defined in the text) which is characterized by an incomplete devil's staircase of SDW between the AFM and the PP phases.

## 5.2. Measurements, manipulations & experimental probing

The entire derivation of the spin chain for effectively describing the $\text{Mott}_1$ phase of $p$-orbital bosons was based on the fact that the spins are encoded in spatial degrees of freedom rather than in internal atomic states. Experimental manipulation/detection in this system requires therefore the ability of controlling the spatial states of the atoms at single sites. This can be done by combining single-site addressing [67] with techniques used in trapped ion physics. And by exploiting the symmetries of the $p_x$- and the $p_y$-orbital states, stimulated Raman transitions can drive both sideband and carrier transitions for the chosen orbitals in the *Lamb-Dicke regime*.

[21] At least by using the total magnetization as the order parameter.

[22] In fact, using similar heuristics, i.e., going up and down the steps of a complete devil's staircase, Chuck Norris counted to infinity - twice [66].

[23] We consider here that the chain with 50 spins is supposed to provide a very good experimental picture of the system that we would like to realize.

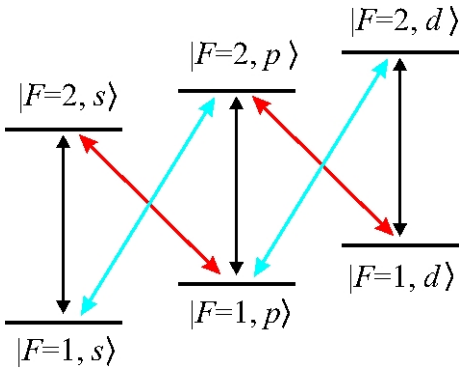


Figure 5.4.: Schematic representation of the coupling between the different orbital states at a single site. While the internal atomic electronic states are coupled by the carrier transition, the different orbital degrees of freedom are coupled by the sideband transitions. As depicted in the figure, the red and blue sideband transitions lower and raise, respectively, the external vibrational state with a single phonon.

Let us consider the two internal atomic electronic states for $^{87}$Rb atoms $F = 1$ and $F = 2$ Raman coupled with two lasers with amplitudes $\Omega_1$ and $\Omega_2$ and wave vectors $\mathbf{k_1}$ and $\mathbf{k_2}$. The matrix element describing this transition is given by

$$\frac{\Omega_1\Omega_2}{\delta}\langle F = 2|e^{i(\mathbf{k}_1-\mathbf{k}_2)\mathbf{x}}|F = 1\rangle, \tag{5.21}$$

where $\delta$ is the detuning of the transitions relative to the ancilla electronic state. In the usual case the spatial dependence of the lasers will induce couplings between vibrational states of the atom, and this, here, corresponds to the different bands. By making the effective *Rabi frequency* very large, $\Omega = \Omega_1\Omega_2/\delta$, the duration of a $\pi/2$-pulse, for example, can be made very short in comparison with any other time scale in the system and therefore it is reasonable to consider that the dynamics in the system is frozen during the applied pulse[24]. Furthermore, accidental degeneracies between other undesired states can be removed by driving resonant two-photon transitions.

In the region of parameters that is interesting for the physics considered here, i.e., deep in the Mott insulator phase, single sites can be approximated with two-dimensional harmonic oscillators with frequencies $\omega_\alpha = \sqrt{2V_\alpha k_\alpha^2/m}$ and the *Lamb-Dicke parameters* [68, 69] become $\eta_\alpha = k_\alpha\sqrt{\hbar/2m\omega_\alpha}$. Moreover, in the Lamb-Dicke regime, when $\eta_\alpha \ll 1$, multi-photon transitions can additionally be neglected, and as illustrated in Fig. 5.4, this leaves three possible transitions for the one-dimensional case:

(I) Carrier transitions - with no change in the vibrational state;

(II) Red sideband transitions - which lower the vibrational state with one quantum;

(III) Blue sideband transitions - which raise the vibrational state with one quantum.

These different transitions are not degenerate, and therefore it is possible to select single transitions by carefully choosing the frequencies of the lasers. And in these terms, or

[24]Indeed, this same assumption applies for experiments with single-site addressing in optical lattices [67].

with the use if these techniques, it is also possible to singly adress the different orbitals. The $p_x$-orbital state, for example, can be addressed by considering $\mathbf{k}_1 - \mathbf{k}_2 = k_x$ such that there is no component in the $y$-direction.

This also provides a means for fully controlling the system, for this is achieved if every unitary $\hat{R}_\beta(\phi) = e^{\hat{S}^\beta \phi}$, where $\beta = \{x, y, z\}$ and $\phi$ is an effective rotation, can be realized. To see that this is the case we discuss implementation of $\hat{R}_z(\phi)$ and $\hat{R}_x(\phi)$. We start with the simplest case, of rotations on the $z$-component of the spin by first noticing that $\hat{S}^z = \hat{S}^+\hat{S}^- - 1$. Here it is enough to realize the operation $\hat{S}^+\hat{S}^-$, which consists of a phase shift of one of the orbitals. This is most easily done by driving the carrier transition off-resonantly for one of the two-orbitals, and since the driving is largely detuned, this corresponds to Stark shifting one of the orbitals.

The $\hat{R}_x(\phi)$ operation can be implemented by simultaneously driving off-resonantly the red sidebands of the two orbitals. Due to the large detuning, the $s$-band will never become populated but the transition between the two orbitals can be made resonant. More explicitly, this operation involves the three states that we denote here as $\{|x, 0, 0\rangle, |0, y, 0\rangle$ and $|0, 0, s\rangle\}$, where the last entry of the ket refers to the state in the $s$-band. The $p$-orbitals are coupled to the $s$-orbital in a $V$-configuration, that in the *rotating wave approximation* is described by [70]

$$\hat{H}_V = \begin{bmatrix} 0 & 0 & \Omega_1 \\ 0 & 0 & \Omega_2 \\ \Omega_1 & \Omega_2 & \delta \end{bmatrix}, \tag{5.22}$$

where $\Omega_1$ and $\Omega_2$ are considered real and spatially dependent. For $\delta \gg \Omega_1, \Omega_2$ the Hamiltonian that generates a rotation of the $x$-component of the spin, $\hat{R}_x(\phi)$,

$$\hat{H}_x = \begin{bmatrix} 0 & \Omega \\ \Omega & 0 \end{bmatrix} = \Omega \hat{S}_x, \tag{5.23}$$

is then obtained after adiabatic elimination of the state $|0, 0, s\rangle$. Notice, however, that if the Raman transition between the two orbitals is not resonant, then this process will perform a combination of rotations in the $x$ and $z$ components of the spin. Rotations in the $y$ component of the spin, in addition, can be performed in two ways, either by adjusting the phases of the lasers, or either by noticing that $\hat{R}_y(\phi) = \hat{R}_z(\pi/4)\hat{R}_x(\phi)\hat{R}_z(-\pi/4)$.

This method allows thus for any manipulation of single spins at a given site. To measure the state of the spin in a given direction one then combines the rotations with single site resolved fluorescence (which acts as measuring $\hat{S}_i^z$) [71]. More precisely, since the drive laser can couple to the two orbitals individually, one of the orbitals will be transparent to the laser while the other one will show fluorescence. In other words, one then measures $\hat{S}_i^z$ on a single site. The other components of the spin can also be measured in this way, but after the correct rotation to the spin state has been previously implemented. Furthermore, with the help of coincident detection, it is possible to extract correlators of the type $\langle \hat{S}_i^\alpha \hat{S}_j^\beta \rangle$, $\alpha, \beta = \{x, y\}$ [72].

### 5.2.1. External parameter control

The spin mapping carried out in Sec. 5.1 provides a route for obtaining the Hamiltonian that effectively describes the physics of Mott$_1$ phase of $p$-orbital bosons. In that procedure, all the couplings in the spin picture are shown to depend initially on the parameters of the bosonic system, and therefore also on the configuration of the optical potential.

In order to give a qualitative estimate for the couplings in the spin model we make use of the analytical expressions derived in Sec. 2.3.1, where the parameters of the Hamiltonian for $p$-orbital bosons were considered in the harmonic limit. Introducing the widths of $\sigma_\alpha$ of the orbital wave functions for the spatial directions $\alpha = \{x, y, z\}$, the expressions of the couplings in this approximation are given by (see appendix A for the derivation)

$$U_{xx} = U_{yy} = 3U_{xy} = \frac{u_0}{\sigma_x \sigma_y \sigma_z}, \tag{5.24}$$

where $u_0$ is used here to denote an effective strength of the interactions, proportional to the $s$-wave scattering length. According to Eq. (5.15), this reveals that the interactions in the $z$ component of the spin favor primarily for ferromagnetic order, i.e., $\Delta < 0$. In fact, using that $|t_x|^2 \gg |t_y|^2$,

$$\Delta \approx -|t_x|^2 \left( 4 \frac{U_{yy}}{U_{xx} U_{yy} - U_{xy}^2} - \frac{1}{U_{xy}} \right), \tag{5.25}$$

which in the harmonic approximation becomes

$$\Delta = -|t_x|^2 \frac{3\sigma_x \sigma_y \sigma_z}{2u_0} < 0. \tag{5.26}$$

Similar computation yields $\gamma = 1/2$, which gives anti-ferromagnetic couplings for the spin $x$ and $y$ components. We notice in addition that even though computation of the couplings with the lattice Wannier functions yield different values for the couplings, it does not change the qualitative properties of the physics obtained via the harmonic approximation. In particular, we have numerically checked that $\Delta$ is always negative, even outside of this limit.

The fully anti-ferromagnetic regime can be reached, however, with application of the same ideas discussed in the previous section. This is again based on the techniques developed for trapped ion physics, and more explicitly, with driving the carrier transition of either of the two orbitals dispersively, with a spatially dependent field[25]. If the shape of the drive is chosen in such a way that the resulting Stark shift is weaker in the center of the sites, then this procedure will narrow the orbital in one of the directions and we say that the orbital is squeezed. Let us assume that the squeezing is implemented here in the $y$-direction. Then the only requirement is that the spatial profile of the field driving the carrier transition changes in the length scale of the lattice spacing in this direction. The tunneling rates $t_x$ and $t_y$ will not be affected by the squeezing but with this procedure it is possible to change both $U_{yy}$ and $U_{xy}$ and therefore it is also possible

[25] This is nothing but a potential that reshapes the lattice sites in different ways for the different orbitals, and that can be implemented as a change in the $\sigma_y$ widths of the different Wannier functions ($w_x(\vec{r})$ and $w_y(\vec{r})$) of the orbitals, while the widths $\sigma_x$ are kept unaltered.

to tune the coupling constants. To be more specific, let us assume that the ratio $\sigma$ of the harmonic length scales of the $p_x$ and the $p_y$ orbitals is tuned (in the $y$-direction). A straightforward calculation using harmonic oscillator functions yields

$$\alpha \equiv \frac{U_{xx}}{U_{xy}} = 2^{-3/2}3\frac{(1+\sigma^2)^{3/2}}{\sigma} \tag{5.27}$$

and that

$$\beta \equiv U_{yy}/U_{yx} = 2^{-3/2}3(1+\sigma^2)^{3/2}. \tag{5.28}$$

The dependence with $\sigma$ on the coupling constants is given as

$$\Delta/J = 2t_x t_y^{-1}\frac{\beta}{(\alpha\beta-1)} = 2t_y t_x^{-1}\frac{\alpha}{(\alpha\beta-1)} - \frac{t_x t_y^{-1} + t_y t_x^{-1}}{2} \tag{5.29}$$

and

$$\gamma = -\frac{4}{(\alpha\beta-1)}. \tag{5.30}$$

The inset in Fig. 5.5 displays the three coupling parameters as a function of $\sigma$ for $|t_x/t_y| = 0.1$. We see that the relative size and even the sign of the couplings can be tuned by varying $\sigma$. In particular, while interactions in $\hat{S}_y$ always lead to anti-ferromagnetic couplings, the interactions in $\hat{S}_z$ and $\hat{S}_x$ can lead to both ferromagnetic or anti-ferromagnetic couplings. In the main part of Fig. 5.5 we sketch the different possible models as a function of $t_y/t_x$ and $\sigma$. This clearly demonstrates that this method allows for realization of a whole class of $XYZ$ spin chains.

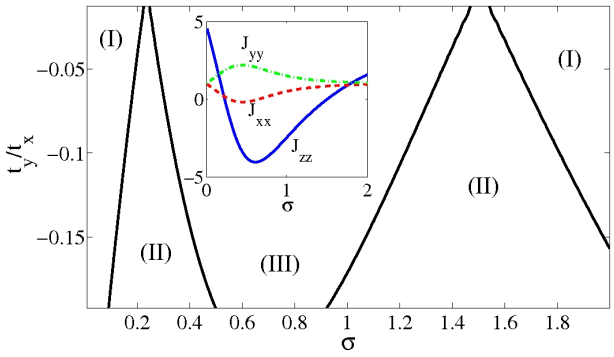


Figure 5.5.: $XYZ$ Heisenberg chains with different types of couplings that can be achieved by varying the relative orbital squeezing and the relative tunneling strength. In (I) the system has anti-ferromagnetic couplings in all the components of the spin with $\Delta > J(1+|\gamma|)$. In (II) the system has both ferromagnetic or anti-ferromagnetic couplings in the $z$ component of the spin and anti-ferromagnetic in the $y$ component with $J(1+|\gamma|) > \Delta$. Finally, (III) has the same characteristics of region (II) but now $|\Delta| > J(1+|\gamma|)$. In the inset we show one example of the spin parameters where $t_y/t_x = -0.1$, and $J_{xx} = (1+\gamma)$, $J_{yy} = (1-\gamma)$ and $J_{zz} = \Delta/J$.

### 5.2.2. Experimental realization

In the experiment described in Ref. [11], the lifetimes reported for bosons occupying the states in the $p$ band of an effective $1D$ optical lattice were surprisingly long. With an

average number of approximately two atoms per site, the atoms could tunnel hundreds of times before decaying to the $s$ band. Here the main decay mechanism stem from atom-atom collisions [7, 11], and therefore an increase in the lifetime is expected for the case where there is only one atom per site[26]

The typical values for the tunneling times can be estimated from the overlap integrals of neighboring Wannier functions. Considering $^{87}$Rb atoms, for example, and $\lambda_{lat} = 843\,nm$ to be the wavelength (in the $y$-direction) which sets the recoil energy $E_R$, we obtain $J/E_R \sim 0.01$ and the characteristic tunneling time $\tau = \hbar/J \sim 5$ms for the system with $V_x = 30E_R$, $V_y = 50E_R$ and $V_z = 60E_R$. This corresponds to a few dozens of times smaller than the expected lifetimes [11], which should allow for experimental explorations of our results. In addition, it is possible to use the external driving discusses in section 5.2.1 to increase the lifetimes even further.

A last remark is in time which regards the temperatures required for observation of the spin correlations. The physics discussed here will emerge for temperatures of the order of $k_B T \lesssim J \sim t^2/U$ [49]. Although it might be very difficult to experimentally achieve such temperatures, this reflects the frontier of experimental realizations and it is being currently attacked by several experimental groups.

## 5.3. Effective model including imperfections due to $s$-orbital atoms

Difficulties for experimental implementations that are related to the low temperatures required for accessing the physics explored here were already pointed out in the last section. The other main difficulty related to experiments regards the existence of imperfections in the system. These imperfections consist of residual $s$-orbital atoms, that result from the process of loading atoms in the $p$-band. Although the possibility of promoting atoms from the $s$ to the $d$ band with 99% fidelity was recently reported [73], the fidelity for promoting atoms from the $s$ to the $p$ band is currently at 80%. This means that 20% of the atoms will still remain in the orbital states of the $s$ band and that it is necessary to investigate the extent of which the presence of ($s$-orbital atom) impurities are capable of changing the physics of the clean system.

We notice first that due to the large amplitudes of the optical potential (required by the Mott insulator phase), the atoms occupying orbital states of the $s$ band can be declared immobile. As a consequence, random sites will contain localized impurities. The next factor to consider is related to the energy scales. Double occupation of states with one $s$- and one $p$-orbital atom has a larger energy cost than the double occupation of states with two atoms in the $p$-orbital states. In other words, $U_{ps} > U_{\alpha\beta}$, where $\alpha, \beta = \{x, y\}$ and

$$U_{ps} = U_0 \int d\mathbf{r} |w_i^{\alpha}(\mathbf{r})|^2 |w_i^{s}(\mathbf{r})|^2 \tag{5.31}$$

is the interaction energy between an $s$- and a $p$-orbital atom[27]. Accordingly, repeated experimental realizations will prepare the system in different random configurations as

[26] In fact, Ref. [11] estimates an increase of up to a factor of 5 in the lifetimes for the situation with unit filling of the lattice sites.

[27] Notice here that $w_i^s(\mathbf{r})$ is used to denote the $s$ orbital at the site $i$.

illustrated in Fig. 5.6. This means that an additional step must be carried out, in principle, in order to integrate out degrees of freedom corresponding to atoms in the $s$-orbitals. This is possible by averaging over all the different configurations which contain a fixed ratio of $s$- to $p$-orbital atoms.

We now repeat the reasoning of Sec. 5.1, to include in the effective Hamiltonian contributions stemming from the presence of impurities in the model. Let us consider two neighboring sites, $i$ and $j$, one with an $s$ and the other with a $p$ orbital atom. After the steps of the perturbative calculation are carried out (in second order in $t/U$), we are left with only one additional term,

$$-\frac{t_\alpha^2}{U_{ps}}\hat{a}^\dagger_{\alpha,i}\hat{a}^\dagger_{s,j}\hat{a}_{\alpha,i}\hat{a}_{s,j} = -\frac{t_\alpha^2}{U_{ps}}\hat{n}_{\alpha,i}, \tag{5.32}$$

where again $\alpha = \{x, y\}$ and $\hat{a}_{s,j}$ is the operator that annihilates one atom in the $s$-orbital state at the site $j$, and where in the last equality we used that $\hat{n}_{s,j} = 1$. Since $t_x \neq t_y$, the effect resulting from the presence of an $s$ atom in the system appears as a local fluctuation in the external field. We therefore obtain an $XYZ$ chain with disorder in the field, i.e.,

$$\hat{H}^{(\mathrm{dis})}_{Mott} = -\sum_{\langle i,j\rangle}\left(J^{zz}\hat{S}^z_i\hat{S}^z_j + J^{xx}\hat{S}^x_i\hat{S}^x_j + J^{yy}\hat{S}^y_i\hat{S}^y_j\right) - \sum_i J_i\hat{S}^z_i. \tag{5.33}$$

If the system contains a small number of atoms on the states of the lowest band, this effect should not be too drastic and we expect the disorder to be irrelevant[28] [74]. As the fraction of impurity atoms increases and the disorder in the external field covers a larger number of sites, we expect the disorder to become relevant and the qualitative picture to change. In fact, one possible scenario is the appearance of a localized phase [74]. We remark here that the physics of disordered one dimensional quantum systems contain a plethora of interesting phenomena, as e.g., Anderson phases[29] [54, 61, 62], Mott-glass phases[30] [54], and many of its questions are in the frontier of the current research[31]. The analysis of the random field $XYZ$ chain discussed here, however, is out of the scope of the present thesis and is left to the future.

[28] In the language of real space renormalization group.

[29] The Anderson transition is a transition between a localized and a metallic state, that appears in disordered systems. Nowadays, after many advances on the physics of disordered systems that happened in the 70's and 80's, the term Anderson transition is used in a broader sense [75] and in addition to the transition from metal-insulator, it also includes critical points with transitions that separate localized phases [75].

[30] The Mott-Glass phase is an incompressible gapless insulator phase that is conjectured to appear in the phase diagram of random $1D$ superfluid to insulator phase transition [62].

[31] The phase diagram of the system known by the name of *random bosons*, for example, is still a matter of 'lively debates' in the community [62].

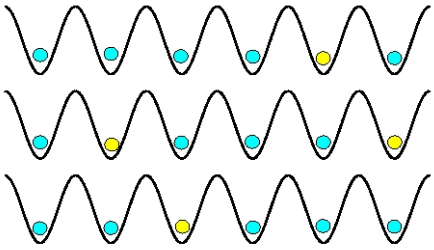

Figure 5.6.: Three random experimental realizations of the insulating state are schematically depicted. The yellow balls are used to represent $s$-orbital atoms, while $p$-orbital atoms are represented by the blue balls.

## 5.4. A quick remark regarding alternative systems for implementing quantum simulators

Alternative scenarios for implementing simulators of quantum systems rely on experimental realizations with trapped ions and polar molecules. Systems of trapped ions have already been used to implement both a small [76, 77, 78, 79] and a large [80] number of spins, but one easily looses control in these setups as the system size increases. In addition, due to trapping potentials the experiments are currently limited to approximately 25 spins, and due to the inherent long range character of the interactions, the construction of paradigmatic spin models becomes a non-trivial task with systems of trapped ions.

Similar limitations appear when using polar molecules, where the effective spin interactions [81, 82] are obtained from the intrinsic dipole-dipole interactions. Here again the character of the dipolar interaction yields effective spin models that are typically long range and in addition, the couplings feature spatial anisotropies [81]. While this spatial anisotropy in the couplings might be in favor of anisotropic models as is the case of the $XYZ$ chain, restricting the range of the interactions might still be tricky for this type of systems.

In summary, even though the temperatures required for simulating the $XYZ$ model with bosons in the $p$ band are very low and in the frontier of the current research, these alternative proposals have different drawbacks and it is not yet clear whether they provide an easier route for experimental implementation of this system.

## 5.5. Remarks on the effective Hamiltonian of the 3-orbital system

In the previous sections we discussed how to use $p$ orbitals to explore the physics of paradigmatic spin 1/2 Hamiltonians. The next question which arises, maybe even natu-

rally, regards the effective Hamiltonian that is obtained from the three orbital system. More explicitly, what is the effective 'spin model' that describes the $\text{Mott}_1$ phase of a $1D$ system with three orbital states?

While this is still in the category of 'work in progress', we present some preliminary discussions regarding the derivation of the effective spin Hamiltonian for a system of (polarized) fermionic atoms in the $p$ band. We restrict ourselves to the fermionic case for the moment, for this considerably simplifies the interaction part of the Hamiltonian (in Eq. (5.1)). In fact, polarized fermions in the $p$ band are described by

$$\hat{H}_f = -\sum_{ij,\alpha} t_{ij}^{\alpha} \hat{a}_{i\alpha}^{\dagger} \hat{a}_{j\alpha} + \sum_{i,\alpha\neq\beta} U_{\alpha\beta} \hat{n}_{i\alpha} \hat{n}_{i\beta} + \sum_{i,\alpha} E_{\alpha}^{p} \hat{n}_{i\alpha}, \tag{5.34}$$

which in addition to the tunneling and on-site energy terms contains only density-density interactions between the different orbital states. Notice here that $\hat{a}_{i\alpha}$ and $\hat{a}_{i\alpha}^{\dagger}$ are operators that destroy and create, respectively, a fermionic atom in the site $i$, and that they satisfy the anti-commutation relations $\{\hat{a}_{i\alpha}, \hat{a}_{i\alpha}^{\dagger}\} = 1$ and $\{\hat{a}_{i\alpha}, \hat{a}_{i\alpha}\} = \{\hat{a}_{i\alpha}^{\dagger}, \hat{a}_{i\alpha}^{\dagger}\} = 0$.

We now apply the same reasoning that was used in Sec. 5.1, and obtain the effective Hamiltonian from second order perturbation theory in $t/U$. For the three orbital system, the basis of states in the subspaces $\mathcal{H}_P$ and $\mathcal{H}_Q$ is taken as

$$\mathcal{H}_P \rightarrow \{|X,X\rangle, |X,Y\rangle, |X,Z\rangle, |Y,X\rangle, |Y,Y\rangle, |Y,Z\rangle, |Z,X\rangle, |Z,Y\rangle, |Z,Z\rangle\} \tag{5.35}$$

and

$$\mathcal{H}_Q \rightarrow \{|0,2X\rangle, |0,XY\rangle, |0,XZ\rangle, |0,2Y\rangle, |0,YZ\rangle, |0,2Z\rangle\}, \tag{5.36}$$

and since the matrix elements which account for transitions of the type $\langle\alpha,\beta|\hat{H}_Q^{-1}|\beta,\alpha\rangle$ will be non-vanishing even for the fermionic case[32], the effective Hamiltonian will contain onsite terms that convert any atom in the $p_\alpha$-orbital state into an atom in the $p_\beta$-orbital state for any $\alpha,\beta$. In order to account for all these dynamical processes we are required to choose a representation for the generators of the $SU(3)$ group[33]. We therefore introduce the *Gell-Mann matrices* [33]

$$\lambda_1 = \begin{pmatrix} 0 & 1 & 0 \\ 1 & 0 & 0 \\ 0 & 0 & 0 \end{pmatrix}, \quad \lambda_2 = \begin{pmatrix} 0 & -i & 0 \\ i & 0 & 0 \\ 0 & 0 & 0 \end{pmatrix}, \quad \lambda_3 = \begin{pmatrix} 1 & 0 & 0 \\ 0 & -1 & 0 \\ 0 & 0 & 0 \end{pmatrix},$$

$$\lambda_4 = \begin{pmatrix} 0 & 0 & 1 \\ 0 & 0 & 0 \\ 1 & 0 & 0 \end{pmatrix}, \quad \lambda_5 = \begin{pmatrix} 0 & 0 & -i \\ 0 & 0 & 0 \\ i & 0 & 0 \end{pmatrix}, \tag{5.37}$$

$$\lambda_6 = \begin{pmatrix} 0 & 0 & 0 \\ 0 & 0 & 1 \\ 0 & 1 & 0 \end{pmatrix}, \quad \lambda_7 = \begin{pmatrix} 0 & 0 & 0 \\ 0 & 0 & -i \\ 0 & i & 0 \end{pmatrix}, \quad \lambda_8 = \frac{1}{\sqrt{3}} \begin{pmatrix} 1 & 0 & 0 \\ 0 & 1 & 0 \\ 0 & 0 & -2 \end{pmatrix}.$$

[32] Notice that it is the density-density interaction term in Eq. (5.35) that allow for such processes to happen.

[33] Maybe an intuitive way of understanding why this is not a spin-1 case, is by noticing that any of the orbital states can be directly converted into each other, i.e., $p_x \rightleftharpoons p_y \rightleftharpoons p_z \rightleftharpoons p_x$. In order for the system to mimic the spin-1 case the conversion between the orbital states should obey a rule as $p_x \rightleftharpoons p_y \rightleftharpoons p_z$, for example, where an atom occupying a $p_x$-orbital state can only be made to occupy a $p_z$-orbital state by being in a $p_y$-orbital state first.

They are traceless Hermitian matrices that satisfy the commutation relations [33]

$$[\lambda_i, \lambda_j] = 2if^{ijk}\lambda_k, \tag{5.38}$$

with $i, j, k = 1, ..8$ and where the $f^{ijk}$ are completely anti-symmetric structure constants given by [33]

$$f^{123} = 1, \;\; f^{147} = f^{165} = f^{246} = f^{257} = f^{345} = f^{376} = \frac{1}{2}, \;\; f^{458} = f^{678} = \frac{\sqrt{3}}{2}. \tag{5.39}$$

In terms of these objects, the correspondence between the SU(3)-spin operators and the operators in the fermionic picture follows as

$$\begin{aligned}
&\lambda_1^i = \hat{a}_{ix}^\dagger \hat{a}_{iy} + \hat{a}_{iy}^\dagger \hat{a}_{ix}, \quad \lambda_2^i = i\hat{a}_{iy}^\dagger \hat{a}_{ix} - i\hat{a}_{ix}^\dagger \hat{a}_{iy} \\
&\lambda_4^i = \hat{a}_{ix}^\dagger \hat{a}_{iz} + \hat{a}_{iz}^\dagger \hat{a}_{ix}, \quad \lambda_5^i = i\hat{a}_{iz}^\dagger \hat{a}_{ix} - i\hat{a}_{ix}^\dagger \hat{a}_{iz} \\
&\lambda_6^i = \hat{a}_{iy}^\dagger \hat{a}_{iz} + \hat{a}_{iz}^\dagger \hat{a}_{iy}, \quad \lambda_7^i = i\hat{a}_{iy}^\dagger \hat{a}_{iz} - i\hat{a}_{iz}^\dagger \hat{a}_{iy} \\
&\lambda_3^i = \hat{n}_i^x - \hat{n}_i^y \\
&\lambda_8^i = \tfrac{1}{\sqrt{3}}\hat{n}_i^x + \tfrac{1}{\sqrt{3}}\hat{n}_i^y - \tfrac{2}{\sqrt{3}}\hat{n}_i^z.
\end{aligned} \tag{5.40}$$

In analogy with the routine executed previously for analysis of the spin-1/2 case, we also impose here the constraint of a unit filling of the lattice sites: $\hat{n}_i^x + \hat{n}_i^y + \hat{n}_i^z = 1$. We therefore obtain

$$\begin{aligned}
\hat{n}_i^x &= \tfrac{1}{3} + \tfrac{1}{2}\lambda_3^i + \tfrac{\sqrt{3}}{6}\lambda_8^i \\
\hat{n}_i^y &= \tfrac{1}{3} - \tfrac{1}{2}\lambda_3^i + \tfrac{\sqrt{3}}{6}\lambda_8^i \\
\hat{n}_i^z &= \tfrac{1}{3} - \tfrac{\sqrt{3}}{3}\lambda_8^i,
\end{aligned} \tag{5.41}$$

and also rewrite the following expressions:

$$\begin{aligned}
\hat{a}_{ix}^\dagger \hat{a}_{iy} &= \tfrac{\lambda_1^i + i\lambda_2^i}{2} \\
\hat{a}_{ix}^\dagger \hat{a}_{iz} &= \tfrac{\lambda_4^i + i\lambda_5^i}{2} \\
\hat{a}_{iy}^\dagger \hat{a}_{iz} &= \tfrac{\lambda_6^i - i\lambda_7^i}{2}.
\end{aligned} \tag{5.42}$$

Now after conducting the steps of the perturbative calculation, the expression for the effective Hamiltonian describing the Mott$_1$ phase of fermions in the three $p$-orbital system follows as

$$\begin{aligned}
H \;= \sum_i \;& \left(t_x^2 + t_y^2\right) \mathcal{J}_1 \left(\hat{n}_i^x \hat{n}_j^y + \hat{n}_i^y \hat{n}_j^x\right) + \left(t_x^2 + t_z^2\right) \mathcal{J}_2 \left(\hat{n}_i^x \hat{n}_j^z + \hat{n}_i^z \hat{n}_j^x\right) \\
&+ \left(t_y^2 + t_z^2\right) \mathcal{J}_3 \left(\hat{n}_i^y \hat{n}_j^z + \hat{n}_i^z \hat{n}_j^y\right) \\
&+ 2t_x t_y \mathcal{J}_4 \hat{a}_{iy}^\dagger \hat{a}_{ix} \hat{a}_{jx}^\dagger \hat{a}_{jy} + 2t_x t_y \mathcal{J}_5 \hat{a}_{iz}^\dagger \hat{a}_{ix} \hat{a}_{jx}^\dagger \hat{a}_{jz} + 2t_y t_z \mathcal{J}_6 \hat{a}_{iz}^\dagger \hat{a}_{iy} \hat{a}_{jy}^\dagger \hat{a}_{jz} \\
&+ 2t_x t_y \mathcal{J}_7 \hat{a}_{ix}^\dagger \hat{a}_{iy} \hat{a}_{jy}^\dagger \hat{a}_{jx} + 2t_x t_y \mathcal{J}_8 \hat{a}_{ix}^\dagger \hat{a}_{iz} \hat{a}_{jz}^\dagger \hat{a}_{jx} + 2t_y t_z \mathcal{J}_9 \hat{a}_{iy}^\dagger \hat{a}_{iz} \hat{a}_{jz}^\dagger \hat{a}_{jy},
\end{aligned} \tag{5.43}$$

where the $\mathcal{J}_n$, $n = 1...9$ are used to denote the inverse of the intensity of the exchange interaction. In fact, due to the absence of orbital-changing terms in the Hamiltonian of fermions in the $p$ band, the interaction Hamiltonian is diagonal in the basis of the intermediate states of the perturbative calculation, and therefore $\mathcal{J} = \frac{1}{2U_{\alpha\beta}}$, where $\alpha, \beta = \{x, y, z\}$. While explicit computation of each term of the effective Hamiltonian is shown in the appendix, we quote here the final result,

$$\begin{aligned} H &= \sum_i \left( \frac{\sqrt{3}}{9} \frac{(t_x^2+t_y^2)}{U_{xy}} - \frac{\sqrt{3}}{9} \frac{(t_x^2+t_z^2)}{U_{xz}} - \frac{\sqrt{3}}{9} \frac{(t_y^2+t_z^2)}{U_{yz}} \right) \lambda_8^i \\ &+ \sum_i \left( \frac{(t_x^2+t_z^2)}{6U_{xz}} - \frac{(t_y^2+t_z^2)}{6U_{yz}} \right) \lambda_3^i \\ &+ \sum_{\langle i,j \rangle} -\frac{(t_x^2+t_y^2)}{4U_{xy}} \lambda_3^i \lambda_3^j + \left( \frac{(t_x^2+t_y^2)}{12U_{xy}} - \frac{(t_y^2+t_z^2)}{6U_{yz}} - \frac{(t_x^2+t_z^2)}{6U_{xz}} \right) \lambda_8^i \lambda_8^j \\ &+ \sum_{\langle i,j \rangle} \left( \frac{\sqrt{3}}{12} \frac{(t_y^2+t_z^2)}{U_{yz}} - \frac{\sqrt{3}}{12} \frac{(t_x^2+t_z^2)}{U_{xz}} \right) \left( \lambda_8^i \lambda_3^j + \lambda_3^i \lambda_8^j \right) \\ &+ \sum_{\langle i,j \rangle} \frac{t_x t_y}{2U_{xy}} (T_i^+ T_j^- + T_i^- T_j^+) + \frac{t_x t_z}{2U_{xz}} (V_i^+ V_j^- + V_i^- V_j^+) + \frac{t_y t_z}{2U_{zy}} (U_i^+ U_j^- + U_i^- U_j^+) \end{aligned} \tag{5.44}$$

where $T^\pm = \lambda_1 \pm i\lambda_2$, $V^\pm = \lambda_4 \pm i\lambda_5$ and $U^\pm = \lambda_6 \pm i\lambda_7$ are the $SU(3)$ ladder operators. While analysis of this system is left for the future, we conclude this section by noticing that cold atoms in the $p$ band offer interesting prospects to unravel the physics of spin chains beyond spin-1/2.

# B. Computation of the effective $SU(3)$-spin chain Hamiltonian

The following steps show a term-by-term computation of the Hamiltonian shown in Eq. (5.44) with explicit use of Eqs. (5.41) and (5.42). This is added here just for 'reference purposes', in what is related to the continuation of this work.

$$\begin{aligned}
\hat{n}_i^x \hat{n}_j^y &= \left(\tfrac{1}{3} + \tfrac{1}{2}\lambda_3^i + \tfrac{\sqrt{3}}{6}\lambda_8^i\right)\left(\tfrac{1}{3} - \tfrac{1}{2}\lambda_3^j + \tfrac{\sqrt{3}}{6}\lambda_8^j\right) \\
&= \tfrac{1}{6}(\lambda_3^i - \lambda_3^j) + \tfrac{\sqrt{3}}{18}(\lambda_8^i + \lambda_8^j) - \tfrac{1}{4}\lambda_3^i\lambda_3^j + \tfrac{\sqrt{3}}{12}(\lambda_3^i\lambda_8^j - \lambda_8^i\lambda_3^j) + \tfrac{1}{12}\lambda_8^i\lambda_8^j \\
\hat{n}_i^y \hat{n}_j^x &= \left(\tfrac{1}{3} - \tfrac{1}{2}\lambda_3^i + \tfrac{\sqrt{3}}{6}\lambda_8^i\right)\left(\tfrac{1}{3} + \tfrac{1}{2}\lambda_3^j + \tfrac{\sqrt{3}}{6}\lambda_8^j\right) \\
&= -\tfrac{1}{6}(\lambda_3^i - \lambda_3^j) + \tfrac{\sqrt{3}}{18}(\lambda_8^i + \lambda_8^j) - \tfrac{1}{4}\lambda_3^i\lambda_3^j - \tfrac{\sqrt{3}}{12}(\lambda_3^i\lambda_8^j - \lambda_8^i\lambda_3^j) + \tfrac{1}{12}\lambda_8^i\lambda_8^j \\
\hat{n}_i^x \hat{n}_j^y + \hat{n}_i^y \hat{n}_j^x &= \tfrac{\sqrt{3}}{9}(\lambda_8^i + \lambda_8^j) - \tfrac{1}{2}\lambda_3^i\lambda_3^j + \tfrac{1}{6}\lambda_8^i\lambda_8^j
\end{aligned} \tag{B.1}$$

$$\begin{aligned}
\hat{n}_i^x \hat{n}_j^z &= \left(\tfrac{1}{3} + \tfrac{1}{2}\lambda_3^i + \tfrac{\sqrt{3}}{6}\lambda_8^i\right)\left(\tfrac{1}{3} - \tfrac{\sqrt{3}}{3}\lambda_8^j\right) \\
&= -\tfrac{\sqrt{3}}{9}\lambda_8^j + \tfrac{\sqrt{3}}{18}\lambda_8^i + \tfrac{1}{6}\lambda_3^i - \tfrac{\sqrt{3}}{6}\lambda_3^i\lambda_8^j - \tfrac{1}{6}\lambda_8^i\lambda_8^j \\
\hat{n}_i^z \hat{n}_j^x &= \left(\tfrac{1}{3} - \tfrac{\sqrt{3}}{3}\lambda_8^i\right)\left(\tfrac{1}{3} + \tfrac{1}{2}\lambda_3^j + \tfrac{\sqrt{3}}{6}\lambda_8^j\right) \\
&= -\tfrac{\sqrt{3}}{9}\lambda_8^i + \tfrac{\sqrt{3}}{18}\lambda_8^j + \tfrac{1}{6}\lambda_3^j - \tfrac{\sqrt{3}}{6}\lambda_8^i\lambda_3^j + \tfrac{1}{6}\lambda_8^i\lambda_8^j \\
\hat{n}_i^x \hat{n}_j^z + \hat{n}_i^z \hat{n}_j^x &= -\tfrac{\sqrt{3}}{9}(\lambda_8^i + \lambda_8^j) + \tfrac{1}{6}(\lambda_3^i + \lambda_3^j) - \tfrac{\sqrt{3}}{6}(\lambda_3^i\lambda_8^j + \lambda_8^i\lambda_3^j) - \tfrac{1}{3}\lambda_8^i\lambda_8^j
\end{aligned} \tag{B.2}$$

$$\begin{aligned}
\hat{n}_i^y \hat{n}_j^z &= \left(\tfrac{1}{3} - \tfrac{1}{2}\lambda_3^i + \tfrac{\sqrt{3}}{6}\lambda_8^i\right)\left(\tfrac{1}{3} - \tfrac{\sqrt{3}}{3}\lambda_8^j\right) \\
&= -\tfrac{\sqrt{3}}{9}\lambda_8^j - \tfrac{1}{6}\lambda_3^i + \tfrac{\sqrt{3}}{6}\lambda_3^i\lambda_8^j + \tfrac{\sqrt{3}}{18}\lambda_8^i - \tfrac{1}{6}\lambda_8^i\lambda_8^j \\
\hat{n}_i^z \hat{n}_j^y &= \left(\tfrac{1}{3} - \tfrac{\sqrt{3}}{3}\lambda_8^i\right)\left(\tfrac{1}{3} - \tfrac{1}{2}\lambda_3^j + \tfrac{\sqrt{3}}{6}\lambda_8^j\right) \\
&= -\tfrac{1}{6}\lambda_3^j + \tfrac{\sqrt{3}}{18}\lambda_8^j - \tfrac{\sqrt{3}}{9}\lambda_8^i + \tfrac{\sqrt{3}}{6}\lambda_8^i\lambda_3^j - \tfrac{1}{6}\lambda_8^i\lambda_8^j \\
\hat{n}_i^y \hat{n}_j^z + \hat{n}_i^z \hat{n}_j^y &= -\tfrac{1}{6}(\lambda_3^i + \lambda_3^j) - \tfrac{\sqrt{3}}{9}(\lambda_8^i + \lambda_8^j) + \tfrac{\sqrt{3}}{6}(\lambda_8^i\lambda_3^j + \lambda_3^i\lambda_8^j) - \tfrac{1}{3}\lambda_8^i\lambda_8^j
\end{aligned} \tag{B.3}$$

$$\begin{aligned}
\hat{a}^{\dagger}_{iy}\hat{a}_{ix}\hat{a}^{\dagger}_{ix}\hat{a}_{jy} &= \tfrac{1}{4}(\lambda^i_1\lambda^j_1 + i(\lambda^i_1\lambda^j_2 - \lambda^i_2\lambda^j_1) + \lambda^i_2\lambda^j_2) \\
\hat{a}^{\dagger}_{iz}\hat{a}_{ix}\hat{a}^{\dagger}_{jx}\hat{a}_{jz} &= \tfrac{1}{4}(\lambda^i_4\lambda^j_4 + i(\lambda^i_4\lambda^j_5 - \lambda^i_5\lambda^j_4) + \lambda^i_5\lambda^j_5) \\
\hat{a}^{\dagger}_{iz}\hat{a}_{iy}\hat{a}^{\dagger}_{jy}\hat{a}_{jz} &= \tfrac{1}{4}(\lambda^i_6\lambda^j_6 - i(\lambda^i_6\lambda^j_7 - \lambda^i_7\lambda^i_6) + \lambda^i_7\lambda^j_7)
\end{aligned} \tag{B.4}$$

# 6. Conclusions

In this thesis we presented different aspects of the physics of $p$-orbital bosons that range to properties of both the mean-field and more strongly correlated levels. The main part of this text covers the material of Papers I and II that are attached after the bibliographic references.

We started by introducing the band structure and the orbital states in Chapter 2, where we also constructed the Hamiltonian for describing the many-body system. This framework was used in Chapter 3 as the basis for the mean-field analysis. There we have shown that the term describing orbital changing collisions in the Hamiltonian of $p$-orbital bosons leads to the formation of structures in the ground-state of the system: in the $2D$ system, for example, this corresponds to the staggered-vortex solution. We continued with Chapter 4, where we studied the physics of $p$-orbital bosons in the presence of an external confining trap. This part presents the study developed in Paper I. In addition to characterizing the ground state propeties and, in particular, the fate of the staggered-vortex solution due to the presence of the trap, we also studied finite temperature physics of the ideal gas and properties of the system in anisotropic lattices.

In Chapter 5 we presented the content of Paper II, where we studied properties of the strongly correlated regime of $p$-orbital bosons. More explicitly, we have shown that for the two-orbital case, the dynamics of the Mott phase with a unit filling of the lattice sites can be effectively described by the spin-1/2 anisotropic Heisenberg (the $XYZ$) model in external field. We studied the phase diagram in the thermodynamic limit and also finite size effects relevant to experimental realizations. We have also proposed manipulation and detection schemes that allow for experimental probing of the physics discussed. In addition to what is covered in Paper II, in this chapter we also discussed extensions of the spin model and directions for future research. As mentioned in Sec. 5.5, generalization to the $3D$ lattice and the three orbital system of the study presented here offers an interesting prospect for studying the physics of models beyond spin-1/2. Along these lines, it is also interesting to engineer spin-1 chains, which in terms of the orbital states in the $p$ band, can be constructed by using the $p_x$, the $p_y$ and the $p_{xy}$[1] orbitals of a $2D$ lattice. Due to recent experimental advances in manipulating bosons in excited bands of optical lattices, and in particular, in the $d$ band [73], characterization of such systems are also of experimental relevance. At the same time, there are still open questions for the spin-1/2 system that we intend to investigate in future work. These include a thorough study of the system with impurities discussed in Sec. 5.3, studying the dynamics, propagation of Lieb-Robinson bounds and characterization of the system when it is coupled to an external bath.

[1]The $p_{xy}$ orbital is the orbital state that is odd both in the $x$ and the $y$ directions.

# Bibliography


[1] Matthew PA Fisher, Peter B Weichman, G Grinstein, and Daniel S Fisher. Boson localization and the superfluid-insulator transition. *Physical Review B*, 40(1):546, 1989.

[2] Markus Greiner, Olaf Mandel, Tilman Esslinger, Theodor W Hänsch, and Immanuel Bloch. Quantum phase transition from a superfluid to a Mott insulator in a gas of ultracold atoms. *Nature*, 415(6867):39–44, 2002.

[3] Maciej Lewenstein, Anna Sanpera, Veronica Ahufinger, Bogdan Damski, Aditi Sen, and Ujjwal Sen. Ultracold atomic gases in optical lattices: mimicking condensed matter physics and beyond. *Advances in Physics*, 56(2):243–379, 2007.

[4] Immanuel Bloch and Markus Greiner. Exploring quantum matter with ultracold atoms in optical lattices. *Advances in Atomic, Molecular, and Optical Physics*, 52:1–47, 2005.

[5] John Hubbard. Electron correlations in narrow energy bands. *Proceedings of the Royal Society of London. Series A. Mathematical and Physical Sciences*, 276(1365):238–257, 1963.

[6] Dieter Jaksch, Ch Bruder, Juan Ignacio Cirac, Crispin W Gardiner, and Peter Zoller. Cold bosonic atoms in optical lattices. *Physical Review Letters*, 81(15):3108–3111, 1998.

[7] A Isacsson and SM Girvin. Multiflavor bosonic hubbard models in the first excited bloch band of an optical lattice. *Physical Review A*, 72(5):053604, 2005.

[8] J Larson, A Collin, and J-P Martikainen. Multiband bosons in optical lattices. *Physical Review A*, 79(3):033603, 2009.

[9] A Collin, J Larson, and J-P Martikainen. Quantum states of p-band bosons in optical lattices. *Physical Review A*, 81(2):023605, 2010.

[10] Georg Wirth, Matthias Ölschläger, and Andreas Hemmerich. Evidence for orbital superfluidity in the p-band of a bipartite optical square lattice. *Nature Physics*, 7(2):147–153, 2010.

[11] Torben Müller, Simon Fölling, Artur Widera, and Immanuel Bloch. State preparation and dynamics of ultracold atoms in higher lattice orbitals. *Physical Review Letters*, 99(20):200405, 2007.

[12] Ofir E Alon, Alexej I Streltsov, and Lorenz S Cederbaum. Zoo of quantum phases and excitations of cold bosonic atoms in optical lattices. *Physical Review Letters*, 95(3):030405, 2005.

[13] Gretchen K Campbell, Jongchul Mun, Micah Boyd, Patrick Medley, Aaron E Leanhardt, Luis G Marcassa, David E Pritchard, and Wolfgang Ketterle. Imaging the Mott insulator shells by using atomic clock shifts. *Science*, 313(5787):649–652, 2006.

[14] Sebastian Will, Thorsten Best, Ulrich Schneider, Lucia Hackermüller, Dirk-Sören Lühmann, and Immanuel Bloch. Time-resolved observation of coherent multi-body interactions in quantum phase revivals. *Nature*, 465(7295):197–201, 2010.

[15] PR Johnson, E Tiesinga, JV Porto, and CJ Williams. Effective three-body interactions of neutral bosons in optical lattices. *New Journal of Physics*, 11(9):093022, 2009.

[16] Maciej Lewenstein and W Vincent Liu. Optical lattices: Orbital dance. *Nature Physics*, 7:101–103, 2011.

[17] VW Scarola and S Das Sarma. Quantum phases of the extended Bose-Hubbard hamiltonian: Possibility of a supersolid state of cold atoms in optical lattices. *Physical review letters*, 95(3):033003, 2005.

[18] VW Scarola, E Demler, and S Das Sarma. Searching for a supersolid in cold-atom optical lattices. *Physical Review A*, 73(5):051601, 2006.

[19] Congjun Wu, W Vincent Liu, Joel Moore, and Sankar Das Sarma. Quantum stripe ordering in optical lattices. *Physical Review Letters*, 97(19):190406, 2006.

[20] Cenke Xu and Matthew PA Fisher. Bond algebraic liquid phase in strongly correlated multiflavor cold atom systems. *Physical Review B*, 75(10):104428, 2007.

[21] Fernanda Pinheiro, Georg M Bruun, Jani-Petri Martikainen, and Jonas Larson. *XYZ* quantum Heisenberg models with *p*-orbital bosons. *arXiv preprint arXiv:1304.3178*, 2013.

[22] W Vincent Liu and Congjun Wu. Atomic matter of nonzero-momentum Bose-Einstein condensation and orbital current order. *Physical Review A*, 74(1):013607, 2006.

[23] Richard P Feynman. Simulating physics with computers. *International Journal of Theoretical Physics*, 21(6):467–488, 1982.

[24] J Ignacio Cirac and Peter Zoller. Goals and opportunities in quantum simulation. *Nature Physics*, 8(4):264–266, 2012.

[25] Gregory H Wannier et al. *Elements of solid state theory*. University Press Cambridge, 1959.

[26] Neil W Ashcroft and N David Mermin. *Solid State Physics*, volume 19761. Cengage Learning; 1 edition (January 2, 1976), 1976.

[27] Fernanda Pinheiro, Jani-Petri Martikainen, and Jonas Larson. Confined p-band Bose-Einstein condensates. *Physical Review A*, 85(3):033638, 2012.

[28] Lev P Pitaevskii and Sandro Stringari. *Bose-Einstein Condensation*, volume 116. Clarendon Press, 2003.

[29] Christopher J Pethick and Henrik Smith. *Bose-Einstein condensation in dilute gases*. Cambridge University Press, 2002.

[30] AFR Piza. Bose-Einstein condensation in dilute atomic gases. *Brazilian journal of physics*, 34(3B):1102–1157, 2004.

[31] Anthony J Leggett. *Quantum liquids: Bose condensation and Cooper pairing in condensed-matter systems*, volume 34. Oxford University Press Oxford, 2006.

[32] Tomasz Sowiński, Mateusz Łacki, Omjyoti Dutta, Joanna Pietraszewicz, Piotr Sierant, Mariusz Gajda, Jakub Zakrzewski, and Maciej Lewenstein. Dynamical restoration of symmetry breaking in realistic optical lattices. *arXiv preprint arXiv:1304.6299*, 2013.

[33] Walter Greiner and Berndt Müller. *Quantum Mechanics. Symmetries*, volume 2. Springer Verlag, 1994.

[34] Nigel Goldenfeld. *Lectures on phase transitions and the renormalization group*. Frontiers in Physics (Book 85). Westview Press, 1992.

[35] Alexander Altland and Ben Simons. *Condensed matter field theory*. Cambridge University Press, 2006.

[36] Marlan O Scully, M Suhail Zubairy, and Ian A Walmsley. *Quantum Optics*, volume 67. Cambridge University Press; 1 edition (September 28, 1997), 1999.

[37] M Aunola. The discretized harmonic oscillator: Mathieu functions and a new class of generalized Hermite polynomials. *Journal of Mathematical Physics*, 44(5):1913–1936, 2003.

[38] P. Behroozi. http://large.stanford.edu/courses/2008/ph372/behroozi2/.

[39] MD Feit, JA Fleck Jr, and A Steiger. Solution of the Schrödinger equation by a spectral method. *Journal of Computational Physics*, 47(3):412–433, 1982.

[40] Matthias Ölschläger, Georg Wirth, Thorge Kock, and Andreas Hemmerich. Topologically induced avoided band crossing in an optical checkerboard lattice. *Physical Review Letters*, 108(7):075302, 2012.

[41] Alexander Altland, V Gurarie, T Kriecherbauer, and A Polkovnikov. Nonadiabaticity

and large fluctuations in a many-particle Landau-Zener problem. *Physical Review A*, 79(4):042703, 2009.

[42] B Damski. The simplest quantum model supporting the Kibble-Zurek mechanism of topological defect production: Landau-Zener transitions from a new perspective. *Physical Review Letters*, 95(3):035701, 2005.

[43] Andreas Hemmerich. Private communication. February 2013.

[44] Hans-Jürgen Mikeska and Alexei K Kolezhuk. One-dimensional Magnetism. In *Quantum Magnetism*, pages 1–83. Springer, 2004.

[45] Assa Auerbach. *Interacting Electrons and Quantum Magnetism*. Springer Verlag, 1994.

[46] Rodney J Baxter. *Exactly Solved Models in Statistical Mechanics*. Dover Publications, 2007.

[47] Fabian HL Essler, Holger Frahm, Frank Göhmann, Andreas Klümper, and Vladimir E Korepin. *The One-dimensional Hubbard Model*. Cambridge University Press, 2005.

[48] Jun John Sakurai. Modern Quantum Mechanics. *Addison Wesley, 1985, edited by Tuan, San Fu*, 1, 1985.

[49] L-M Duan, E Demler, and MD Lukin. Controlling spin exchange interactions of ultracold atoms in optical lattices. *Physical Review Letters*, 91(9):090402, 2003.

[50] Ehud Altman, Walter Hofstetter, Eugene Demler, and Mikhail D Lukin. Phase diagram of two-component bosons on an optical lattice. *New Journal of Physics*, 5(1):113, 2003.

[51] Eduardo Fradkin. *Field Theories of Condensed Matter Systems*, volume 226. Addison-Wesley Redwood City, 1991.

[52] A Yu Kitaev. Unpaired Majorana fermions in quantum wires. *Physics-Uspekhi*, 44(10S):131, 2001.

[53] Thierry Giamarchi. *Quantum Physics in One Dimension*. International Series of Monographs on Physics (Book 121). Oxford University Press, USA, 2004.

[54] Thierry Giamarchi. Boulder Summer School Lecture Notes, July 2013.

[55] Leon A Takhtajan. The quantum inverse problem method and the XYZ Heisenberg model. *Physica D: Nonlinear Phenomena*, 3(1):231–245, 1981.

[56] Eran Sela, Alexander Altland, and Achim Rosch. Majorana fermions in strongly interacting helical liquids. *Physical Review B*, 84(8):085114, 2011.

[57] E Miranda. Introduction to bosonization. *Brazilian Journal of Physics*, 33(1):3–35, 2003.

[58] Christopher L. Henley. http://people.ccmr.cornell.edu/~clh/p654/5.6.pdf.

[59] Per Bak. Commensurate phases, incommensurate phases and the devil's staircase. *Reports on Progress in Physics*, 45(6):587–629, 1982.

[60] Thomas Vojta. Phases and phase transitions in disordered quantum systems. *arXiv preprint arXiv:1301.7746*, 2013.

[61] Thomas Vojta. Boulder Summer School Lecture Notes, July 2013.

[62] Gil Refael. Boulder Summer School Lecture Notes, July 2013.

[63] Henrik Jeldtoft Jensen. http://www.mit.edu/~levitov/8.334/notes/xynotes1.pdf.

[64] David George Ferguson. http://guava.physics.uiuc.edu/~nigel/courses/569/Essays-Spring2006/files/ferguson.pdf.

[65] Subir Sachdev. *Quantum Phase Transitions*. Wiley Online Library, 2007.

[66] Chuck Norris facts.

[67] Christof Weitenberg, Manuel Endres, Jacob F Sherson, Marc Cheneau, Peter Schauß, Takeshi Fukuhara, Immanuel Bloch, and Stefan Kuhr. Single-spin addressing in an atomic Mott insulator. *Nature*, 471(7338):319–324, 2011.

[68] D Leibfried, R Blatt, C Monroe, and D Wineland. Quantum dynamics of single trapped ions. *Reviews of Modern Physics*, 75(1):281, 2003.

[69] Dong Wang, Tony Hansson, Åsa Larson, Hans O Karlsson, and Jonas Larson. Quantum interference structures in trapped-ion dynamics beyond the Lamb-Dicke and rotating wave approximations. *Physical Review A*, 77(5):053808, 2008.

[70] Bruce W Shore. *Manipulating quantum structures using laser pulses*. Cambridge University Press, 2011.

[71] Serge Haroche, Jean-Michel Raimond, and Pierre Meystre. Exploring the quantum: atoms, cavities, and photons. *Physics Today*, 60(8):61, 2007.

[72] Michael Knap, Adrian Kantian, Thierry Giamarchi, Immanuel Bloch, Mikhail D Lukin, and Eugene Demler. Probing real-space and time resolved correlation functions with many-body Ramsey interferometry. *arXiv preprint arXiv:1307.0006*, 2013.

[73] Yueyang Zhai, Xuguang Yue, Yanjiang Wu, Xuzong Chen, Peng Zhang, and Xiaoji Zhou. Effective preparation and collisional decay of atomic condensate in excited bands of an optical lattice. *arXiv preprint arXiv:1306.3313*, 2013.

[74] Curtis A Doty and Daniel S Fisher. Effects of quenched disorder on spin-1/2 quantum XXZ chains. *Physical Review B*, 45(5):2167, 1992.

[75] Ferdinand Evers and Alexander D Mirlin. Anderson transitions. *Reviews of Modern Physics*, 80(4):1355, 2008.

[76] Axel Friedenauer, Hector Schmitz, Jan Tibor Glueckert, Diego Porras, and Tobias Schätz. Simulating a quantum magnet with trapped ions. *Nature Physics*, 4(10):757–761, 2008.

[77] Kihwan Kim, M-S Chang, S Korenblit, R Islam, EE Edwards, JK Freericks, G-D Lin, L-M Duan, and C Monroe. Quantum simulation of frustrated Ising spins with trapped ions. *Nature*, 465(7298):590–593, 2010.

[78] R Islam, EE Edwards, K Kim, S Korenblit, C Noh, H Carmichael, G-D Lin, L-M Duan, C-C Joseph Wang, JK Freericks, et al. Onset of a quantum phase transition with a trapped ion quantum simulator. *Nature Communications*, 2:377, 2011.

[79] Philip Richerme, Crystal Senko, Simcha Korenblit, Jacob Smith, Aaron Lee, Wesley C Campbell, and Christopher Monroe. Trapped-ion quantum simulation of an Ising model with transverse and longitudinal fields. *arXiv preprint arXiv:1303.6983*, 2013.

[80] Joseph W Britton, Brian C Sawyer, Adam C Keith, C-C Joseph Wang, James K Freericks, Hermann Uys, Michael J Biercuk, and John J Bollinger. Engineered two-dimensional Ising interactions in a trapped-ion quantum simulator with hundreds of spins. *Nature*, 484(7395):489–492, 2012.

[81] A Micheli, GK Brennen, and P Zoller. A toolbox for lattice-spin models with polar molecules. *Nature Physics*, 2(5):341–347, 2006.

[82] Bo Yan, Steven A Moses, Bryce Gadway, Jacob P Covey, Kaden RA Hazzard, Ana Maria Rey, Deborah S Jin, and Jun Ye. Realizing a lattice spin model with polar molecules. *arXiv preprint arXiv:1305.5598*, 2013.